# ICI Calculations of the Exact Wave Functions of Atoms and Molecules and Theoretical Studies of the Reversible $O_2$ Binding of Hemes

Hiroyuki Nakashima

2006

# ICI Calculations of the Exact Wave Functions of Atoms and Molecules and Theoretical Studies of the Reversible $O_2$ Binding of Hemes

Hiroyuki Nakashima

2006

# - Preface -

Solving the Schrödinger equation (SE) and Dirac-Coulomb equation (DCE) is a central theme of theoretical chemistry because of its scientific and practical importance. On the other side, in a complicated system like biological system, a discovery of the role of the essential quantum mechanical principle becomes also a main theme and its prediction is important contribution of quantum chemistry.

Recently, Nakatsuji proposed the general method of solving the Schrödinger equation and established Iterative Configuration or Complements Interaction (ICI) method for obtaining the exact wave functions. Therefore, solving the SE became not a dream but realistic. However, for practical applications of the ICI theory, some formulations and extending theory are necessary especially for many electron systems. Moreover, for the systems including heavy elements, the relativistic effects are rather dominant and therefore extending the ICI theory to the relativistic case is also important. So, the purposes of this thesis are to develop the ICI method for the practical applications to many electron systems and to solve the relativistic DCE. Further, the applications of the present theory to the systems in a magnetic field are performed with both the non-relativistic and relativistic calculations. These systems are interesting from several scientific fields but they are difficult to solve on high precision. These studies are discussed in part I (chapter 1 to 3) of this thesis.

The other purpose of this thesis is to elucidate the reversible $O_2$ binding mechanism of heme. Heme is an active site of hemoglobin and myoglobin, which play indispensable roles in living body on the transport and storage of $O_2$. Several experimental and theoretical studies are found but there is no study for totally understanding this mechanism. In this thesis, theoretical studies are performed for this purpose and we found an important role of the quantum mechanical principles behind the reversible $O_2$ binding mechanism. Based on this study, the $O_2$ binding mechanisms of the isomers of heme are further investigated. They are important as designing the functional proteins. Theoretical predictions are in good agreement with the experimental results. These studies are described in part II (chapter 4, 5).

In chapter 1, the theories of the ICI method are briefly introduced and formulated for many electron systems, and the application to a few-electron atomic systems (from two- to five-electron atoms) has been performed. The formulation given for many electron

systems is general and there is no obstacle to apply the ICI method to these systems. For the application of the two-electron atom (He), the ICI method could achieve the variational energy of incredible high precision. Even for the three-to-five electron atoms (Li to B), very satisfactory results were accomplished.

In chapter 2, the present ICI theories were extended to the relativistic case and a general method of exactly solving the Dirac-Coulomb equation has been proposed for atoms and molecules. For solving the relativistic DCE, an obstacle that often appears in the relativistic field is the so-called variational collapse. Since the lowest electronic state of the DCE is not the lowest state of this equation, the so-called Ritz-type property does not hold. A method to recover Ritz-type property, the inverse Hamiltonian was introduced. Another method of avoiding the variational collapse is to ensure balancing condition on the basis functions. In the ICI formalism, this balancing is automatically done, and we call it ICI balance. The results of the test applications were satisfactory enough to show a high potentiality of the ICI method also for the relativistic case.

Chapter 3 describes the application of the ICI method to the hydrogen and helium atoms in a strong magnetic field with both the non-relativistic and relativistic calculations. Such systems are physically interesting from several scientific fields: astrophysics, chaotic field, condensed matter physics and so on, for example, strong magnetic fields exist on the surface of the white dwarf and neutron stars and the spectroscopic studies are very important for studying what atoms exist there. However they are difficult to be calculated because the systems are extremely distorted by a strong magnetic field and easily cause numerical instability. However, the ICI method showed excellent performance even for these systems and very high precision could be accomplished for both the ground and excited states with both the non-relativistic and relativistic calculations. For the helium atom, this thesis is a first accurate relativistic calculation with explicitly correlated type functions.

In chapter 4, the electronic mechanisms of the reversible $O_2$ binding by heme were studied. The two-dimensional potential energy surfaces for triplet and singlet states were investigated. Since the ground state of the $O_2$ + deoxyheme is triplet and that of oxyheme is singlet, $O_2$ binding process requires relativistic spin-orbit interaction to accomplish the intersystem crossing from triplet to singlet states. The moderate and reversible $O_2$ binding can be accomplished by this crossing. As a result, the spin state (comes from quantum mechanics) and the spin-orbit interaction (comes from relativistic

theories) are governing principles for the reversible $O_2$ binding mechanism of heme.

In chapter 5, the $O_2$ binding mechanisms were investigated further in the Fe-porphyrin (FePor) isomers: Fe-porphycene (FePc) and Fe-corrphycene (FeCor) complexes. The modified proteins, where heme is replaced with these complexes, are important for designing the functional proteins. The experimental studies show that the dramatic increase of the $O_2$ affinity is shown in FePc complex and the decrease in FeCor complex. From theoretical studies of this thesis, it was clear that FePc-$O_2$ complex used only singlet surface without crossing of triplet and singlet surfaces, different from the cases of FePor and FeCor. This is a reason why the high $O_2$ affinity is shown in FePc complex. Estimated equilibrium constants for the $O_2$ binding reasonably reproduced the trends in the experimental results. It is confirmed that the theoretical predictions give satisfactory results and useful for designing the functional molecules.

# - Acknowledgments -

The present thesis is the summary of the author's studies carried out at the Department of Synthetic Chemistry and Biological Chemistry, Graduate School of Engineering at Kyoto University from 2000 to 2006. The author would like to express his heartfelt gratitude to Professor Hiroshi Nakatsuji for his guidance and warm encouragement.

The author is also grateful to Dr. Masahiro Ehara, Dr. Jun-ya Hasegawa and Dr. Ryoichi Fukuda for their critical suggestions and useful advices.

The author would also like to thank Dr. Maho Nakata and Dr. Kei Kuramoto for their helpful discussions and warm encouragements, and Mr. Yusaku Kurokawa, Mr. Atsushi Ishikawa, Dr. Taisuke Nagasawa and Mr. Yu Hijikata for their helps and discussions on the author's work of Part I. He also thanks to Dr. Yasushi Honda, Dr. Tomoo Miyahara, Dr. Yuhki Ohtsuka, Mr. Kazuhiro Fujimoto and all other members of the Nakatsuji Laboratory for their good suggestions, kindness and friendship.

Finally, the author expresses his sincere gratitude to his parents, Mr. Takahiko Nakashima and Ms. Kayo Nakashima for their continuous understanding, financial supports and affectionate encouragement.

2006 January

Hiroyuki Nakashima

# - List of Publications -

**Part I** **Solving Schrödinger and Dirac-Coulomb Equations of Small Atoms and Molecules with the ICI Formalism**

Chapter 1 ICI Calculations of the Exact Wave Functions of a Few-Electron Atoms
H. Nakashima, Y. Kurokawa, H. Nakatsuji, *J. Chem. Phys.*, to be submitted for publication.

Chapter 2 Analytically Solving the Relativistic Dirac-Coulomb Equation for Atoms and Molecules
H. Nakatsuji, H. Nakashima, *Phys. Rev. Lett.*, **95**, 050407, 2005.

Chapter 3 Hydrogen and Helium Atoms in a Strong Magnetic Field
H. Nakashima, H. Nakatsuji, *Phys. Rev. A*, submitted.

**Part II** **Theoretical Study for the Reversible $O_2$ Binding Mechanism of Fe-Porphyrin Complex and its Isomers**

Chapter 4 On the Reversible $O_2$ Binding of Fe-Porphyrin Complex
H. Nakashima, J. Hasegawa, H. Nakatsuji, *J. Comput. Chem.*, **27**, 426, 2006.

Chapter 5 On the $O_2$ Binding of Fe-Porphyrin, Fe-Porphycene and Fe-Corrphycene Complexes
H. Nakashima, J. Hasegawa, H. Nakatsuji, *J. Comput. Chem.* submitted.

**Others** Free Iterative-Complement-Interaction Calculations of the Hydrogen Molecule
Y. Kurokawa, H. Nakashima, H. Nakatsuji, *Phys. Rev. A*, **72**, 062502, 2005.

# - Contents -

# Part I

# Solving Schrödinger and Dirac-Coulomb Equations of Small Atoms and Molecules with the ICI Formalism

# Chapter 1

# ICI Calculations of the Exact Wave Functions of a Few-Electron Atoms

**Abstract:**

The ICI method of solving the exact wave function for atoms and molecules is formulated for many electron systems. Some necessary and useful formulation is derived especially for the spin-free Hamiltonian by using the symmetries. In the ICI formalism, only totally symmetric operators generate the wave function, therefore, the wave function preserves its symmetries from an appropriate initial function, hence symmetry-adopted. For more than two-electron systems, although wave function is inseparable in spatial and spin parts on satisfied the Pauli principle, the ICI method can be performed without any difficulty. For the spin-free Hamiltonian, the more simplified formulation is possible. Test applications for a few electron atoms were almost satisfactory and the ICI method also has a high potentiality for many electron systems.

## 1. Introduction

As noted by Dirac in 1929,[1] the Schrödinger equation (SE) for atoms and molecules,

$$H\psi = E\psi \tag{1.1}$$

$$H = -\frac{1}{2}\sum_i \Delta_i - \sum_i \frac{Z_A}{r_{Ai}} + \sum_{i<j} \frac{1}{r_{ij}} \tag{1.2}$$

is a major quantum principle governing chemistry. So, establishing a general method of exactly solving the SE is a dream of theoretical chemists. In the SE, the exact wave function $\psi$ is determined by the Hamiltonian $H$, so that the exact $\psi$ may be written as a functional of $H$ applied to some appropriate function $\psi_0$ as

$$\psi = f(H)\psi_0 \tag{1.3}$$

Recently, Nakatsuji has studied the structure of the exact wave function – i.e., a possible functional form of $f(H)$, and he proposed the iterative configuration or complement interaction (ICI) method and the simplest extreme coupled cluster (SECC) method as methods of constructing the exact wave function.[2-5] Generally, when $f$ is expanded in a Maclaurin series of $H$, it would include higher powers of $H$, but the integrals of the higher powers of $H$ over approximate wave functions do not exist – i.e., diverge because of the singularity of the Coulomb potentials included in the Hamiltonian.[4,5] Thus, the singularity difficulty commonly occurs in the method of analytically solving the SE of atoms and molecules. He also proposed two methods of solving the singularity problem – i.e., by introducing the inverse Schrödinger equation (ISE) and the scaled Schrödinger equation (SSE).[3-5] Between the two, the latter method was simpler and more general than the former. Combined with the ICI method, it opened a new field of calculating the exact wave functions of atoms and molecules in an analytical expansion form. We have applied the method successfully to hydrogen, Hooke's and helium atom and hydrogen molecule: these calculations have given a basis to confirm the high potentiality of the ICI method.[4-6]

The purpose of this thesis is to extend our theory for many electron systems and to perform test applications to a few-electron atomic systems. For many electron systems, in general, the spatial and spin parts of wave function are inseparable each other on satisfied the Pauli principle for Fermion systems. Therefore, we must treat both spatial and spin coordinates explicitly. This is a different point from one- or two-electron systems. As shown in Eq. (1.3), the ICI method is based on the theory of the structure of

the exact wave function, which is expressed as a functional of the totally symmetric operator $H$. Therefore, the ICI method does not change any symmetry of the wave function from an appropriate initial function $\psi_0$. This indicates that the ICI method is symmetry-adopted and there is no difficulty from spin functions and the Pauli principle. Especially for the spin-free Hamiltonian, the spin part of wave function is not influenced on $H$, which makes formulation simple. In Sec. 2, we introduce the ICI method briefly and explain in details the general method to extend the present method for many electron systems.

Test applications to a few-electron atoms are performed: helium, lithium, beryllium and boron – i.e., from two- to five-electron atoms. The test calculations of helium atom are also shown in the previous papers.[4,5] In this thesis, further calculations are performed to confirm our method can achieve any accuracy results as the iteration proceeds, and detailed computational aspects are also described. By the test calculations of lithium, beryllium and boron atoms, we examine how the ICI method does work for many electron systems. The general formulation to calculate atomic systems is also shown. In Sec. 3, we summarize the computations and mathematics necessary for the present study. In Sec. 4, the results of these calculations are discussed and compared with the existing accurate wave functions in the field of explicitly correlated wave functions. The conclusion is remarked in Sec. 5.

## 2. Theory

### 2.1 The general formalism of the ICI method to solve the Schrödinger equation

In the previous papers,[2-5] the details of the ICI method have been reported. Here, we briefly summarize them.

First, we prepare some equivalent principles and formulas to the SE. One is the variational principle for the wave function $\psi$, written as

$$\langle \psi | H - E | \delta\psi \rangle = 0 \tag{1.4}$$

This is a stationary principle for calculating the best possible $\psi$. Another one is the H-square equation. It is also equivalent to the SE, written as

$$\langle \psi | (H - E)^2 | \psi \rangle = 0 \tag{1.5}$$

Then, Nakatsuji proposed the simplest ICI wave function (SICI) by the recurrence formula,

$$\psi_{n+1} = \left[1 + C_n \left(H - E_n\right)\right] \psi_n \tag{1.6}$$

where $n$ is iteration number and $C$ is a variational parameter. After applied the variational principle to $\psi_{n+1}$, the SICI gives the exact wave function at convergence because we get the H-square equation at convergence.

However, for general atoms and molecules, since Hamiltonian includes the singular Coulomb potentials, the wave function $\psi_{n+1}$ from Eq. (1.6) may include diverging parts. To avoid singular problems, Nakatsuji introduced the scaled Schrödinger equation (SSE),

$$g\left(H - E\right)\psi = 0 \tag{1.7}$$

where $g$ is a positive scalar function, becomes zero only at the singular points $r_0$ of the potential $V$ and should be defined as totally symmetric. Even at the singular point $r_0$, we impose the following condition not to eliminate the information of the Hamiltonian at the singular point,

$$\lim_{r_0 \to 0} gV \neq 0 \tag{1.8}$$

The H-square equation for the SSE is also defined as follows and this is also equivalent to the SE,

$$\left\langle \psi \middle| (H - E) g (H - E) \middle| \psi \right\rangle = 0 \tag{1.9}$$

We also redefine our simplest ICI wave function (SICI) based on the SSE,

$$\psi_{n+1} = \left[1 + C_n g \left(H - E_n\right)\right] \psi_n \tag{1.10}$$

Applied the variational principle, the SICI wave function for the SSE also gives the exact wave function at convergence, because we get the H-square equation for the SSE at convergence. Moreover, we can avoid singular problems. To expect better performance, the free ICI method is introduced. In the free ICI, we take all the independent functions $\{\phi_i\}^{(n)}$ from the ICI wave function and give independent variational parameters to all $\{\phi_i\}^{(n)}$,

$$\psi_{n+1} = \sum_{i}^{all} c_i \phi_i \tag{1.11}$$

This free ICI calculation should converge faster than the SICI from the variational point of view.

## 2.2 The symmetries of the ICI wave function for many electron systems

Next, we introduce some useful formulas from the symmetries to apply the ICI theory to many electron systems. For the non-relativistic Hamiltonian, spin coordinates must be considered together with spatial coordinates and the Pauli principle must be satisfied because electron is a Fermion particle. As shown in Sec. 2.1, the ICI wave function is generated by only totally symmetric operators – i.e., the Hamiltonian $H$, $g$ function and some scalar functions, therefore, the generated wave function preserves its symmetries same as an given initial function $\psi_0$. Therefore, it is necessary to choose the initial function $\psi_0$ with the same symmetry as the state we want to calculate.

First, we must consider the symmetry of the permutation group related to the Pauli principle. Since electron is a Fermion particle, an electronic wave function has to be anti-symmetrized to any exchange of electrons. We define the anti-symmetrizer by

$$A = \frac{1}{\sqrt{N!}} \sum_{i=1}^{N!} (-1)^{p_i} \hat{P}_i \tag{1.12}$$

where $N$ is the number of electrons, $\hat{P}_i$ is the permutation operator and $p_i$ is its parity. To an arbitral wave function $\Psi$, the anti-symmetrized wave function $\psi = A\Psi$ satisfies the Pauli principle (if $A\Psi \neq 0$). We should note that Hamiltonian and $g$ function commute with the permutation operator $\hat{P}_i$, so also commute with the anti-symmetrizer $A$, respectively,

$$[H, \hat{P}_i] = 0 \tag{1.13}$$

$$[H, A] = 0, \ [g, A] = 0 \tag{1.14}$$

Therefore, if we assume the wave function $\psi_n$ at the iteration $n$ as anti-symmetrized one $\psi_n = A\Psi_n$, the generated ICI wave function at the iteration $n+1$ becomes also anti-symmetrized from the recursion formula,

$$\begin{aligned} \psi_{n+1} &= \left[1 + C_n g(H - E_n)\right]\psi_n = \left[1 + C_n g(H - E_n)\right](A\Psi_n) \\ &= A\left[\left(1 + C_n g(H - E_n)\right)\Psi_n\right] \\ &= A\Psi_{n+1} \end{aligned} \tag{1.15}$$

If we choose the initial function as anti-symmetrized one $\psi_0 = A\Psi_0$, the ICI wave function at any iteration number becomes also anti-symmetrized from Eq. (1.15). For many electron systems, the anti-symmetrizer of Eq. (1.12) becomes very complicated because the number of permutations increases in order $N!$. However, from Eq. (1.15),

we can only consider the ICI recursion formula outside from the anti-symmetrizer,

$$\Psi_{n+1} = \left(1 + C_n g\left(H - E_n\right)\right)\Psi_n \tag{1.16}$$

After the iteration proceeds to the final step, the wave function must be anti-symmetrized $\psi_{n+1} = A\Psi_{n+1}$.

Next, to consider other types of symmetries, we should find the operators commute with the Hamiltonian like Eq. (1.13). If the Hamiltonian includes spin-orbit coupling terms, the Hamiltonian may commute with the only total angular momentum operator $\mathbf{J}$. In other cases, the Hamiltonian commutes with the spatial symmetry operator $\mathbf{R}$ and spin angular momentum operator $\mathbf{S}$, separately. In general, if we know the operators commute with the Hamiltonian and these operators also commute each other, the projection operators, make the eigenfunctions of these operators, are also defined like Eq. (1.12). When we define these projection operators as $A_1, A_2, \ldots, A_m$, the commutation relations are written as

$$\begin{aligned} &[H, A_1] = 0, [H, A_2] = 0, \cdots, [H, A_m] = 0 \\ &[A_1, A_2] = 0, [A_1, A_3] = 0, \cdots, [A_{m-1}, A_m] = 0 \end{aligned} \tag{1.17}$$

As discussed for Eq. (1.16), we can only consider the ICI recursion formula outside from these projection operators $A_1, A_2, \ldots, A_m$,

$$\Psi_{n+1} = \left(1 + C_n g\left(H - E_n\right)\right)\Psi_n \tag{1.18}$$

$$\psi_{n+1} = A_1 A_2 \cdots A_m \Psi_{n+1} \tag{1.19}$$

### 2.3 The spin-free Hamiltonian

When we exclude the special cases to have to consider spin-orbit coupling terms, we only have to consider the spin-free Hamiltonian given by Eq. (1.2). Since this Hamiltonian does not operate the spin part of wave function, the spin function is unchanged from the initial function $\psi_0$.

For one- and two-electron systems, since the spatial and spin parts of wave function can be expressed as a separated form each other on satisfied Pauli principle, we only have to treat the spatial part. However, for many electron systems, they are inseparable each other. Therefore, we have to consider explicitly both spatial and spin functions. However, in the sense of Eq. (1.18) and Eq. (1.19), we can exclude the spin part from the ICI recursion formula. Since the spin-free Hamiltonian commutes with $\mathbf{S}$, the eigenfunction of the Hamiltonian becomes a simultaneous eigenfunction of $S^2$ and

$S^z$ operators,

$$\left[H, S^2\right] = 0, \left[H, S^z\right] = 0, \left[S^2, S^z\right] = 0 \tag{1.20}$$

Many papers and books describe how to create eigenfunction of $S^2$ and $S^z$ for many electron systems.[7] When we express the eigenfunction of $S^2$ and $S^z$ as $\chi$, we can write down the wave function satisfies the Pauli principle and also becomes an eigenfunction of the spin angular momentum as

$$\psi = A(\Psi\chi) \tag{1.21}$$

where $A$ is the anti-symmetrizer, $\Psi$ is the spatial part of the wave function. Therefore, if the initial function $\psi_0$ of the ICI formalism is written as

$$\psi_0 = A(\Psi_0\chi) \tag{1.22}$$

the wave function at the iteration $n$ has the same spin angular momentum as the initial function $\psi_0$. The ICI recursion formula can be written as the only spatial part,

$$\Psi_{n+1} = \left(1 + C_n g\left(H - E_n\right)\right)\Psi_n \tag{1.23}$$

However, in some cases, eigenfunctions of $S^2$ and $S^z$ operators are degenerate having same eigenvalues. For example, the doublet state ($S = 1/2$ and $S^z = 1/2$) of three-electron system has two degenerate states,

$$\begin{aligned} \chi^1 &= \alpha(1)\beta(2)\alpha(3) - \beta(1)\alpha(2)\alpha(3) \\ \chi^2 &= 2\alpha(1)\alpha(2)\beta(3) - \beta(1)\alpha(2)\alpha(3) - \alpha(1)\beta(2)\alpha(3) \end{aligned} \tag{1.24}$$

where $\alpha$ and $\beta$ are one-electron spin functions having eigenvalues $S^z = 1/2$ and $S^z = -1/2$, respectively. In this case, we might have to take different spatial functions on different spin eigenfunctions as follows instead of Eq. (1.21),

$$\psi = A\left(\Psi^1\chi^1 + \Psi^2\chi^2\right) \tag{1.25}$$

This may become one choice. However, as Cencek et al. suggested,[8] it is not necessary to use all degenerate functions because the space belonging to different spin functions are covered by extending the spatial space. Since the ICI method extends the spatial space to the exact space, Eq. (1.21) or Eq. (1.22) is a sufficient choice.

For spin-free operators (not only the spin-free Hamiltonian), their expectation values are more easily calculated than for general operators. The most gloomy part of evaluation of expectation values is the permutation of electrons because the number of

permutation operators increases in order $N!$ where $N$ is the number of electrons. However, since spin-free operators do not change the spin part of wave function, the permutation of the unlike spin is negligible from integration of the spin part. We consider the wave function expressed as Eq. (1.21). The spin function is written as a linear combination of the product of the one-electron spin functions. For example of the three-electron system, using the upper spin eigenfunction of Eq. (1.24),

$$\psi = A\left(\Psi(\mathbf{r}_1,\mathbf{r}_2,\mathbf{r}_3)\cdot(\alpha\beta\alpha-\beta\alpha\alpha)\right) \tag{1.26}$$

Eq. (1.26) is rewritten as

$$\psi = A\left(\left(-\Psi(\mathbf{r}_1,\mathbf{r}_2,\mathbf{r}_3)+\Psi(\mathbf{r}_3,\mathbf{r}_2,\mathbf{r}_1)\right)\cdot\alpha\alpha\beta\right) \tag{1.27}$$

Like this, a linear combination of the spin part is replaced as that of spatial part. In general, for the $N$ electron system, we can write the wave function as follows instead of Eq. (1.21),

$$\begin{aligned}\psi &= A\left(\left(\sum_k (-1)^{p_k}\hat{P}_k\Psi(\mathbf{r}_1,\mathbf{r}_2,\ldots,\mathbf{r}_N)\right)\cdot\prod_{i=1}^{N_\alpha}\alpha(i)\cdot\prod_{i=1}^{N_\beta}\beta(i+N_\alpha)\right)\\ &= A\left(\Phi(\mathbf{r}_1,\mathbf{r}_2,\ldots,\mathbf{r}_N)\cdot\Xi(\sigma_1,\sigma_2,\ldots,\sigma_N)\right)\end{aligned} \tag{1.28}$$

where $N_\alpha$ is the number of $\alpha$ spin electrons, $N_\beta$ is the number of $\beta$ spin electrons and $\sigma$ is a spin coordinate. $\Phi$ is the new spatial part and $\Xi$ is the new spin part defined as

$$\begin{aligned}\Phi(\mathbf{r}_1,\mathbf{r}_2,\ldots\mathbf{r}_N) &= \sum_k (-1)^{p_k}\hat{P}_k\Psi(\mathbf{r}_1,\mathbf{r}_2,\ldots\mathbf{r}_N)\\ \Xi(1,2,\ldots N) &= \prod_{i=1}^{N_\alpha}\alpha(i)\cdot\prod_{i=1}^{N_\beta}\beta(i+N_\alpha)\end{aligned} \tag{1.29}$$

The expectation value or matrix element of the spin-free totally symmetric operator $O$ is written as

$$\begin{aligned}\langle\psi'|O|\psi\rangle = \sum_{i=1}^{n!}\sum_{j=1}^{n!}(-1)^{p_i}(-1)^{p_j}&\\ \cdot\int d\mathbf{r}_1\cdots d\mathbf{r}_N\hat{P}_i\Phi'(\mathbf{r}_1,\mathbf{r}_2,\ldots,\mathbf{r}_N)\cdot\left(\hat{O}\hat{P}_j\Phi(\mathbf{r}_1,\mathbf{r}_2,\ldots,\mathbf{r}_N)\right)&\\ \cdot\int d\sigma_1\cdots d\sigma_N\hat{P}_i\Xi'(\sigma_1,\sigma_2,\ldots,\sigma_n)\cdot\hat{P}_j\Xi(\sigma_1,\sigma_2,\ldots,\sigma_n)&\end{aligned} \tag{1.30}$$

Since the operator $O$ is spin-free and totally symmetric and the integration is performed at all electrons (which means the integration is independent from the electron

numbering), the terms of the permutation of unlike spin is negligible in the summation of Eq. (1.30) after the integration is performed in the spin coordinates,

$$\langle\psi'|\hat{O}|\psi\rangle = {}_N C_{N_\alpha} \sum_{i=1}^{N_\alpha!}\sum_{j=1}^{N_\beta!}\sum_{k=1}^{N_\alpha!}\sum_{l=1}^{N_\beta!}(-1)^{p_i}(-1)^{p_j}(-1)^{p_k}(-1)^{p_l} \cdot\int d\mathbf{r}_1\cdots d\mathbf{r}_N \hat{P}_i\hat{P}_j\Phi'(\mathbf{r}_1,\mathbf{r}_2,\ldots,\mathbf{r}_N)\cdot\left(\hat{O}\hat{P}_k\hat{P}_l\Phi(\mathbf{r}_1,\mathbf{r}_2,\ldots,\mathbf{r}_N)\right) \tag{1.31}$$

where the permutation operators in Eq. (1.31) performs only the permutation of like spin. Therefore, if we write the wave function $\psi$ as,

$$\psi = A_\alpha(1,2,\ldots,N_\alpha)A_\beta(1,2,\ldots,N_\beta)\left(\Phi(\mathbf{r}_1,\mathbf{r}_2,\ldots,\mathbf{r}_N)\right) \tag{1.32}$$

the expectation values and matrix elements of the operator $O$ have same values (but multiplied constant ${}_N C_{N_\alpha}$) as Eq. (1.30) and Eq. (1.31) even though the wave function of Eq. (1.32) does not satisfy the Pauli principle and does not contain the spin part. Where $A_\alpha$ and $A_\beta$ are the anti-symmetrizer of $\alpha$ and $\beta$ electrons, respectively. The wave function of Eq. (1.32) becomes very simplified and it is also useful for the Monte Carlo calculation of many electron systems because not only the number of permutation operators is considerably decreased from Eq. (1.21) but also the spin part need not be considered explicitly.

### 3. The ICI method applied to a few-electron atoms

We applied the ICI method to two-to-five electron atomic systems from the helium to boron atoms. For the helium atom, some test calculations have been previously reported and, in this thesis, we show the results of the advanced calculations from the previous ones.[4,5] The calculations of the lithium, beryllium and boron atoms are first applications of the ICI method to many electron systems more than two electrons. Though we show the calculations of only spherically symmetric states, it is not difficult to calculate the states having spatial higher angular momentum. In this section, we derive the formulation and integrals necessary for calculating the helium atom and the general atomic systems more than two electrons. The results of the test calculations are summarized in Sec. 4.

### 3.1 Two-electron atom

Since the helium atom is a two-electron system, the number of independent variables is six. The simplest choice of the independent variables is using polar coordinates of each electron. However, for three-body systems (one nuclear and two electrons), three inter-particle coordinates $(r_1, r_2, r_{12})$ and Euler angles $(\alpha, \beta, \gamma)$ can become another choice with the range of the variables $(r_1, r_2, r_{12})$: $r_1 \geq 0, r_2 \geq 0, r_1 + r_2 \geq r_{12} \geq |r_1 - r_2|$, where $r_i$ is the distance between the electron $i$ and the nucleus and $r_{ij}$ is the distance between the two electrons and the volume element is $8\pi^2 r_1 r_2 r_{12}$. The ground state of the helium atom has a zero spatial angular momentum, – i.e., S state. Therefore, only inter-particle coordinates $(r_1, r_2, r_{12})$ without Euler angles can sufficiently express the wave function of the ground state. Since the calculations in this coordinates consist of the same argument for general many electron atoms in the polar coordinates, the formulation is discussed in the next subsection together with the general atomic systems. We also chose the following coordinates originally defined by Hylleraas with the volume element $8\pi^2(s^2 - t^2)u$,[9]

$$\begin{aligned} s &= r_1 + r_2 \\ t &= r_1 - r_2 \\ u &= r_{12} \end{aligned} \tag{1.33}$$

The Hamiltonian in the coordinates $(s,t,u)$ is written as

$$\begin{aligned} H = &-\left(\frac{\partial^2}{\partial s^2} + \frac{\partial^2}{\partial t^2} + \frac{\partial^2}{\partial u^2}\right) - 2\frac{s(u^2 - t^2)}{u(s^2 - t^2)}\frac{\partial^2}{\partial s \partial u} - 2\frac{t(s^2 - u^2)}{u(s^2 - t^2)}\frac{\partial^2}{\partial u \partial t} \\ &- \frac{4s}{s^2 - t^2}\frac{\partial}{\partial s} - \frac{2}{u}\frac{\partial}{\partial u} + \frac{4t}{s^2 - t^2}\frac{\partial}{\partial t} - \frac{4sZ}{s^2 - t^2} + \frac{1}{u} \end{aligned} \tag{1.34}$$

where the last two terms represent the Coulomb potential operators of the nuclear attraction $V_{Ne} = -4sZ/(s^2 - t^2)$ and electron repulsion $V_{ee} = 1/u$ with the nuclear charge $Z$ and the other terms represent the kinetic operator.

We want to apply the ICI method to the helium atom. For the ground state, the spin part is singlet (anti-symmetric), so the spatial part becomes symmetric. In the free ICI calculations, we have two freedoms: one is the $g$ function and the other is the initial function $\psi_0$. First, we tried the simplest choice of them,

$$g = \frac{u(s^2 - t^2)}{4sZ} \tag{1.35}$$

$$\psi_0 = \exp(-\alpha s) \tag{1.36}$$

where $\alpha$ is a non-linear variational parameter. This type $g$ function has inverse order of the potential functions $g = (V_{Ne}V_{ee})^{-1}$ to avoid nuclear and electron singularity problem.

Second choice of $g$ and $\psi_0$ is

$$g = 1 + \frac{s^2 - t^2}{4sZ} + u \tag{1.37}$$

$$\psi_0 = \exp(-\alpha s) \tag{1.38}$$

This $g$ function is a summation type of inverse order of the potential functions $g = 1 + 1/V_{Ne} + 1/V_{ee}$. In contrast, Eq. (1.35) is a production type. When we use a production type, the orders of $(s,t)$ and $u$ in the wave function increase one order at the same time as the one iteration proceeds. In contrast, when we use a summation type, the orders of $(s,t)$ and $u$ increase one order separately. Therefore, the independent functions are more widely generated by using the summation type $g$. Note that, when we use a summation type $g$ function, the free ICI process may generate diverging functions but they are eliminated since such functions are inappropriate for describing the wave function.

Next, to improve our variational results more, we tried the following type set,

$$g = 1 + \frac{s^2 - t^2}{4sZ} + u \tag{1.39}$$

$$\psi_0 = \left(1 + s^{1/2} + u^{1/2}\right)\exp(-\alpha s) \tag{1.40}$$

Thakkar and Koga introduced the functions include non-integer powers of $s,u$.[10] In our ICI method, when we introduce such functions in the initial function like Eq. (1.40), the ICI method automatically generates the functions of half-integer powers.

The present helium wave function generated by the ICI method is expressed as

$$\psi = \sum_{l,m,n} c_{lmn} s^l t^{2m} u^n \cdot \exp(-\alpha s) \tag{1.41}$$

where $c_{lmn}$ is a free ICI variational parameter. For the generated wave function from the set of Eq. (1.35) and Eq. (1.36), $l$ run both positive and negative integers and $m$ and $n$ run only positive integers. From the set of Eq. (1.37) and Eq. (1.38), in addition to the case of Eq. (1.35) and Eq. (1.36), $n$ run both positive and negative integers.

From the set of Eq. (1.39) and Eq. (1.40), in addition to the case of Eq. (1.37) and Eq. (1.38), $l$ and $n$ run half-integers.

To evaluate matrix elements, it is necessary to calculate the following integral,

$$I = \int_0^\infty ds \int_0^s du \int_0^u dt \cdot s^a u^b t^c \exp(-\alpha s) \tag{1.42}$$

where the ranges of indexes are $c \geq 0, b+c \geq 0, a+b+c \geq 0$. The integration of Eq. (1.42) is elementally evaluated as

$$\begin{aligned} I &= \int_0^\infty ds \int_0^s du \int_0^u dt \cdot s^a u^b t^c \exp(-\alpha s) \\ &= \frac{1}{c+1} \int_0^\infty ds \int_0^s du \cdot s^a u^{b+c+1} \exp(-\alpha s) \\ &= \frac{1}{(c+1)(b+c+2)} \int_0^\infty ds \cdot s^{a+b+c+2} \exp(-\alpha s) \\ &= \frac{1}{(c+1)(b+c+2)} \frac{\Gamma(a+b+c+3)}{\alpha^{a+b+c+3}} \end{aligned} \tag{1.43}$$

### 3.2 Many electron atoms

The Hamiltonian of the general atomic systems is written as

$$H = -\frac{1}{2}\sum_i \Delta_i - \sum_i \frac{Z}{r_i} + \sum_{i<j} \frac{1}{r_{ij}} \tag{1.44}$$

where $Z$ is the nuclear charge. The Hamiltonian commutes with the spin $\mathbf{S}$ and spatial angular momentums $\mathbf{L}$,

$$\left[H, S^2\right] = 0, \left[H, S^z\right] = 0, \left[H, L^2\right] = 0, \left[H, L^z\right] = 0 \tag{1.45}$$

We chose the general polar coordinates of each electron. In this coordinates, the eigenfunction of $L^2$ and $L^z$ is easily expressed by the spherical harmonics.

In the applications of our ICI method to the two-to-five electron atomic systems of the singlet and S symmetry states, we adopted the following simplest $g$ function,

$$g = 1 + \sum_i r_i + \sum_{i<j} r_{ij} \tag{1.46}$$

The initial functions we adopted were follows,

He: $\psi_0 = A\left(\exp(-\alpha_1 r_1) \cdot \exp(-\alpha_2 r_2) \cdot \chi_2\right)$ (1.47)

Li: $\psi_0 = A\left(\exp(-\alpha_1 r_1) \cdot \exp(-\alpha_2 r_2) \cdot (1 - r_3) \exp(-\alpha_3 r_3) \cdot \chi_3\right)$ (1.48)

Be: $\psi_0 = A\left(\exp(-\alpha_1 r_1)\cdot\exp(-\alpha_2 r_2)\cdot(1-r_3)\exp(-\alpha_3 r_3)\cdot(1-r_4)\exp(-\alpha_4 r_4)\cdot\chi_4\right)$ (1.49)

B: $$\psi_0 = A\left(\exp(-\alpha_1 r_1)\cdot\exp(-\alpha_2 r_2)\cdot(1-r_3)\exp(-\alpha_3 r_3)\cdot(1-r_4)\exp(-\alpha_4 r_4)\cdot\left(1-r_5-r_5^2\right)\exp(-\alpha_5 r_5)\cdot\chi_5\right) \quad (1.50)$$

where the term $(1-r_3)$ and $(1-r_4)$ express the node of 2s orbital and similarly $\left(1-r_5-r_5^2\right)$ expresses that of 3s orbital. For simplification, we used the restricted non-linear parameters $\alpha_1=\alpha_2$ and $\alpha_3=\alpha_4$. The spin functions we adopted were written as

He: $\chi_2 = \alpha\beta-\beta\alpha$ (1.51)

Li: $\chi_3 = (\alpha\beta-\beta\alpha)\alpha$ (1.52)

Be: $\chi_4 = (\alpha\beta-\beta\alpha)(\alpha\beta-\beta\alpha)$ (1.53)

B: $\chi_5 = (\alpha\beta-\beta\alpha)(\alpha\beta-\beta\alpha)\alpha$ (1.54)

The spin states are singlet, doublet, singlet and doublet for He, Li, Be and B, respectively.

The spatial part of the wave function generated by the free ICI method has the form,

$$\Psi = \sum_I c_I\left(\prod_i R_i(r_i)Y_{l_i}^{m_i}(\vartheta_i,\varphi_i)\cdot\prod_{i<j} f_{ij}(r_{ij})\right) = \sum_I c_I\phi \quad (1.55)$$

For convenience, we derive the operation of the Laplacian to Eq. (1.55),

$$\nabla_i^2\phi = \left(\nabla_i^2 R_i(r_i)Y_{l_i}^{m_i}(\vartheta_i,\varphi_i)\right)\cdot\prod_{j\neq i}R_j(r_j)Y_{l_j}^{m_j}(\vartheta_j,\varphi_j)\cdot\prod_{j<k}f_{jk}(r_{jk})$$

$$+\prod_j R_j(r_j)Y_{l_j}^{m_j}(\vartheta_j,\varphi_j)\cdot\left\{\sum_{j<i}\left(\nabla_i^2 f_{ji}(r_{ji})\prod_{\substack{k<l\\(k\neq j,l\neq i)}}f_{kl}(r_{kl})\right)+\sum_{j>i}\left(\nabla_i^2 f_{ij}(r_{ij})\prod_{\substack{k<l\\(k\neq i,l\neq j)}}f_{kl}(r_{kl})\right)\right\}$$

$$+2\prod_{j\neq i}R_j(r_j)\cdot\prod_j Y_{l_j}^{m_j}(\vartheta_j,\varphi_j)\cdot\left\{\sum_{j<i}\left(\nabla_i R_i(r_i)\cdot\nabla_i f_{ji}(r_{ji})\prod_{\substack{k<l\\(k\neq j,l\neq i)}}f_{kl}(r_{kl})\right)\right.$$

$$\left.+\sum_{j>i}\left(\nabla_i R_i(r_i)\cdot\nabla_i f_{ij}(r_{ij})\prod_{\substack{k<l\\(k\neq i,l\neq j)}}f_{kl}(r_{kl})\right)\right\}$$

$$+2\prod_j R_j(r_j)\cdot\prod_{j\neq i}Y_{l_j}^{m_j}(\vartheta_j,\varphi_j)\cdot\left\{\sum_{j<i}\left(\nabla_i Y_{l_i}^{m_i}(\vartheta_i,\varphi_i)\cdot\nabla_i f_{ji}(r_{ji})\prod_{\substack{k<l\\(k\neq j,l\neq i)}}f_{kl}(r_{kl})\right)\right.$$

$$\left.+\sum_{j>i}\left(\nabla_i Y_{l_i}^{m_i}(\vartheta_i,\varphi_i)\cdot\nabla_i f_{ij}(r_{ij})\prod_{\substack{k<l\\(k\neq i,l\neq j)}}f_{kl}(r_{kl})\right)\right\}$$

$$+2\prod_j R_j(r_j)Y_{l_j}^{m_j}(\vartheta_j,\varphi_j)\cdot\left\{\sum_{j<i}\left(\nabla_i f_{ji}(r_{ji})\cdot\left(\sum_{k>j,k<i}\nabla_i f_{ki}(r_{ki})\prod_{\substack{l<m\\(lm\neq ji,ki)}}f_{lm}(r_{lm})\right.\right.\right.$$

$$\left.\left.\left.+\sum_{k>j,k>i}\nabla_i f_{ik}(r_{ik})\prod_{\substack{l<m\\(lm\neq ji,ki)}}f_{lm}(r_{lm})\right)\right)\right. \tag{1.56}$$

$$\left.+\sum_{j<i}\left(\nabla_i f_{ji}(r_{ji})\cdot\sum_{k>j}\nabla_i f_{ik}(r_{ik})\prod_{\substack{l<m\\(lm\neq ij,ik)}}f_{lm}(r_{lm})\right)\right\}$$

The Laplacian is written by the polar coordinate as

$$\begin{aligned}\nabla^2&=\frac{1}{r^2}\frac{\partial}{\partial r}\left(r^2\frac{\partial}{\partial r}\right)+\frac{1}{r^2}\left\{\frac{1}{\sin\vartheta}\frac{\partial}{\partial\vartheta}\left(\sin\vartheta\frac{\partial}{\partial\vartheta}\right)+\frac{1}{\sin^2\vartheta}\frac{\partial^2}{\partial\varphi^2}\right\}\\&=\xi^2-\frac{L^2}{r^2}\end{aligned} \tag{1.57}$$

where $\xi^2$ operates $r$ and $\mathbf{L}$ is the spatial angular momentum who operates the angular coordinates $\vartheta$ and $\varphi$,

$$\xi^2=\frac{1}{r^2}\frac{\partial}{\partial r}\left(r^2\frac{\partial}{\partial r}\right) \tag{1.58}$$

$$L^2=\frac{1}{\sin\vartheta}\frac{\partial}{\partial\vartheta}\left(\sin\vartheta\frac{\partial}{\partial\vartheta}\right)+\frac{1}{\sin^2\vartheta}\frac{\partial^2}{\partial\varphi^2} \tag{1.59}$$

The spherical harmonic becomes a simultaneous eigenfunction of $L^2$ and $L^z$. We derive some useful relations of the spherical harmonics for convenience,

$$\cos\theta\cdot Y_l^m(\vartheta,\varphi)=\sqrt{\frac{(l+m)(l-m)}{(2l+1)(2l-1)}}Y_{l-1}^m(\vartheta,\varphi)+\sqrt{\frac{(l-m+1)(l+m+1)}{(2l+1)(2l+3)}}Y_{l+1}^m(\vartheta,\varphi)$$

$$\sin\vartheta e^{i\varphi}\cdot Y_l^m(\vartheta,\varphi)=\sqrt{\frac{(l+m+1)(l+m+2)}{(2l+1)(2l+3)}}Y_{l+1}^{m+1}(\vartheta,\varphi)-\sqrt{\frac{(l-m-1)(l-m)}{(2l-1)(2l+1)}}Y_{l-1}^{m+1}(\vartheta,\varphi)$$

$$\sin\vartheta e^{-i\varphi}\cdot Y_l^m(\vartheta,\varphi)=\sqrt{\frac{(l+m-1)(l+m)}{(2l-1)(2l+1)}}Y_{l-1}^{m-1}(\vartheta,\varphi)-\sqrt{\frac{(l-m+1)(l-m+2)}{(2l+1)(2l+3)}}Y_{l+1}^{m-1}(\vartheta,\varphi)$$

$$L^2Y_l^m(\vartheta,\varphi)=l(l+1)Y_l^m(\vartheta,\varphi)$$

$$L^zY_l^m(\vartheta,\varphi)=mY_l^m(\vartheta,\varphi)$$

$$L^{\pm}Y_l^m(\vartheta,\varphi)=\sqrt{(l\mp m)(l\pm m+1)}Y_l^{m\pm1}(\vartheta,\varphi) \tag{1.60}$$

The first term of Eq. (1.56) is calculated as

$$\nabla_i^2R_i(r_i)Y_{l_i}^{m_i}(\vartheta_i,\varphi_i)=Y_{l_i}^{m_i}(\vartheta_i,\varphi_i)\left(\xi_i^2R_i(r_i)\right)-\frac{R_i(r_i)}{r_i^2}\left(L_i^2Y_{l_i}^{m_i}(\vartheta_i,\varphi_i)\right) \tag{1.61}$$

The right hand side of Eq. (1.61) is easily calculated by using Eq. (1.60). The evaluation of the second term of Eq. (1.56) is also easy as

$$\nabla_i^2f_{ij}(r_{ij})=\frac{d^2f_{ij}}{dr_{ij}^2}+\frac{2}{r_{ij}}\frac{df_{ij}}{dr_{ij}} \tag{1.62}$$

The third term of Eq. (1.56) includes the inner product of the gradient operators. This is evaluated as

$$\nabla_iR_i(r_i)\cdot\nabla_if_{ij}(r_{ij})=\frac{dR_i}{dr_i}\frac{df_{ij}}{dr_{ij}}\left(\hat{\mathbf{r}}_i\cdot\hat{\mathbf{r}}_{ij}\right)=\frac{dR_i}{dr_i}\frac{df_{ij}}{dr_{ij}}\frac{r_i^2+r_{ij}^2-r_j^2}{2r_ir_{ij}} \tag{1.63}$$

The fourth term of Eq. (1.56) also includes the inner product of the gradient operators. The operation of the gradient operator to the spherical harmonic is not obvious but the following equations are available,

$$\nabla_iY_{l_i}^{m_i}(\vartheta_i,\varphi_i)\cdot\nabla_if_{ij}(r_{ij})=\frac{1}{r_{ij}}\frac{df_{ij}}{dr_{ij}}\frac{r_j}{r_i}\left(\mathbf{L}_iY_{l_i}^{m_i}(\vartheta_i,\varphi_i)\right)\cdot\hat{\mathbf{r}}_j \tag{1.64}$$

$$\left(\mathbf{L}_iY_{l_i}^{m_i}(\vartheta_i,\varphi_i)\right)\cdot\hat{\mathbf{r}}_j=\frac{1}{2}L_i^+Y_{l_i}^{m_i}\cdot\sin\vartheta_je^{i\varphi_j}+\frac{1}{2}L_i^-Y_{l_i}^{m_i}\cdot\sin\vartheta_je^{i\varphi_j}+L_i^zY_{l_i}^{m_i}\cdot\cos\vartheta_j \tag{1.65}$$

The fifth term of Eq. (1.56) is evaluated as

$$\nabla_if_{ij}(r_{ij})\cdot\nabla_if_{ik}(r_{ik})=\frac{df_{ij}}{dr_{ij}}\frac{df_{ik}}{dr_{ik}}\left(\hat{\mathbf{r}}_{ij}\cdot\hat{\mathbf{r}}_{ik}\right)=\frac{df_{ij}}{dr_{ij}}\frac{df_{ik}}{dr_{ik}}\frac{r_{ij}^2+r_{ik}^2-r_{jk}^2}{2r_{ij}r_{ik}} \tag{1.66}$$

Thus, we derived the evaluations of all terms of Eq. (1.56). The formulation is quite general. For the atomic systems, although the angular parts are almost restricted by the spatial angular momentum operators, various choices are possible for the radial $R(r_i)$ and correlated parts $f(r_{ij})$. In the ICI formalism, the $g$ and initial functions

determine the function forms of $R(r_i)$ and $f(r_{ij})$. In this thesis, although we only select the simplest one given by Eq. (1.46) to Eq. (1.50), another choice may give good performance. For example, $g = r/(r+a)$ is one choice with $a$ being constant. But, this choice gives the difficult functions to evaluate integrals. To overcome the difficulty of integration, the Monte Carlo strategy is useful.[11]

When we use the $g$ and initial functions given by Eq. (1.46) to Eq. (1.50), the integral form to evaluate matrix elements is expressed as

$$I = \int \prod_i r_i^{\nu_i} \exp(-\alpha_i r_i) \cdot \prod_i Y_{l_i}^{m_i}(\vartheta_i, \varphi_i) \cdot \prod_{i<j} r_{ij}^{\nu_{ij}} \cdot \prod_i d\mathbf{r}_i \tag{1.67}$$

where the index $\nu_i$ and $\nu_{ij}$ run the integer values with $\nu_i \geq -1$ and $\nu_{ij} \geq -1$. For $N$ electron systems, the $N$-electron integrals are appeared in the ICI method. This is very difficult to calculate in the analytical form. The simple and popular way to calculate the integrals of Eq. (1.67) is using the Perkins method based on the Sack expansion.[12,13] These integration methods have been studied by several authors for three- and four-electron atomic systems.[13-17] The Perkins expansion is written as

$$r_{ij}^{\nu_{ij}} = \sum_{q_{ij}=0}^{L_{ij}^1} P_{q_{ij}}(\cos\vartheta_{ij}) \sum_{k_{ij}=0}^{L_{ij}^2} c_{\nu_{ij},q_{ij},k_{ij}} r_{<ij}^{\,q_{ij}+2k_{ij}} r_{>ij}^{\,\nu_{ij}-q_{ij}-2k_{ij}} \tag{1.68}$$

where, for even values of $\nu_{ij}$ : $L_{ij}^{\,1} = 1/2 \cdot \nu_{ij}$, $L_{ij}^{\,2} = 1/2 \cdot \nu_{ij} - q_{ij}$, for odd values of $\nu_{ij}$ : $L_{ij}^{\,1} = \infty$, $L_{ij}^{\,2} = 1/2 \cdot (\nu_{ij}+1)$ and $r_{<ij} = \min(r_i, r_j)$ and $r_{>ij} = \max(r_i, r_j)$. $P_q(x)$ is the Legendre polynomial. The coefficient $c_{\nu_{ij},q_{ij},k_{ij}}$ is given by

$$c_{\nu_{ij},q_{ij},k_{ij}} = \frac{2q_{ij}+1}{\nu_{ij}+2} \cdot {}_{\nu_{ij}+2}C_{2k_{ij}+1} \cdot \prod_{t=0}^{\min(q_{ij}-1,\frac{1}{2}(\nu_{ij}+1))} \frac{2k_{ij}+2t-\nu_{ij}}{2k_{ij}+2q_{ij}-2t+1} \tag{1.69}$$

Eq. (1.68) is substituted for Eq. (1.67) and we get

$$\begin{aligned} I = \int \prod_i d\mathbf{r}_i \cdot \sum_{q_{12}=0}^{L_{12}^1} \sum \cdots \sum_{q_{N-1,N}=0}^{L_{N-1,N}^1} P_{q_{12}}(\cos\vartheta_{12}) \cdots P_{q_{N-1,N}}(\cos\vartheta_{N-1,N}) \cdot \prod_i Y_{l_i}^{m_i}(\vartheta_i, \varphi_i) \\ \cdot \sum_{k_{12}=0}^{L_{12}^2} \sum \cdots \sum_{k_{N-1,N}=0}^{L_{N-1,N}^2} \frac{r_{<12}^{\,q_{12}+2k_{12}}}{r_{>12}^{\,q_{12}+2k_{12}-\nu_{12}}} \cdots \frac{r_{<N-1,N}^{\,q_{N-1,N}+2k_{N-1,N}}}{r_{>12}^{\,q_{N-1,N}+2k_{N-1,N}-\nu_{N-1,N}}} \cdot \prod_i r_i^{\nu_i} \exp(-\alpha_i r_i) \end{aligned} \tag{1.70}$$

The Legendre polynomial is expanded by the spherical harmonics as

$$P_{q_{ij}}(\cos\vartheta_{ij}) = \frac{4\pi}{2q_{ij}+1} \sum_{m_{ij}=-q_{ij}}^{q_{ij}} Y_{q_{ij}}^{m_{ij}*}(\vartheta_i, \varphi_i) Y_{q_{ij}}^{m_{ij}}(\vartheta_j, \varphi_j) \tag{1.71}$$

Substitute Eq. (1.71) for Eq. (1.70) and we can separate the integral to the angular and

radial integrations,

$$I = \sum_{q_{12}=0}^{L_{12}^{1}} \sum \cdots \sum_{q_{N-1,N}=0}^{L_{N-1,N}^{1}} \prod_{i<j} \frac{4\pi}{2q_{ij}+1}$$
$$\cdot \sum_{m_{12}=-q_{12}}^{q_{12}} \sum \cdots \sum_{m_{N-1,N}=-q_{N-1,N}}^{q_{N-1,N}} \int_0^{\pi}\int_0^{2\pi} Y(\vartheta_1,\varphi_1)\cdots d\vartheta_1 d\varphi_1 \cdots \int_0^{\pi}\int_0^{2\pi} Y(\vartheta_N,\varphi_N)\cdots d\vartheta_N d\varphi_N$$
$$\cdot \sum_{k_{12}=0}^{L_{12}^{2}} \sum \cdots \sum_{k_{N-1,N}=0}^{L_{N-1,N}^{2}} \int_0^{\infty} dr_1 \cdots \int_0^{\infty} dr_N \cdot \frac{r_{<12}^{\,q_{12}+2k_{12}}}{r_{>12}^{\,q_{12}+2k_{12}-\nu_{12}}} \cdots \frac{r_{<N-1,N}^{\,q_{N-1,N}+2k_{N-1,N}}}{r_{>12}^{\,q_{N-1,N}+2k_{N-1,N}-\nu_{N-1,N}}} \cdot \prod_i r_i^{\nu_i+2} \exp(-\alpha_i r_i)$$

(1.72)

In the angular part, by Edmonds book,[7] a product of the spherical harmonics is written by using the Wigner 3j-symbols and is reduced to a summation of the single spherical harmonic,

$$Y_{l_a}^{m_a*}(\vartheta_i,\varphi_i) Y_{l_b}^{m_b}(\vartheta_i,\varphi_i)$$
$$= (-1)^{m_a} \sum_{l=|l_a-l_b|}^{l_a+l_b} \left\{ \frac{(2l_a+1)(2l_b+1)(2l+1)}{4\pi} \right\}^{1/2} \begin{pmatrix} l_a & l_b & l \\ 0 & 0 & 0 \end{pmatrix} \begin{pmatrix} l_a & l_b & l \\ -m_a & m_b & -m \end{pmatrix} Y_l^m(\vartheta_1,\varphi_1)$$

(1.73)

By Eq. (1.73), the angular part is easily calculated. The radial part of the integration is expressed as a linear combination of the following integration,

$$I_R = \int_0^{\infty} dr_1 \int_0^{r_1} dr_2 \cdots \int_0^{r_{N-1}} dr_N \cdot \prod_i r_i^{n_i} \exp(-\alpha_i r_i) \qquad (1.74)$$

The integration of $I_R$ is complicated but various authors derive the recursion formula and the formulation for the direct evaluation.[14-17] The Ref. 17 is useful.[17]

In this procedure, for many electron systems, we must calculate quite large number of terms appeared in Eq. (1.72). Especially, when the index $\nu_{ij}$ is odd number, the Perkins expansion becomes infinity series. The Levin's u transformation procedure is useful to accelerate the convergence speed.[18] For three-electron atoms, Hill and several authors suggested how to evaluate atomic integrals by the closed form.[19] This method is useful because we need not worry about discontinuity of infinite loop. However, for more than three-electron atoms, such closed form has not been found yet. We must study analytical integration methods for many electron systems or the Monte Carlo strategy becomes a substitute for analytical evaluations of many-electron integrals.

**Table I.** Free ICI calculation for the helium atom with $g$ and $\psi_0$ given in Eq. (1.35) and Eq. (1.36).

| n[a] | M[b] | $\alpha$ [c] | Energy (a.u.) |
|---|---|---|---|
| 0 | 1 | 1.688 | **-2.**84 765 624 500 |
| 1 | 6 | 1.673 | **-2.90** 157 701 247 |
| 2 | 26 | 1.880 | **-2.90 37**0 867 501 |
| 3 | 74 | 2.033 | **-2.90 372 3**90 061 |
| 4 | 159 | 2.200 | **-2.90 372 43**4 707 |
| 5 | 291 | 2.331 | **-2.90 372 437** 274 |
| 6 | 481 | 2.450 | **-2.90 372 437** 636 |
| 7 | 738 | 2.680 | **-2.90 372 437 6**83 |
| Ref. 24[d] | 10257 | | -2.90 372 437 703 411 959 831 1 |

a Iteration number.

b Number of the independent functions.

c Non-linear parameter.

d Hylleraas type including the logarithm term.

## 4. Results

### 4.1 Helium

Our first application of the present method is the helium atom. Helium is the simplest atom which the exact solution is unknown. However, there were a lot of calculations with various types of functions and the solutions could be achieved very high precision.[9,10,20-25] Therefore, the energy calculation of the helium atom is often used as a rather benchmark calculation. We also use helium as a test calculation how our ICI method can reach to the exact solution in finite iterations. The coordinates and the Hamiltonian were already discussed in the previous section. We have to determine the $g$ and initial functions $\psi_0$ in the ICI method.

First, we tried the functions given by Eq. (1.35) and Eq. (1.36), whose $g$ function was a production type. Table I shows the results of the free ICI energy. The non-linear parameter $\alpha$ was optimized by the Newton-Raphson method. As shown in Table I, at the iteration 4, the energy was correct to micro-hartree order and, at the iteration 7, the energy was achieved nano-hartree accuracy. Clearly, by continuing the iteration, we can achieve any accuracy results. This combination of $g$ and $\psi_0$ automatically generates the wave functions close to the Kinoshita type.[20] But, the ICI and Kinoshita type functions are slightly different each other. Though the Kinoshita type functions include negative powers of $u$, but the functions generated from Eq. (1.35) and Eq. (1.36) do not appear such negative powers.

**Table II.** Free ICI calculation for the helium atom with $g$ and $\psi_0$ given in Eq. (1.37) and Eq. (1.38).

| n[a] | M[b] | $\alpha$ [c] | Energy (a.u.) |
|---|---|---|---|
| 0 | 1 | 1.688 | **-2.**84 765 625 000 |
| 1 | 5 | 1.701 | **-2.90** 143 777 880 |
| 2 | 23 | 1.732 | **-2.90 36**6 045 230 |
| 3 | 59 | 1.776 | **-2.90 372** 108 471 |
| 4 | 121 | 1.836 | **-2.90 372 4**04 918 |
| 5 | 216 | 1.920 | **-2.90 372 43**2 447 |
| Ref. 24[d] | 10257 | | -2.90 372 437 703 411 959 831 1 |

a Iteration number.

b Number of the independent functions.

c Non-linear parameter.

d Hylleraas type including the logarithm term.

Second, we chose $g$ and $\psi_0$ given by Eq. (1.37) and Eq. (1.38), whose $g$ was a summation type. In this choice, the generated functions are very closer to the Kinoshita type. Table II shows the results. Compared the results given in Table I and II, at the iteration 4 in Table I, the energy was -2.90 372 434 with the dimension 159 and, at the iteration 5 in Table II, the energy was -2.90 372 432 with the dimension 216. The former is slightly better than the latter from the variational point of view. However, this is a rare case in our calculations. As discussed in Sec. 3, the generated functions by using the summation type $g$ function cover the wider range of the functional space than by the production type. The functions generated by Eq. (1.37) and Eq. (1.38) contain the functions generated by Eq. (1.35) and Eq. (1.36) by continuing the iteration.

Next, we chose $g$ and $\psi_0$ given by Eq. (1.46) and Eq. (1.47) expressed in the polar coordinates $(r_1, r_2, r_{12})$ with the spin function of Eq. (1.51). In Eq. (1.47), after the operation of the anti-symmetrizer, the spatial and spin parts are separated each other. Table III summarizes the results. Compared to the results in Table I and Table III, at the iteration 6 in Table I, the energy was -2.90 372 437 636 with the dimension 481, at the iteration 14 in Table III, the energy was -2.90 372 437 656 with the dimension 372. The behavior of the energy convergence of Table III related to the dimension of the free ICI is slightly better than that of Table I although the iteration number is large in Table III. It indicates that using the $g$ function given by Eq. (1.46) and using the polar coordinates are not so worse choice even though the $g$ function is not exactly inverse function of the potential.

**Table III.** Free ICI calculation for the helium atom with $g$ and $\psi_0$ given in Eq. (1.46) and Eq. (1.47).

| n[a] | M[b] | $\alpha$ [c] | Energy (a.u.) |
|---|---|---|---|
| 0 | 1 | 1.687 | **-2.84** 765 625 000 |
| 1 | 3 | 1.812 | **-2.89** 123 235 194 |
| 2 | 7 | 1.814 | **-2.90 3**42 585 480 |
| 3 | 13 | 1.906 | **-2.90 3**64 047 050 |
| 4 | 22 | 2.038 | **-2.90 37**1 394 501 |
| 5 | 34 | 2.112 | **-2.90 372** 096 780 |
| 6 | 50 | 2.235 | **-2.90 372 3**70 190 |
| 7 | 70 | 2.309 | **-2.90 372 4**10 501 |
| 8 | 95 | 2.426 | **-2.90 372 43**0 538 |
| 9 | 125 | 2.502 | **-2.90 372 43**4 387 |
| 10 | 161 | 2.614 | **-2.90 372 436** 643 |
| 11 | 203 | 2.688 | **-2.90 372 437** 161 |
| 12 | 252 | 2.801 | **-2.90 372 437** 503 |
| 13 | 308 | 2.861 | **-2.90 372 437** 592 |
| 14 | 372 | 2.941 | **-2.90 372 437 6**56 |
| Ref. 24[d] | 10257 | | -2.90 372 437 703 411 959 831 1 |

a Iteration number.

b Number of the independent functions.

c Non-linear parameter.

d Hylleraas type including the logarithm term.

Finally, to improve our variational results more, we tried $g$ and $\psi_0$ given by Eq. (1.39) and Eq. (1.40). This choice automatically generates the wave functions close to the Thakkar-Koga type.[10] Table IV summarizes the results. We performed the free ICI calculations until large iteration number with very high dimension (until the iteration is 10 and the dimension is 4358). So, we could achieve the energy of very high precision, which reached 20 digits: -2.90 372 437 703 411 959 830 7. It means that our ICI method can be calculated to any precision of accuracy by increasing iterations. However, some authors reported on the results of higher precision than those of us.[23-25] These level of accuracy is significant only as a bench mark calculation and it is no physically significant because the relativistic effect already appears in 4 or 5 digits according to the solution of the relativistic Dirac-Coulomb equation[26] and QED and/or mass polarization effect also appear less than 20 digits.[27]

When we choose any other set of $g$ and $\psi_0$, the ICI method can generate various type functions. For example, the Hylleraas type is expanded by using the set,[9]

**Table IV.** Free ICI calculation for the helium atom with $g$ and $\psi_0$ given in Eq. (1.39) and Eq. (1.40).

| n[a] | M[b] | $\alpha$ [c] | Energy (a.u.) |
|---|---|---|---|
| 0 | 3 | 1.653 | **-2.89** 046 871 962 722 |
| 1 | 18 | 1.658 | **-2.90 37**1 133 601 506 |
| 2 | 74 | 1.630 | **-2.90 372 43**4 035 477 |
| 3 | 186 | 1.593 | **-2.90 372 437 6**97 816 |
| 4 | 377 | 1.641 | **-2.90 372 437 703** 322 433 148 |
| 5 | 668 | 1.688 | **-2.90 372 437 703 410** 779 431 |
| 6 | 1080 | 1.736 | **-2.90 372 437 703 411** 931 551 |
| 7 | 1634 | 1.784 | **-2.90 372 437 703 411 958** 735 |
| 8 | 2351 | 1.831 | **-2.90 372 437 703 411 959** 772 |
| 9 | 3252 | 1.880 | **-2.90 372 437 703 411 959 826** 8 |
| 10 | 4358 | 1.927 | **-2.90 372 437 703 411 959 830** 7 |
| Ref. 24[d] | 10257 | | -2.90 372 437 703 411 959 831 1 |

a Iteration number.

b Number of the independent functions.

c Non-linear parameter.

d Hylleraas type including the logarithm term.

$$g = 1 + \left(s^2 - t^2\right) + u \tag{1.75}$$

$$\psi_0 = \exp(-\alpha s) \tag{1.76}$$

If you want to include logarithm singularity based on the three particle cusp condition,[25] you only have to include the logarithm functions in the $g$ and/or initial functions. Examinations of another choice of $g$ and $\psi_0$ will be given elsewhere.

### 4.2 Lithium, Beryllium and Boron

Lithium is the first atom more than two electrons and spin coordinates must be treated explicitly. However, the precision attainable is very high (cannot compete that of helium). Therefore, as well as helium, the lithium atom is one of test system for verifying theories.[28-30] The lithium atom is important not only as a benchmark but also as having some interesting physical properties: hyperfine spectra, magnetic properties, Lamb shift, relativistic effects, QED effects and so on. The coordinates and Hamiltonian were already discussed in the previous section. In the ICI calculation, the $g$ function is given by Eq. (1.46) and the initial function $\psi_0$ is given by Eq. (1.48) with the spin eigenfunction of Eq. (1.52). In this initial function, the electrons 1 and 2 have singlet

**Table V.** Free ICI energies for the lithium atom with $g$ and $\psi_0$ given in Eq. (1.46) and Eq. (1.48).

| n[a] | M[b] | $\alpha_1 = \alpha_2$, $\alpha_3$ [c] | Energy (a.u.) |
|---|---|---|---|
| 0 | 2 | 2.69, 0.691 | **-7.41** 918 357 |
| 1 | 9 | 2.85, 0.676 | **-7.46** 619 235 |
| 2 | 31 | 2.93, 0.695 | **-7.47 7**60 268 |
| 3 | 82 | 3.08, 0.698 | **-7.47 7**95 920 |
| 4 | 190 | 3.25, 0.755 | **-7.47 80**4 315 |
| 5 | 392 | 3.30, 0.746 | **-7.47 805** 552 |
| 6 | 748 | 3.42, 0.764 | **-7.47 805** 914 |
| 7 | 1334 | 3.54, 0.782 | **-7.47 805** 996 |
| 8 | 2260 | 3.66, 0.800 | **-7.47 806 0**20 |
| 9 | 3661 | 3.78, 0.818 | **-7.47 806 028** |
| Ref. 30[d] | 3502 | | -7.47 806 032 |

a Iteration number.

b Number of the independent functions.

c Non-linear parameters.

d Hylleraas type.

**Table VI.** The expectation values of the delta function and Fermi contact term by the Free ICI calculation for the lithium atom with $g$ and $\psi_0$ given in Eq. (1.46) and Eq. (1.48).

| n[a] | M[b] | Delta function | Fermi contact |
|---|---|---|---|
| 0 | 2 | 12.5063 | 1.54272 |
| 1 | 9 | 13.1186 | 2.13518 |
| 2 | 31 | 13.8466 | 2.97295 |
| 3 | 82 | 13.8212 | 2.93671 |
| 4 | 190 | 13.8423 | 2.91211 |
| 5 | 392 | 13.839 | 2.9065 |
| 6 | 748 | 13.8416 | 2.90954 |
| 7 | 1334 | 13.8416 | 2.90828 |
| Ref. 30[c] | 3502 | 13.8425 | 2.90598 |

a Iteration number.

b Number of the independent functions.

c Hylleraas type.

coupling nature each other and the electron 3 is occupied 2s orbital. The spin state is doublet. The non-linear parameters were optimized by the Newton-Raphson method. Table V shows the free ICI energies. Our results exceeded micro-hartree accuracy at the iteration 9 with the dimension 3661. Yan et al. showed very good results by using the Hylleraas type functions,[30] they achieved pico-hartree accuracy. The Hylleraas type

**Table VII.** Free ICI calculation for the beryllium atom with $\psi_0$ and $g$ given in Eq. (1.46) and Eq. (1.49).

| n[a] | M[b] | $\alpha_1 = \alpha_2$, $\alpha_3 = \alpha_4$ [c] | Energy (a.u.) |
|---|---|---|---|
| 0 | 3 | 3.70, 1.00 | **-14.5** 599 4 |
| 1 | 18 | 3.70, 1.00 | **-14.6** 491 2 |
| 2 | 82 | 3.90, 1.10 | **-14.6 654** 6 |
| 3 | 290 | 4.00, 1.00 | **-14.6 672** 0 |
| 4 | 885 | 4.10, 1.10 | **-14.6 673** 0 |
| Ref. 32[d] | 3700 | | -14.6 673 5 |

a Iteration number.

b Number of the independent functions.

c Non-linear parameters.

d ECG type.

functions they used are similar to our ICI functions generated by using the set of Eq. (1.46) and Eq. (1.48). However, they used the many unrestricted type non-linear parameters. At least, our ICI method indicated good performance converging to the exact wave function even for three-electron system. We calculated other properties of the expectation values of the delta function and the Fermi contact term except the energies. The results are shown in Table VI. These values also converge to the reference values.[30] The studies for the physically interesting properties like relativistic effects, hyperfine spectra and magnetic properties will be appeared elsewhere.

The beryllium atom has four electrons with the ground state $1s^2 2s^2$ ($^1S_0$). In molecular orbital theories, near degeneracy problem is sometimes discussed since the orbital 2s and 2p locate near region and the configurations $1s^2 2s^2$ and $1s^2 2s^2$ are almost degenerate. However, in our ICI method, this problem does not occur because the correlated term $r_{ij}$ is explicitly appeared in the wave function. We chose the $g$ and $\psi_0$ as well as the case of the lithium atom, given in Eq. (1.46) and Eq. (1.49). The spin function is given by Eq. (1.53), in which the electrons 1 and 2 are coupled as singlet and the electrons 3 and 4 also have singlet coupling nature. The total spin state is singlet. Table VII summarizes the results. Our results exceeded milli-hartree accuracy at the iteration 4 with the dimension 885. The references were calculated by using the explicitly correlated Gaussian functions (ECG) with large number of parameters (3700 term) and the Hylleraas-CI procedure with large number of linear independent functions.[31,32] The ECG method is a very powerful tool to get variationally good results since integration (even three and four electron integrations) is not so difficult, but the optimization

**Table VIII.** Free ICI calculation for the boron atom ($^2$S Excited state) with $\psi_0$ and $g$ given in Eq. (1.46) and Eq. (1.50).

| n[a] | M[b] | $\alpha_1 = \alpha_2$, $\alpha_3 = \alpha_4$, $\alpha_5$ [c] | Energy (a.u.) |
|---|---|---|---|
| 0 | 9 | 5.00, 1.20, 0.20 | **-24.**2 036 |
| 1 | 78 | 5.00, 1.20, 0.20 | **-24.4** 330 |
| 2 | 484 | 5.00, 1.20, 0.20 | **-24.4 628** |
| Ref. 33[d] | 4997 | | -24.4 698 |

a Iteration number.

b Number of the independent functions.

c Non-linear parameters.

d MCHF type.

of very large number of non-linear parameters is difficult in general. In our ICI method, although a few non-linear parameters are included in the wave function, basically variational parameters are linear hence simple. However, the ECG method has already achieved micro-hartree accuracy. We are advancing our calculations to gain more accurate results.

The boron atom is a five-electron atom with the ground state $1s^2 2s^2 2p^2$ ($^2P_{1/2}$) but we focused the lowest spherically symmetric state $1s^2 2s^2 3s^2$ ($^2S_{1/2}$). Several theoretical studies are found but the level of accuracy is lower, compared to the lithium and beryllium atoms.[33] For the boron atom, very high accurate calculations are too difficult because the boron has five electrons correlated each other. In our ICI , we chose the $g$ and $\psi_0$ given by Eq. (1.46) and Eq. (1.50) as well as the cases of the lithium and beryllium atoms. The spin function is given by Eq. (1.54), the electron 5 is attached to the beryllium atomic shell and occupies 3s orbital. Table VIII shows the result. The reference calculation was performed by MCHF calculation with very large number of configurations.[33] Our result reached the reference value but could not achieve milli-hartree accuracy yet. The time consuming step is the integration part of many electron correlated terms, as discussed in Sec. 3. The integration method we adopted was straightforward, which was based on the expansion of the correlated term $r_{ij}$.[12] Therefore, for many electron systems, the summations from the expansions become enormous and exponentially increasing. Though many electron integrals have been studied by various researches all over the world, the wonderful results are not found yet. The Monte Carlo method is another choice, which is a powerful tool for many electron integrals although contains statistical error.[11] We have already applied the Monte Carlo strategy to our method and obtained some good results for many electron systems.

## 5. Conclusion

In this chapter, the theories of the ICI method were formulated for many electron systems more than two electrons and some necessary and useful formulas were derived especially for the spin-free Hamiltonian from using the symmetries. And as test calculations, we applied our method to two-to-five electron atoms from the helium to boron atoms.

For many electron systems, the spatial and spin part of wave function cannot be separated each other on satisfied the Pauli principle. The ICI wave function is generated by the totally symmetric operators: the Hamiltonian $H$ and $g$ function, therefore, the permutation symmetries, angular momentums and the other quantum symmetries are unchanged from the initial function $\psi_0$. Therefore, the generation of the ICI wave function can be performed outside from the projection operators of the symmetries. This simplifies the application of the ICI method to many electron systems especially for the spin-free Hamiltonian.

For the application to the helium atom, we achieved the energy having very high precision. It means that our ICI method can be calculated to any precision of accuracy by increasing iterations. Moreover, by the combination of $g$ and $\psi_0$, various types of functions can be generated automatically. For example, the Hylleraas type corresponds to choosing:[9] $g = u\left(s^2 - t^2\right)$ and $\psi_0 = \exp(-\alpha s)$ and, the Kinoshita type:[20] $g = 1 + \left(s^2 - t^2\right)/s + u$ and $\psi_0 = \exp(-\alpha s)$ and, the Thakkar-Koga type:[10] $g = 1 + \left(s^2 - t^2\right)/s + u$ and $\psi_0 = \left(1 + s^{1/2} + u^{1/2}\right)\exp(-\alpha s)$. The best choice of this combination will be discussed elsewhere.

For the lithium, beryllium and boron atoms, these are first applications of the ICI method to many electron systems more than two electrons. Even for many electron systems, the ICI method generated the wave functions converging to the exact ones. For many electron systems, the most difficult problem is in the integration part. Analytical integrations are difficult in general, so the Monte Carlo method may provide a useful tool.[11] We have already applied the Monte Carlo strategy to our method and obtained some good results for many electron systems.

## ACKNOWLEDGMENTS

This study has been supported financially by a Grant for Creative Scientific Research from the Ministry of Education, Science, Culture, and Sports of Japan.

**REFERENCES**


1. P. A. M. Dirac, *Proc. R. Soc. A* **123**, 714, 1929.
2. H. Nakatsuji, *J. Chem. Phys.* **113**, 2949, 2000., H. Nakatsuji, E. R. Davidson, *J. Chem. Phys.* **115**, 2000, 2001. H. Nakatsuji, *J. Chem. Phys.* **115**, 2465, 2001. H. Nakatsuji, *J. Chem. Phys.* **116**, 1811, 2002. H. Nakatsuji, M. Ehara, *J. Chem. Phys.* **117**, 9, 2002. H. Nakatsuji, M. Ehara, *J. Chem. Phys.* **122**, 194108, 2005.
3. H. Nakatsuji, *Phys. Rev. A* **65**, 052122, 2002.
4. H. Nakatsuji, *Phys. Rev. Lett.* **93**, 030403, 2004.
5. H. Nakatsuji, *Phys. Rev. A* **65**, 062110, 2005.
6. Y. Kurokawa, H. Nakashima, H. Nakatsuji, *Phys. Rev. A* **72**, 062502, 2005.
7. A. R. Edmonds, *Angular Momentum in Quantum Mechanics* (Princeton University Press, Princeton, 1957).
8. W. Cencek, J. Rychlewski, *J. Chem. Phys.* **98**, 1252, 1993.
9. E. A. Hylleraas, *Z. Phys.* **54**, 347, 1929.
10. A. J. Thakkar, T. Koga, *Phys. Rev. A* **50**, 854, 1994.
11. B. L. Hammond, W. A. Lester, Jr., and P. J. Reynolds, *Monte Carlo Methods in Ab Initio Quantum Chemistry* (World Scientific, Singapore, 1994).
12. R. A. Sack, *J. Math. Phys.* **5**, 245, 1964.
13. J. F. Perkins, *J. Chem. Phys.* **48**, 1985, 1968.
14. G. W. F. Drake, Z. C. Yan, *Phys. Rev. A* **52**, 3681, 1995.
15. S. Larsson, *Phys. Rev.* 169, **49**, 1968.
16. F. W. King, *Phys. Rev. A* **40**, 1735, 1989.
17. H. Kleindienst, G. Büsse, A. Lüchow, *Int. J. Quantum Chem.* **53**, 575, 1995.
18. D. Levin, *Int. J. Comput. Math. B* **3**, 371, 1973.
19. D. M. Fromm, R. N. Hill, *Phys. Rev. A* **36**, 1013, 1987.
20. T. Kinoshita, *Phys. Rev.* **105**, 1490, 1957.
21. C. L. Pekeris, *Phys. Rev.* **112**, 1649, 1958.
22. V. I. Korobov, *Phys. Rev. A* **61**, 064503, 2000.
23. G. W. F. Drake, M. M. Cassar, R. A. Nistor, *Phys. Rev. A* **65**, 054501, 2002.
24. C. Schwartz, *J. Comput. Methods Sci. Eng.* **4**, 13, 2004.
25. R. C. Forrey, *Phys. Rev. A* **69**, 022504, 2004.
26. H. Nakatsuji, H. Nakashima, *Phys. Rev. Lett.* **95**, 050407, 2005.
27. J. Rychlewski, J. Komasa, *in Explicitly Correlated Wave Functions in Chemistry*

*and Physics – Theory and Applications, edited by J. Rychlewski (Kluwer, Dordrecht, 2003)*, pp. 91-147.

28. F. W. King, *J. Mol. Struct. (Theochem)* **400**, 7, 1997.
29. Z. C. Yan, G. W. F. Drake, *Phys. Rev. A* **52**, 3711, 1995.
30. Z. C. Yan, M. Tambasco, G. W. F. Drake, *Phys. Rev. A* **57**, 1652, 1998.
31. G. Büsse, H. Kleindienst, A. Lüchow, *Int. J. Quantum Chem.* **66**, 241, 1998.
32. J. Komasa, *Chem. Phys. Lett.* **363**, 307, 2002.
33. P. Jönsson, C. F. Fischer, *Phys. Rev. A* **50**, 3080, 1994.

# Chapter 2

# Analytically Solving the Relativistic Dirac-Coulomb Equation for Atoms and Molecules

**Abstract:**

A method of solving the Schrödinger equation in an analytically expanded form reported previous chapter (ICI method) is extended to the relativistic case and a general method of exactly solving the Dirac-Coulomb equation (DCE) has been proposed for atoms and molecules. For solving the relativistic DCE, the so-called variational collapse may often become an obstacle in the relativistic field. To avoid this problem, the inverse Hamiltonian and inverse DCE is introduced. By using the inverse DCE, the Ritz-type property of variational calculations holds and the electronic ground state is the highest solution against the complete vacuum. Another method of avoiding the variational collapse is to hold the strict relation connecting small and large components. In the ICI formalism, this relation is automatically ensured and we call it ICI balance. Formulation and integrals to solve the DCE are obtained in analytical expressions. The new integration method based on the Fourie transformation is proposed for singular integrals of two-electron atoms. As a result, the systems including heavy elements or in a strong magnetic field, which cause numerical instability easily, can be calculated on high precision. Test applications to the Dirac oscillator, hydrogenlike and heliumlike atoms were satisfactory, implying a high potentiality of the ICI method also for the relativistic case.

## 1. Introduction

As noted by Dirac in 1929,[1] the Schrödinger equation (SE) provides a fundamental principle to predict physical and chemical phenomena. So, for theoretical chemistry, it is one of the most important subjects to solve the SE as accurately as possible. Despite its importance, there was no general method of solving the SE.

Recently, Nakatsuji has studied the structure of the exact wave functions to establish and develop a general method of solving the SE.[2-5] In the SE, the Hamiltonian $H$ determines the exact wave function $\psi$, so the exact $\psi$ may be expressed as a functional of $H$ applied to some appropriate function $\psi_0$,

$$\psi = f(H)\psi_0 \tag{2.1}$$

Based on the theory of the exact wave function,[2-5] a possible functional form of $f(H)$ is proposed by the iterative configuration or complement interaction (ICI) method and the simplest extreme coupled cluster (SECC) method, which construct the exact wave functions in Eq. (2.1).

However, the Hamiltonian for atoms and molecules includes the singularity of the Coulomb potential $V$. At the singular origin, the Hamiltonian diverges and a general form of Eq. (2.1) may also diverge. This is a serious problem because the function $\psi$ does not satisfy the conditions as wave function: square-integrable, one-valued and continuity. Nakatsuji has also proposed two methods to overcome this problem. One is to introduce the inverse Schrödinger equation (ISE) and the other is to introduce the scaled Schrödinger equation (SSE).[3-5] Both the ISE and SSE are equivalent to the SE, but the latter method (SSE) is simpler and more general for formulation. As a result, we can successfully apply the ICI method to solve the exact wave function in the sense of Eq. (2.1).

Now, we want to extend the ICI theory to the relativistic case. If atoms and molecules include heavier elements, the relativistic effect becomes very important and even dominant. For a one-electron system, the Dirac equation (DE) describes the relativistic equation of motion for electron although pair-annihilation and creation effect is not considered. It has an explicit Hamiltonian that obeys the Lorentz transformation. For many-electron systems, however, we do not have such relativistic equations as compact as the one-electron DE. The Dirac-Coulomb equation (DCE) and the Dirac-Coulomb-Breit equation (DCBE) are approximate and do not exactly obey the Lorentz transformation, but they are expected to be very accurate for atoms and

molecules. For more accurate formulation, we can use quantum electrodynamics (QED), but we do not have explicit Hamiltonians in QED.

The DE for one-electron system and the DCE for $N$-electron system are written as

$$\widehat{H}\psi = E\psi \tag{2.2}$$

where the Hamiltonian $\widehat{H}$ is defined by

$$\widehat{H} = \sum_{i}^{N} \widehat{H}_N(i) + \hat{I}_{(N)} \sum_{i<j}^{N} w_{ij} \tag{2.3}$$

$$\widehat{H}_N(i) = \hat{I}_{(i-1)} \otimes \hat{h}_i \otimes \hat{I}_{(N-i)} \tag{2.4}$$

$$\hat{h}_i = \begin{pmatrix} \left(v_i + c^2\right)\hat{I}_2 & c\left(\sigma \cdot \mathbf{p}_i\right) \\ c\left(\sigma \cdot \mathbf{p}_i\right) & \left(v_i - c^2\right)\hat{I}_2 \end{pmatrix} \tag{2.5}$$

where $w_{ij} = 1/r_{ij}$, $\hat{I}_n$ and $\hat{I}_{(n)}$ are the unit matrices of orders $n$ and $4^n$, respectively. $\hat{h}_i$ is the $4\times4$ matrix one-electron Hamiltonian and $v_i = -\sum_A Z_A / r_{Ai}$ is the nuclear attraction operator for electron $i$. $\sigma$ and $\mathbf{p}_i$ are the Pauli spin matrix and the momentum operator of electron $i$. The relativistic Hamiltonian $\widehat{H}$ is a $4^N \times 4^N$ operator matrix and the wave function is a vector composed of $4^N$ elements. The term $E\psi$ in Eq. (2.2) is also written as $E\hat{I}_{(N)}\psi$: mostly we use the simpler expression. For the one-electron case ($N=1$), the DCE reduces to the DE. In the nonrelativistic limit, the DCE reduces to the SE. So, the DCE should be very accurate for atoms and molecules. In this thesis, our aim is to formulate a general method of solving the exact $\psi$ of the DE and DCE in an analytical expansion form.

In the relativistic case, there are no theories dealing with the structure of the exact wave function, nor the theories for constructing the exact wave function. So, we first generalize our theory for the SE to the relativistic case. The Coulomb singularity problem is common to both the nonrelativistic and relativistic cases and is solved by introducing the scaled equations.[4,5] Another problem that often appears in the relativistic field is the variational instability and collapse. Though some studies using kinetic and other balances were reported,[6,7] there seems to be no established method. It was impressive that Pestka and Karwowski closed their important chapter of the Rychlewski's book in 2003 by noting "The Hylleraas CI approach to solving the Dirac-Coulomb eigenvalue problem is still in its infancy.[6] However, it certainly offers a perspective of highly accurate benchmark results, at least for two-electron systems."

The test applications of the present theory to the Dirac oscillator, hydrogenlike and heliumlike atoms are performed. The Dirac oscillator is a simple one-particle system, which is a relativistic extension of the nonrelativistic harmonic oscillator and one of the rare examples that the DE is exactly solvable and various mathematical and physical properties have been investigated.[8,9] The Hamiltonian of the Dirac oscillator does not contain the Coulomb singularity, hence simple, but the force field is expressed through vector potential, like in a magnetic field. The hydrogenlike atoms are also one-electron systems and exist the exact solutions.[10] The Hamiltonian contains the Coulomb singularity expressed in scalar potential. The heliumlike atoms are two-electron systems and the Hamiltonian contains the Coulomb singularity and the two-electron interaction term. This is a complicated system but interesting because both the nuclear and electron singularities are included in the Coulomb potential. In the next chapter, we apply our method to the systems in a magnetic field, which includes the force field and interactions through both vector and scalar potentials.

We derive the formulation and integrals necessary to solve the DE and DCE of these systems in analytical expressions. For solving the DE of the Dirac oscillator and hydrogenlike atoms, very difficult formulation and integrals are not appeared. For solving the DCE of the heliumlike atoms, however, complicated formulation and integrals are appeared. Previously, to evaluate matrix elements for the Hylleraas-CI basis functions, some of the formulation and integrals were derived by Pestka.[11] However, in our method, the operation of the Hamiltonian is needed not only for the estimation of matrix elements but also for the generation of wave function. Therefore, more general formulas have to be derived. Pestka also proposed the necessary integrals to evaluate matrix elements, based on the Sack expansion method.[11,12] However, he did not focus on the integrals including singular and/or mild singular potentials. When using his method based on the Sack expansion for integration, the convergence to the exact value is very slow especially for the integrals including singular potentials. Therefore, the systems including heavy elements or in a strong magnetic field, which cause numerical instability easily, cannot be treated because of the lack of precision. These systems are physically interesting and the relativistic effect is important and dominant. To calculate these integrals on high precision, we propose the new method based on the Fourie transformation. As a result, we can calculate these systems without any numerical instability.

In Sec. 2, we extend the ICI theory to the relativistic case and the methods of variational calculations in the relativistic field are discussed. In Sec. 3, we apply our theory to the Dirac oscillator, hydrogenlike and heliumlike atoms and derive the mathematical formulation and integrals necessary to solve the DE and DCE of these systems. In Sec. 4, the results of the calculations are discussed. The conclusion is remarked in Sec. 5.

## 2. Theory

### 2.1 Formulation of the exact wave function for the relativistic case

Now the first step of our project is to clarify the structure of the exact relativistic wave function $\psi$ and then to give a general method of constructing it in an analytical form. We follow the same arguments as in the nonrelativistic case.[2-5] First, the variational principle for $\psi$ is written as

$$\langle \psi | \widehat{H} - E | \delta\psi \rangle = 0 \tag{2.6}$$

This is a stationary principle for calculating the best possible $\psi$. The H-square equation is formulated as

$$\langle \psi | (\widehat{H} - E)^2 | \psi \rangle = 0 \tag{2.7}$$

and is satisfied only with the exact $\psi$. Then, we have the following theorem.

*Theorem*: When $\psi$ includes only one variable matrix $\widehat{C}$ (diagonal) with the element $C_n$ ($n = 1 \ldots 4^N$) and when an arbitrary variation of $\psi$ satisfies

$$\delta\psi = \delta\widehat{C}\left(\widehat{H} - E\right)\psi \tag{2.8}$$

then this $\psi$ has the structure of the exact wave function.

*Proof*: When we define $\left(\widehat{H} - E\right)\psi = \chi$, $\chi$ is a column vector of the elements $\chi_n$ ($n = 1 \ldots 4^N$). When we substitute $\delta\psi$ given by Eq. (2.8) into the variational principle, Eq. (2.6), we obtain

$$0 = \langle \psi | (\widehat{H} - E)\delta\widehat{C}(\widehat{H} - E) | \psi \rangle = \sum_n^{4^N} \delta C_n \left\langle |\chi_n|^2 \right\rangle \tag{2.9}$$

Since $\delta C_n$ is arbitrary, this means $\left\langle |\chi_n|^2 \right\rangle = 0$ for all $n$, which is equivalent to Eq. (2.7). So, among $\psi$ with the form of Eq. (2.8), variationally optimal wave functions are the exact solutions of the DE and the DCE. *Proof ends.*

This theorem is a generalization of the similar theorem given previously for the nonrelativistic case[2-5] and the argument is free from the technical arguments like variational collapse, since the H-square equation is valid only for the exact wave function.

Based on the above theorem, we propose the relativistic ICI method just as in the nonrelativistic case. We define the simplest ICI (SICI) wave function by the recurrence formula,

$$\psi_{n+1} = \left[1 + \hat{C}_n\left(\hat{H} - E_n\right)\right]\psi_n \tag{2.10}$$

where $n$ is an iteration number. The variation of $\psi_{n+1}$, $\delta\psi_{n+1} = \delta\hat{C}_n\left(\hat{H} - E_n\right)\psi_n$, becomes equal to that given by Eq. (2.8) at convergence where everything becomes $n$ independent, so that the SICI gives the exact wave function at convergence. We can also formulate a more general ICI method by dividing the operator $\hat{H}$ in the $N_D$ parts (ICIND).[2-5]

The DC Hamiltonian includes the Coulomb potentials that cause the singularity problem. To avoid it, we introduce the scaled DE and DCE that are given by

$$g\left(\hat{H} - E\hat{I}_{(N)}\right)\psi = 0 \tag{2.11}$$

where the scaling function $g$ is a positive scalar function of electron coordinates and can become zero only at the singular points $r_0$ of the potential $V$ but satisfies

$$\lim_{r \to r_0} gV \neq 0 \tag{2.12}$$

By this introduction of the scaled equation, we can avoid the singularity problem as in the nonrelativistic case.[4,5] Since this idea is very general, we can use it for singular potentials that appear in other fields of physics. Based on the scaled DCE, we introduce the SICI method that is free from the singularity problem by

$$\psi_{n+1} = \left[1 + \hat{C}_n g\left(\hat{H} - E_n\right)\right]\psi_n \tag{2.13}$$

The SICI includes only one variable matrix $\hat{C}_n$ at each iteration step and its convergence may be slow. A better performance is expected by introducing the free ICI method as in the nonrelativistic case.[4,5] In the free ICI, we take all the independent functions $\{\phi_i\}^n$ from the right hand side of Eq. (2.13) and give independent coefficients to all such functions $\phi_i$ – i.e.,

$$\psi_{n+1} = \sum_{i}^{all} c_i \phi_i \tag{2.14}$$

From the variational point of view, this free ICI should converge faster than the SICI. Note that $\phi_i$ is a column vector of $4^N$ dimension and $c_i$ is a diagonal matrix with $4^N$ elements. In the free ICI, each iteration does not depend on the results of the former iterations and so no accumulation of error occurs. In some choice of $g$, the right hand side of Eq. (2.13) may include diverging functions but they are eliminated in the free ICI process since such functions are inappropriate for describing the wave function.

### 2.2 Variational calculations by using the inverse Hamiltonian

Now, we have an analytical function having the structure of the exact wave function in the form of free ICI (Eq. (2.14)). The next step is to perform the variational calculation of the variables $\{c_i\}$ and the corresponding energy, which we call the diagonalization step. Here, an obstacle that often appears in the relativistic field is the so-called variational collapse. Since the lowest electronic state of the DE and the DCE is not the lowest state of these equations, the so-called Ritz-type property does not hold. However, a method to recover Ritz-type property was proposed by Hill and Krauthauser for one-electron DC calculations with basis set expansion method.[13] They introduced the inverse Hamiltonian and wrote the DE as

$$\hat{H}^{-1}\psi = E^{-1}\psi \tag{2.15}$$

As shown in the paper of the inverse Schrödinger equation,[3] it is easy to show the equivalence between the original equation and the inverse one. For the inverse DE, the electronic ground state is the highest solution against the complete vacuum and therefore we have the Ritz-like variational principle,

$$E^{-1} = \frac{\left\langle \tilde{\psi} \middle| \hat{H}^{-1} \middle| \tilde{\psi} \right\rangle}{\left\langle \tilde{\psi} \middle| \tilde{\psi} \right\rangle} \leq E_0^{-1} \tag{2.16}$$

where $\tilde{\psi}$ is a variational trial function for exact $\psi$ and $E_0$ is the true energy of the ground electronic state. The image of this inverse procedure is illustrated in Fig. 1. Now, how do we explicitly write down the inverse Hamiltonian? A clever trick is to take our variational function in the form of[13]

$$\tilde{\psi} = \hat{H}\varphi \tag{2.17}$$

with $\varphi$ representing a free variation. Then, the above variational equation is rewritten as

$$E^{-1} = \frac{\langle\varphi|\hat{H}|\varphi\rangle}{\langle\varphi|\hat{H}^2|\varphi\rangle} \le E_0^{-1} \tag{2.18}$$

and the variance is formulated as

$$\begin{aligned}\sigma^2 &= \frac{\langle\tilde{\psi}|(\hat{H}^{-1} - E^{-1})^2|\tilde{\psi}\rangle}{\langle\tilde{\psi}|\tilde{\psi}\rangle} \\ &= \frac{1}{\langle\varphi|\hat{H}^2|\varphi\rangle}\left(\langle\varphi|\varphi\rangle - 2E^{-1}\langle\varphi|\hat{H}|\varphi\rangle + E^{-2}\langle\varphi|\hat{H}^2|\varphi\rangle\right)\end{aligned} \tag{2.19}$$

which we can calculate. For the exact wave function, $\sigma^2$ must be zero: this is the inverse H-square theorem.[3]

At the diagonalization step of the relativistic free ICI, we utilize the above Ritz-like variational equation to ensure the bound property. Though it was introduced originally for the one-electron DE,[13] we utilize it for solving the many-electron DCE. We know from the ICI theory that our free ICI function $\varphi_n$ approaches the exact wave function, and therefore it is easy to show that our variational function $\tilde{\psi}_n$ also approaches the exact wave function,

$$\tilde{\psi}_{n+1} = \hat{H}\varphi_{n+1} = \hat{H}\left\{\prod_{i=1}^{n}\left(1 + \hat{C}_{i-1}g\left(\hat{H} - E_{i-1}\right)\right)\varphi_0\right\} \tag{2.20}$$

$$\left(\hat{H} - E\right)\varphi = 0 \Leftrightarrow \left(\hat{H}^{-1} - E^{-1}\right)\tilde{\psi} = 0 \tag{2.21}$$

Since $\hat{H}$ must not be singular to define its inverse, we often have to shift it by a constant $W$,

$$\hat{H}' = \hat{H} + W\hat{I}_{(N)} \tag{2.22}$$

Further, since Eq. (2.18) includes the integral of $\hat{H}^2$ that is more strongly singular than $\hat{H}$, we have to eliminate a larger number of diverging functions from our ICI basis than in the ordinary case that involves only $\hat{H}$. This may make the inverse variation method rather slowly converging. Nevertheless, the bound property of this variational method is

useful in actual calculations where we do not know the true energy. In the ICI formulation, the excited states are calculated as the higher solutions: an appropriate choice of $\psi_0$ is necessary for obtaining a reasonable convergence speed.

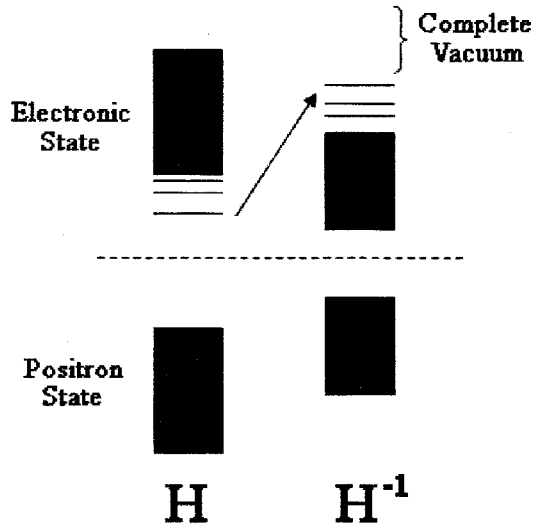


**Fig.1** The image of the energy spectra of the DE and inverse DE. For the regular Hamiltonian, the lowest electronic state is not the lowest state of the DE. For the inverse Hamiltonian, the highest electronic state is the highest solution against complete vacuum.

### 2.3 Variational calculations satisfied the balance conditions

Another method of avoiding the variational collapse is to ensure some balance conditions – i.e., kinetic balance, etc. on the basis functions.[6,7,14] From the DE, we obtain a relation connecting small and large components as

$$\phi^S = \frac{c\sigma \cdot \mathbf{p}}{E - V + c^2}\phi^L \tag{2.23}$$

A strict use of this relation is called atomic balance and an approximate one kinetic balance. These balance conditions have been studied in details by several authors[6,7,14] but the strict balance condition of Eq. (2.23) contains the energy $E$, which is an unknown parameter determined after the diagonalization step. Therefore, the exact and strict relation can not be satisfied by practical calculations. For the electronic state to become upper bounds to the eigenvalues of the DE, these conditions between large and small components are expressed as[14]

Atomic balance condition: $$\bigcup_j \left( \frac{1}{E_j + c^2 - V} (\sigma \cdot \mathbf{p}) H_l \right) \subset H_s \tag{2.24}$$

Asymptotic balance condition: $$\bigcup_j \left( r^j (\sigma \cdot \mathbf{p}) H_l \right) \subset H_s \tag{2.25}$$

Kinetic balance condition: $$(\sigma \cdot \mathbf{p}) H_l \subset H_s \tag{2.26}$$

where $H_l$ and $H_s$ are the large and small component spaces, respectively. We note here that the balancing similar to the atomic and asymptotic balance is automatically done in the ICI formalism. In ICI, $\psi_{n+1}$ is generated by applying the DC operator to $\psi_n$ (Eq. (2.13)) and this is essentially a balancing that is theoretically valid even for many-electron systems. We call this balancing ICI balance,

$$\begin{aligned} \psi_{n+1}{}^L &\supset g(\sigma \cdot \mathbf{p}) \psi_n{}^S \\ \psi_{n+1}{}^S &\supset g(\sigma \cdot \mathbf{p}) \psi_n{}^L \end{aligned} \tag{2.27}$$

Eq. (2.27) means that the terms necessary to satisfy the balancing condition are certainly included at the next iteration step in both the large and small component spaces. However, in an earlier stage of the ICI calculation, the number of the basis functions is small and the ICI balancing would be insufficient. So, practically, we may need to do an additional balancing before diagonalization. Detailed examinations of such balancing methods will be given elsewhere.

## 3. ICI method applied to the Dirac oscillator, hydrogenlike and heliumlike atoms

### 3.1 Dirac oscillator

First, we introduce the Hamiltonian and exact solutions of the Dirac oscillator. The DE of the Dirac oscillator is expressed as

$$\left( c\boldsymbol{\alpha} \cdot (\mathbf{p} - i\omega \mathbf{r}\boldsymbol{\beta}) + c^2 \boldsymbol{\beta} \right) \psi = E\psi \tag{2.28}$$

The external potential is given by the substitution: $\mathbf{p} \rightarrow \mathbf{p} - i\omega \mathbf{r}\boldsymbol{\beta}$, where $\omega$ is an oscillator frequency. The Hamiltonian is linear to both $\mathbf{p}$ and $\mathbf{r}$, so the nonrelativistic limit becomes quadratic of $\mathbf{r}$. The square root of the Hamiltonian is expressed as

$$H^2 = c^2 \left( p^2 + \omega^2 r^2 + c^2 \right) \hat{I} + c^2 \left( 4\mathbf{S} \cdot \mathbf{L} - 3 \right) \omega \boldsymbol{\beta} \tag{2.29}$$

where $\mathbf{S}$ and $\mathbf{L}$ are the spin and spatial angular momentums, respectively. The second term of Eq. (2.29) is a strong spin-orbit coupling term and is not appeared in the

nonrelativistic harmonic oscillator. Eq. (2.28) is the three-dimensional DE and simplification to the one-dimensional case is given by

$$\begin{pmatrix} c^2 & c\left(-\frac{d}{dx}+\omega x\right) \\ c\left(\frac{d}{dx}+\omega x\right) & -c^2 \end{pmatrix} \psi = E\psi \tag{2.30}$$

The exact solution of Eq. (2.30) is written as[9]

$$E_m = \pm c^2 \sqrt{1+2|m|\frac{\omega}{c^2}} \tag{2.31}$$

$$\begin{aligned} \psi_m{}^L &= C_m{}^L H_{|m|}(\lambda x)\cdot \exp(-\lambda^2/2\cdot x^2) \\ \psi_m{}^S &= C_m{}^S H_{|m|-1}(\lambda x)\cdot \exp(-\lambda^2/2\cdot x^2) \end{aligned} \tag{2.32}$$

$$\begin{aligned} C_m{}^L &= \sqrt{\frac{\lambda\left(E_m+c^2\right)}{2^{|m|+1}|m|!\sqrt{\pi}E_m}} \\ C_m{}^S &= \sqrt{\frac{\lambda\left(E_m-c^2\right)}{2^{|m|}\left(|m|-1\right)!\sqrt{\pi}E_m}} \end{aligned} \tag{2.33}$$

where $E_m$ and $\psi_m$ are the exact energy and wave function with quantum number $m$: $m = 0, \pm 1, \pm 2, \ldots$, respectively. In Eq. (2.32), $H_{|m|}(\lambda x)$ and $H_{|m|-1}(\lambda x)$ are the Hermite polynomials and $\lambda = \sqrt{\omega}$.

We apply our ICI method to solve the DE of Eq. (2.30). Since the solution for $m = 0$ is quite obvious, we perform the calculation for $m = 1$ which contains the spin-orbit coupling effect in Eq. (2.29). The parity of the wave function is determined by $m$: odd and even parity for the large and small components, respectively. The initial functions should be chosen as satisfied these symmetries. Since the Hamiltonian does not contain any singularity term, the $g$ function need not be introduced. As a result, we adopted the following $g$ and initial functions,

$$g = 1 \tag{2.34}$$

$$\begin{aligned} \psi_0{}^L &= x\cdot \exp(-\alpha x^2) \\ \psi_0{}^S &= \exp(-\alpha x^2) \end{aligned} \tag{2.35}$$

Gaussian type function is suitable for this system because there is no singularity point in the Hamiltonian and cusp property is not appeared in the wave function. We examined

two different calculations to avoid the variational collapse. One is to use the inverse Hamiltonian and we confirm the Ritz-type variational property holds. The other is the normal ICI calculation by using the regular Hamiltonian without any constraint to the wave function, in which we examine that the ICI method automatically satisfies the balancing condition (ICI balance). The results are discussed in Sec. 4.

### 3.2 Hydrogenlike atoms

The next application is to the hydrogen isoelectronic atoms for which the exact analytical wave functions are also known same as Dirac oscillator. The DE is written as

$$\begin{pmatrix} \left(V+c^2\right)\hat{I}_2 & c\left(\sigma\cdot\mathbf{p}\right) \\ c\left(\sigma\cdot\mathbf{p}\right) & \left(V-c^2\right)\hat{I}_2 \end{pmatrix}\psi = E\psi \tag{2.36}$$

where $V=-Z/r$. Separated from the angular part, we can write the radial part alone,

$$\begin{pmatrix} c^2-\dfrac{Z}{r} & c\left(-\dfrac{d}{dr}-\dfrac{1-k}{r}\right) \\ c\left(\dfrac{d}{dr}+\dfrac{1+k}{r}\right) & -c^2-\dfrac{Z}{r} \end{pmatrix}\psi = E\psi \tag{2.37}$$

where $k=\pm\left(j+1/2\right)$ and $l=j\pm1/2$. $j$ is a quantum number of the total angular momentum. Exact solution of Eq. (2.37) is written as[10]

$$E_{m,k}=\pm c^2\left(1+\left(\frac{Z}{c\left(m-|k|+\gamma_k\right)}\right)^2\right)^{-1/2} \tag{2.38}$$

$$\gamma_k=\sqrt{k^2-\left(Z/c\right)^2} \tag{2.39}$$

$$\begin{aligned} \psi_{m,k}{}^{L} &= r^{\gamma_k-1}e^{-\lambda_{m,k}r}w_{m,k}{}^{L} \\ \psi_{m,k}{}^{S} &= -r^{\gamma_k-1}e^{-\lambda_{m,k}r}\left(\frac{\lambda_{m,k}}{E_{m,k}+c^2}\right)w_{m,k}{}^{S} \end{aligned} \tag{2.40}$$

$$\begin{aligned} w_{m,k}{}^{L} &= x^{1-\left(A_{m,k}+\gamma_k-k\right)}\frac{d}{dx}\left\{x^{A_{m,k}+\gamma_k-k}\,{}_1F_1(\alpha_{m,k};\beta_k;x)\right\} \\ w_{m,k}{}^{S} &= -x^{1-\left(\gamma_k+k-B_{m,k}\right)}\frac{d}{dx}\left\{x^{\gamma_k+k-B_{m,k}}\,{}_1F_1(\alpha_{m,k};\beta_k;x)\right\} \end{aligned} \tag{2.41}$$

$$A_{m,k} = \frac{Z\lambda_{m,k}}{c^2 + E_{m,k}}, B_{m,k} = \frac{Z\lambda_{m,k}}{c^2 - E_{m,k}} \tag{2.42}$$

$$\alpha_{m,k} = \gamma_k + \left(A_{m,k} - B_{m,k}\right)/2, \beta_k = 1 + \gamma_k \tag{2.43}$$

where $E_{m,k}$ and $\psi_{m,k}$ are the exact energy and wave function with quantum number $m$ and $k$, respectively. $\lambda_{m,k}$ and $x$ are defined as $\lambda_{m,k} = \sqrt{c^4 - E_{m,k}{}^2}$ and $x = 2\lambda_{m,k} r$, respectively. ${}_1F_1$ is the confluent hypergeometric function. Thus, the relativistic exact wave function has a mild singularity at the position of the nucleus.[10]

In the ICI calculations, since the Hamiltonian of the hydrogenlike atoms contains the Coulomb singularity, we have to introduce the $g$ function with the scaled DE (SDE). We tried three sets of the $g$ and initial functions. First is the simplest one,

$$g = r \tag{2.44}$$

$$\psi_0{}^L = \psi_0{}^S = \exp(-\alpha r) \tag{2.45}$$

This set has been adopted in the nonrelativistic calculation of the hydrogen atom.[4,5] Slater type function is suitable to express a cusp condition at the singularity point. However, this set can not generate any function expresses a mild singularity at the nucleus position. Therefore, this set may not be a good choice for the relativistic case. Second choice is

$$g = r \tag{2.46}$$

$$\psi_0{}^L = \psi_0{}^S = r^{\gamma_k - 1} \exp(-\alpha r) \tag{2.47}$$

This is an improved type of the set of Eq. (2.44) and Eq. (2.45). A mild singularity is included in the initial function. The third choice is

$$g = r^{\delta} \tag{2.48}$$

$$\psi_0{}^L = \psi_0{}^S = \exp(-\alpha r) \tag{2.49}$$

where $\delta$ is a non-integer number with the region: $1/2 < \delta < 1$. A mild singularity is included in the $g$ function. Moreover, several types of scaling mild singularities are included to the wave function during the iteration process.

When using these sets of the $g$ and initial functions, we must calculate the following form integration to evaluate matrix elements,

$$I = \int_0^\infty r^\gamma \exp(-\alpha r) \cdot dr \tag{2.50}$$

where $\gamma > -1$. This integral is quite easily calculated by

$$I = \frac{1}{\alpha^{\gamma+1}} \Gamma(\gamma+1) \tag{2.51}$$

We took H (Z=1) and $Fe^{25+}$ (Z=26) as the hydrogenlike atoms: the relativistic effect is larger for the latter. We performed the calculations by using both the inverse DE and regular DE.

### 3.3 Heliumlike atoms

The final application of our method is to heliumlike two-electron atoms, whose DCE is the matrix equation of dimension 16. The Hamiltonian is written as

$$\widehat{H} = \begin{pmatrix} (V+2c^2)\hat{I}_4 & c(\boldsymbol{\sigma}_2 \cdot \mathbf{p}_2) & c(\boldsymbol{\sigma}_1 \cdot \mathbf{p}_1) & 0 \\ c(\boldsymbol{\sigma}_2 \cdot \mathbf{p}_2) & V\hat{I}_4 & 0 & c(\boldsymbol{\sigma}_1 \cdot \mathbf{p}_1) \\ c(\boldsymbol{\sigma}_1 \cdot \mathbf{p}_1) & 0 & V\hat{I}_4 & c(\boldsymbol{\sigma}_2 \cdot \mathbf{p}_2) \\ 0 & c(\boldsymbol{\sigma}_1 \cdot \mathbf{p}_1) & c(\boldsymbol{\sigma}_2 \cdot \mathbf{p}_2) & (V-2c^2)\hat{I}_4 \end{pmatrix} \tag{2.52}$$

where $\mathbf{p}_1$ and $\mathbf{p}_2$ are the momentum operators of electron 1 and 2, respectively. $V$ is the scalar potential operator with nuclear charge $Z$, written as $V = -Z/r_1 - Z/r_2 + 1/r_{12}$. The wave function is composed of $\psi^{ll}$, $\psi^{ls}$, $\psi^{sl}$ and $\psi^{ss}$, each being 4-vector. The following operators are appeared in the Hamiltonian,

$$T_1 = \boldsymbol{\sigma}_1 \cdot \mathbf{p}_1, \quad T_2 = \boldsymbol{\sigma}_2 \cdot \mathbf{p}_2, \quad \frac{Z}{r_1}, \quad \frac{Z}{r_2}, \quad \frac{1}{r_{12}} \tag{2.53}$$

$$\boldsymbol{\sigma}_1 \cdot \mathbf{p}_1 = \left(\sigma \otimes \hat{I}_2\right) \cdot \mathbf{p}_1, \quad \boldsymbol{\sigma}_2 \cdot \mathbf{p}_2 = \left(\hat{I}_2 \otimes \sigma\right) \cdot \mathbf{p}_2 \tag{2.54}$$

where $\sigma$ and $\hat{I}_2$ are the Pauli spin matrices and $2 \times 2$ unit matrices, respectively. Explicit forms of $\boldsymbol{\sigma}_1$ and $\boldsymbol{\sigma}_2$ are expressed as

$$\boldsymbol{\sigma}_1 = \sigma \otimes \hat{I}_2 = \begin{pmatrix} \boldsymbol{\sigma}_{11} & 0 & \boldsymbol{\sigma}_{12} & 0 \\ 0 & \boldsymbol{\sigma}_{11} & 0 & \boldsymbol{\sigma}_{12} \\ \boldsymbol{\sigma}_{21} & 0 & \boldsymbol{\sigma}_{22} & 0 \\ 0 & \boldsymbol{\sigma}_{21} & 0 & \boldsymbol{\sigma}_{22} \end{pmatrix}, \quad \boldsymbol{\sigma}_2 = \mathbf{I}_2 \otimes \boldsymbol{\sigma} = \begin{pmatrix} \boldsymbol{\sigma}_{11} & \boldsymbol{\sigma}_{12} & 0 & 0 \\ \boldsymbol{\sigma}_{21} & \boldsymbol{\sigma}_{22} & 0 & 0 \\ 0 & 0 & \boldsymbol{\sigma}_{11} & \boldsymbol{\sigma}_{12} \\ 0 & 0 & \boldsymbol{\sigma}_{21} & \boldsymbol{\sigma}_{22} \end{pmatrix} \tag{2.55}$$

The wave function must be satisfied anti-symmetric property as

$$\begin{aligned}\psi^{ll}(1,2) &= -\psi^{ll}(2,1)\\ \psi^{ls}(1,2) &= -\psi^{sl}(2,1)\\ \psi^{ss}(1,2) &= -\psi^{ss}(2,1)\end{aligned} \tag{2.56}$$

In the ICI calculations, we took the $g$ and initial functions as

$$g = 1 + r_1 + r_2 + r_{12} \tag{2.57}$$

$$\begin{aligned}\psi_0^{\,ll} &= A\left(s_{1/2,1/2} \otimes s_{1/2,-1/2}\right)\\ \psi_0^{\,ls} &= s_{1/2,1/2} \otimes p_{1/2,-1/2} - s_{1/2,-1/2} \otimes p_{1/2,1/2}\\ \psi_0^{\,ss} &= A\left(p_{1/2,1/2} \otimes p_{1/2,-1/2}\right)\end{aligned} \tag{2.58}$$

with $A$ being an anti-symmetrizer. $s_{j,m}$ means the one-electron orbital of the exact solution of the hydrogenlike atom with the total angular momentum $j$, its $z$ component $m$ and spatial angular momentum $l = 0$ ($l$ is not a quantum number in the relativistic case). $p_{j,m}$ is similarly defined with $l = 1$. The radial part of $s_{j,m}$ and $p_{j,m}$ is written as

$$\chi = r^{\gamma_k - 1}\exp(-Zr) \tag{2.59}$$

with a mild singularity $\gamma_k = \sqrt{k^2 - (Z/c)^2}$ at the nucleus position.

We performed the calculations for He (Z=2) and $Th^{88+}$ (Z=90) by using both the inverse DCE and regular DCE. The results are shown in Sec. 4.

In the ICI calculations of two-electron systems, the correlated terms $r_{12}$ are explicitly appeared in the wave function. Therefore, the formulation becomes very complicated both for the generation of the ICI wave function and the evaluation of matrix elements. In the nonrelativistic case, after Hylleraas first found in 1929 that the correlated terms $r_{12}$ were so important to represent electron correlation and rapidly converge to the exact solution,[15] a quite large number of studies about the explicitly correlated wave functions have been performed. However, in the relativistic case, there is little study about the correlated type wave functions. The more accurate solution is needed not only for the electron correlation but also for the variational calculation in the relativistic case. In the following subsections 3.3.1 and 3.3.2, we derive the necessary formulation and integrals for our ICI calculations and they should be useful not only for the ICI but also for the Hylleraas type correlated wave functions.

### 3.3.1 The generation of the ICI wave functions and the evaluation of matrix elements

Since the ICI wave functions are generated by the Hamiltonian $\hat{H}$ and $g$ function, these operators are used in both the generation of the wave function and evaluation of matrix elements. In the ICI formalism, as described later, the functions of each ll, ls, sl and ss components are expressed as linear combinations of the following form,

$$\zeta = \left(T_i f(r_{12})\right) \cdot g(r_{12}) \cdot R(r_1, r_2)\Theta(\hat{\mathbf{r}}_1, \hat{\mathbf{r}}_2) \quad (i = 1, 2) \tag{2.60}$$

where $f(r_{12})$ and $g(r_{12})$ are the functions of $r_{12}$. $R(r_1, r_2)$ and $\Theta(\hat{\mathbf{r}}_1, \hat{\mathbf{r}}_2)$ are the functions of the radial and angular part, respectively. The angular part $\Theta(\hat{\mathbf{r}}_1, \hat{\mathbf{r}}_2)$ is also composed of four components as the tensor product of one-electron angular function, which is composed as preserved the total angular momentum and parities by the angular momentum composite theorem.[16] In Eq. (2.60), $T_i f(r_{12})$ may be expanded by means of the equation,

$$T_i f(r_{12}) = -i \frac{1}{r_{12}} \frac{df}{dr_{12}} \left(\boldsymbol{\sigma}_i \cdot \mathbf{r}_i - \boldsymbol{\sigma}_i \cdot \mathbf{r}_j\right) \quad (i, j = 1, 2) \tag{2.61}$$

However, in some cases, for example $f(r_{12}) = r_{12}$, Eq. (2.61) cannot become square integrable form since it may gives $\infty - \infty$ formula. Therefore, we use the no expansion form of $T_i f(r_{12})$ like Eq. (2.60) until the stage of the evaluation of matrix elements.

We derive the formulation of some operators to $\zeta$ (Eq. (2.60)). The operation of the scalar potential $V$ and $g$ function is obvious. However, the operation of the kinetic part $T_i = \boldsymbol{\sigma}_i \cdot \mathbf{p}_i$ $(i = 1, 2)$ is very complicated,

$$\begin{aligned} T_i\zeta &= T_i\left\{\left(T_j f(r_{12})\right) \cdot g(r_{12}) \cdot R(r_1, r_2)\Theta(\hat{\mathbf{r}}_1, \hat{\mathbf{r}}_2)\right\} \\ &= \left(T_j f(r_{12})\right) \cdot g(r_{12}) \cdot \left(T_i\left(R(r_1, r_2)\Theta(\hat{\mathbf{r}}_1, \hat{\mathbf{r}}_2)\right)\right) \\ &\quad + \left(T_i T_j f(r_{12})\right) \cdot g(r_{12}) \cdot R(r_1, r_2)\Theta(\hat{\mathbf{r}}_1, \hat{\mathbf{r}}_2) \\ &\quad + \left(T_j f(r_{12})\right) \cdot \left(T_i g(r_{12})\right) \cdot R(r_1, r_2)\Theta(\hat{\mathbf{r}}_1, \hat{\mathbf{r}}_2) \quad (i, j = 1, 2) \end{aligned} \tag{2.62}$$

For the first term of Eq. (2.62), it is convenient to use the following equation,

$$\begin{aligned} T_i &= \boldsymbol{\sigma}_i \cdot \mathbf{p}_i = \frac{\boldsymbol{\sigma}_i \cdot \mathbf{r}_i}{r_i^2}\left(\boldsymbol{\sigma}_i \cdot \mathbf{r}_i\right)\left(\boldsymbol{\sigma}_i \cdot \mathbf{p}_i\right) = \frac{\boldsymbol{\sigma}_i \cdot \mathbf{r}_i}{r_i^2}\left(\mathbf{r}_i \cdot \mathbf{p}_i + i\boldsymbol{\sigma}_i\left(\mathbf{r}_i \times \mathbf{p}_i\right)\right) \\ &= -i\left(\boldsymbol{\sigma}_i \cdot \hat{\mathbf{r}}_i\right)\left(\frac{\partial}{\partial r_i} - \frac{1}{r_i}\left(\boldsymbol{\sigma}_i \cdot \mathbf{L}_i\right)\right) \end{aligned} \tag{2.63}$$

where $\mathbf{L}_i$ is the spatial angular momentum operator (not total angular momentum operator): $\mathbf{L}_i = \mathbf{r}_i \times \mathbf{p}_i$. $\boldsymbol{\sigma}_i \cdot \hat{\mathbf{r}}_i$ and $\boldsymbol{\sigma}_i \cdot \mathbf{L}_i$ operate the angular part: $\Theta(\hat{\mathbf{r}}_1, \hat{\mathbf{r}}_2)$. The explicit forms of these angular operators are expressed as follows related to Eq. (2.55),

$$\boldsymbol{\sigma}_1 \cdot \boldsymbol{\eta}_i = \begin{pmatrix} \boldsymbol{\sigma}_{11} \cdot \boldsymbol{\eta}_i & 0 & \boldsymbol{\sigma}_{12} \cdot \boldsymbol{\eta}_i & 0 \\ 0 & \boldsymbol{\sigma}_{11} \cdot \boldsymbol{\eta}_i & 0 & \boldsymbol{\sigma}_{12} \cdot \boldsymbol{\eta}_i \\ \boldsymbol{\sigma}_{21} \cdot \boldsymbol{\eta}_i & 0 & \boldsymbol{\sigma}_{22} \cdot \boldsymbol{\eta}_i & 0 \\ 0 & \boldsymbol{\sigma}_{21} \cdot \boldsymbol{\eta}_i & 0 & \boldsymbol{\sigma}_{22} \cdot \boldsymbol{\eta}_i \end{pmatrix} \tag{2.64}$$

where $\boldsymbol{\eta}_i$ means $\hat{\mathbf{r}}_i$ or $\mathbf{L}_i$. $\boldsymbol{\sigma}_{jk}$ means the $j,k$ element of the Pauli spin matrices $\sigma$. Each element is written in the polar coordinates as

$$\begin{aligned} \boldsymbol{\sigma}_{11} \cdot \hat{\mathbf{r}}_i &= \cos\vartheta_i & \boldsymbol{\sigma}_{11} \cdot \mathbf{L}_i &= L_i^z \\ \boldsymbol{\sigma}_{12} \cdot \hat{\mathbf{r}}_i &= \sin\vartheta_i e^{-i\varphi_i} & \boldsymbol{\sigma}_{12} \cdot \mathbf{L}_i &= L_i^- \\ \boldsymbol{\sigma}_{21} \cdot \hat{\mathbf{r}}_i &= \sin\vartheta_i e^{i\varphi_i} & \boldsymbol{\sigma}_{21} \cdot \mathbf{L}_i &= L_i^+ \\ \boldsymbol{\sigma}_{22} \cdot \hat{\mathbf{r}}_i &= -\cos\vartheta_i & \boldsymbol{\sigma}_{22} \cdot \mathbf{L}_i &= -L_i^z \end{aligned} \tag{2.65}$$

When the angular part $\Theta(\hat{\mathbf{r}}_1, \hat{\mathbf{r}}_2)$ is expressed by the spherical harmonics, the following relations are useful,

$$\begin{aligned} \cos\vartheta \cdot Y_l^m(\vartheta,\varphi) &= \sqrt{\frac{(l+m)(l-m)}{(2l+1)(2l-1)}} Y_{l-1}^m(\vartheta,\varphi) + \sqrt{\frac{(l-m+1)(l+m+1)}{(2l+1)(2l+3)}} Y_{l+1}^m(\vartheta,\varphi) \\ \sin\vartheta e^{i\varphi} \cdot Y_l^m(\vartheta,\varphi) &= \sqrt{\frac{(l+m+1)(l+m+2)}{(2l+1)(2l+3)}} Y_{l+1}^{m+1}(\vartheta,\varphi) - \sqrt{\frac{(l-m-1)(l-m)}{(2l-1)(2l+1)}} Y_{l-1}^{m+1}(\vartheta,\varphi) \\ \sin\vartheta e^{-i\varphi} \cdot Y_l^m(\vartheta,\varphi) &= \sqrt{\frac{(l+m-1)(l+m)}{(2l-1)(2l+1)}} Y_{l-1}^{m-1}(\vartheta,\varphi) - \sqrt{\frac{(l-m+1)(l-m+2)}{(2l+1)(2l+3)}} Y_{l+1}^{m-1}(\vartheta,\varphi) \\ L^z Y_l^m(\vartheta,\varphi) &= m Y_l^m(\vartheta,\varphi) \\ L^{\pm} Y_l^m(\vartheta,\varphi) &= \sqrt{(l \mp m)(l \pm m + 1)}\, Y_l^{m\pm1}(\vartheta,\varphi) \end{aligned}$$

(2.66)

For the second term of Eq. (2.62), we derive the expansion form of the function $T_i T_j f(r_{12})$. For the case of $i = j$, $T_i T_i$ is the same operator as the kinetic part of the nonrelativistic Hamiltonian,

$$T_i T_i = (\boldsymbol{\sigma}_i \cdot \mathbf{p}_i)(\boldsymbol{\sigma}_i \cdot \mathbf{p}_i) = \mathbf{p}_i^2 = -\Delta_i \tag{2.67}$$

Therefore, this operator is easily calculated by

$$T_i T_i f(r_{12}) = -\frac{d^2 f}{dr_{12}^{\,2}} - \frac{2}{r_{12}}\frac{df}{dr_{12}} \tag{2.68}$$

For the case of $i \neq j$, we expand $T_j f(r_{12})$ first,

$$\begin{aligned} T_i T_j f(r_{12}) &= T_i\left\{-i\frac{1}{r_{12}}\frac{df}{dr_{12}}\left(\boldsymbol{\sigma}_j \cdot \mathbf{r}_j - \boldsymbol{\sigma}_j \cdot \mathbf{r}_i\right)\right\} \\ &= -iT_i\left(\frac{1}{r_{12}}\frac{df}{dr_{12}}\right)\left(\boldsymbol{\sigma}_j \cdot \mathbf{r}_j - \boldsymbol{\sigma}_j \cdot \mathbf{r}_i\right) - i\frac{1}{r_{12}}\frac{df}{dr_{12}}\left(T_i\left(\boldsymbol{\sigma}_j \cdot \mathbf{r}_j\right) - T_i\left(\boldsymbol{\sigma}_j \cdot \mathbf{r}_i\right)\right) \end{aligned} \tag{2.69}$$

The first term of Eq. (2.69) is reduced to the form of Eq. (2.60), as $\boldsymbol{\sigma}_j \cdot \mathbf{r}_j$ and $\boldsymbol{\sigma}_j \cdot \mathbf{r}_i$ are already discussed in the above paragraph. The second term of Eq. (2.69) is also reduced to the form of Eq. (2.60) by using the following equations,

$$\begin{aligned} T_i\left(\boldsymbol{\sigma}_j \cdot \mathbf{r}_j\right) &= 0 \\ T_i\left(\boldsymbol{\sigma}_j \cdot \mathbf{r}_i\right) &= \left(\boldsymbol{\sigma}_i \cdot \mathbf{p}_i\right)\left(\boldsymbol{\sigma}_j \cdot \mathbf{r}_i\right) = -i\boldsymbol{\sigma}_i \cdot \boldsymbol{\sigma}_j \end{aligned} \tag{2.70}$$

The operation of $\boldsymbol{\sigma}_i \cdot \boldsymbol{\sigma}_j$ is obvious and it operate the angular part.

For the third term of Eq. (2.62), we derive the formulation of the function $\left(T_j f(r_{12})\right)\cdot\left(T_i g(r_{12})\right)$. For the case of $i = j$, the following equation is easily obtained,

$$\left(T_i f(r_{12})\right)\cdot\left(T_i g(r_{12})\right) = \left(-i\frac{df}{dr_{12}}\boldsymbol{\sigma}_i \cdot \hat{\mathbf{r}}_{ij}\right)\left(-i\frac{dg}{dr_{12}}\boldsymbol{\sigma}_i \cdot \hat{\mathbf{r}}_{ij}\right) = -\frac{df}{dr_{12}}\frac{dg}{dr_{12}} \tag{2.71}$$

For the case of $i \neq j$, when we consider the special case $f(r_{12}) = r_{12}^{\,p}$, $g(r_{12}) = r_{12}^{\,q}$ and $p+q \neq 0$ and $p+q \neq 2$, we can use the following relationship,[11]

$$\left(T_j f(r_{12})\right)\cdot\left(T_i g(r_{12})\right) = \frac{pq}{(p+q)(p+q-2)}\left(T_j T_i r_{12}^{\,p+q}\right) + \frac{pq}{p+q-2} r_{12}^{\,p+q-2}\boldsymbol{\sigma}_j \cdot \boldsymbol{\sigma}_i \tag{2.72}$$

The right hand side of this equation is already discussed and, as a result, the third term of Eq. (2.62) is also reduced to the form of Eq. (2.60).

Thus, after the Hamiltonian operates $\zeta$ (Eq. (2.60)), the derived functions are also reduced to linear combination of $\zeta$. Therefore, the ICI wave function is expressed as only linear combination of $\zeta$.

Next, we introduce how to evaluate matrix elements. As discussed above, since the wave function can be written as the form $\zeta$, we only have to consider the matrix elements composed by the following bra and ket,

$$\begin{aligned} (bra) &= \left(T_i f_b(r_{12})\right)\cdot g_b(r_{12})\cdot R_b(r_1, r_2)\Theta_b(\hat{\mathbf{r}}_1, \hat{\mathbf{r}}_2) \\ (ket) &= \left(T_j f_k(r_{12})\right)\cdot g_k(r_{12})\cdot R_k(r_1, r_2)\Theta_k(\hat{\mathbf{r}}_1, \hat{\mathbf{r}}_2) \end{aligned} \tag{2.73}$$

As a result, the following integral is obtained,

$$I=\left\langle R_b(r_1,r_2)\Theta_b(\hat{\mathbf{r}}_1,\hat{\mathbf{r}}_2)\middle| g(r_{12})\cdot\left(T_i f(r_{12})\right)\middle| R_k(r_1,r_2)\Theta_k(\hat{\mathbf{r}}_1,\hat{\mathbf{r}}_2)\right\rangle \tag{2.74}$$

When evaluating the matrix element, the $T_i f(r_{12})$ part may be expanded by using Eq. (2.61) but singular type functions may be generated. These type integrals are singular but integrable, which are discussed in the next subsection. In special case $f(r_{12})=r_{12}{}^q$ and $g(r_{12})=r_{12}{}^p$, it is convenient to use the relations derived by Pestka,[11]

$$r_{12}{}^p\left(T_i r_{12}{}^q\right)=\begin{cases}\dfrac{q}{p+q}\left(T_i r_{12}{}^{p+q}\right) & (p+q\neq 0)\\ q\left(T_i \ln r_{12}\right) & (p+q=0)\end{cases} \tag{2.75}$$

$$\begin{aligned}&\left\langle R_b(r_1,r_2)\Theta_b(\hat{\mathbf{r}}_1,\hat{\mathbf{r}}_2)\middle|\left(T_i f(r_{12})\right)\middle| R_k(r_1,r_2)\Theta_k(\hat{\mathbf{r}}_1,\hat{\mathbf{r}}_2)\right\rangle\\ &=\left\langle T_i\left(R_b(r_1,r_2)\Theta_b(\hat{\mathbf{r}}_1,\hat{\mathbf{r}}_2)\right)\middle| f(r_{12})\middle| R_k(r_1,r_2)\Theta_k(\hat{\mathbf{r}}_1,\hat{\mathbf{r}}_2)\right\rangle\\ &\quad-\left\langle R_b(r_1,r_2)\Theta_b(\hat{\mathbf{r}}_1,\hat{\mathbf{r}}_2)\middle| f(r_{12})\middle| T_i\left(R_k(r_1,r_2)\Theta_k(\hat{\mathbf{r}}_1,\hat{\mathbf{r}}_2)\right)\right\rangle\end{aligned} \tag{2.76}$$

In the next subsection, although we discuss about these integrals, the logarithm function $\ln r_{12}$ is not considered. If you want to use our derived integration method, you should not use Eq. (2.75) but use Eq. (2.61) for $p+q=0$.

### 3.3.2 Integration including mild singular and/or singular potential, based on the Fourie transformation

In a general case, the integral we want to calculate is written as not spherically symmetric type,

$$I_1=\int f(r_1,r_2,r_{12})\cdot Y_{l_a}^{m_a*}(\vartheta_1,\varphi_1)Y_{l_b}^{m_b*}(\vartheta_2,\varphi_2)Y_{l_c}^{m_c}(\vartheta_1,\varphi_1)Y_{l_d}^{m_d}(\vartheta_2,\varphi_2)\cdot d\tau_1 d\tau_2 \tag{2.77}$$

Although this integral includes the spherical harmonics, we can reduce it to linear combination of spherically symmetric integrals. First, we formulate this procedure. By Edmonds book,[16] a product of the spherical harmonics is given by using the Wigner 3j-symbols and is reduced to a summation of the single spherical harmonic,

$$\begin{aligned}&Y_{l_a}^{m_a*}(\vartheta_1,\varphi_1)Y_{l_c}^{m_c}(\vartheta_1,\varphi_1)\\ &=(-1)^{m_a}\sum_{l=|l_a-l_c|}^{l_a+l_c}\left\{\frac{(2l_a+1)(2l_c+1)(2l+1)}{4\pi}\right\}^{1/2}\begin{pmatrix}l_a & l_c & l\\ 0 & 0 & 0\end{pmatrix}\begin{pmatrix}l_a & l_c & l\\ -m_a & m_c & -m\end{pmatrix}Y_l^m(\vartheta_1,\varphi_1)\end{aligned} \tag{2.78}$$

where $m = -m_a + m_c$ . A similar expression is appeared for electron 2: $Y_{l_b}^{m_b *}(\vartheta_2, \varphi_2) Y_{l_d}^{m_d}(\vartheta_2, \varphi_2)$. Therefore, the integral $I_1$ is reduced to a linear combination of the following type integral,

$$I_2 = \int f(r_1, r_2, r_{12}) \cdot Y_{l_1}^{m_1}(\vartheta_1, \varphi_1) Y_{l_2}^{m_2}(\vartheta_2, \varphi_2) \cdot d\tau_1 d\tau_2 \tag{2.79}$$

The integral variables can be separated into radial ( $r_1$, $r_2$, $r_{12}$ ) and angular ( $\vartheta_1$, $\varphi_1$, $\chi$ ) types with the volume element,

$$d\tau_1 d\tau_2 = r_1 r_2 r_{12} dr_1 dr_2 dr_{12} \cdot \sin\vartheta_1 d\vartheta_1 d\varphi_1 d\chi \tag{2.80}$$

where $\chi$ is the angle of rotation of the triangle formed by $\mathbf{r}_1$, $\mathbf{r}_2$ and $\mathbf{r}_{12}$ vectors. Although $\vartheta_2$ and $\varphi_2$ are not independent variables, $Y_{l_2}^{m_2}(\vartheta_2, \varphi_2)$ can be transformed as following by the rotation matrix relations,[16]

$$Y_{l_2}^{m_2}(\vartheta_2, \varphi_2) = \sum_m D_{m_2,m}^{l_2 *}(\varphi_1, \vartheta_1, \chi) Y_{l_2}^{m}(\vartheta_{12}, \varphi_{12}) \tag{2.81}$$

where $\vartheta_{12}$ and $\varphi_{12}$ are the polar angles of $\mathbf{r}_2$ relative to $\mathbf{r}_1$ and $D_{m_2,m}^{l_2}$ is the matrix element of the rotation operator defined in Edmonds book.[16,17] When substitution of this formula into the integral $I_2$ and integration over $\vartheta_1$, $\varphi_1$ and $\chi$ are performed,[18] we can obtain spherical symmetric type integral,

$$I_2 = 2\pi\delta_{m_1,m_2}\delta_{l_1,l_2} I_3(l_1) \tag{2.82}$$

$$I_3(l) = \int_0^\infty r_1 dr_1 \int_0^\infty r_2 dr_2 \int_{|r_1 - r_2|}^{r_1 + r_2} r_{12} dr_{12} \cdot f(r_1, r_2, r_{12}) P_l(\cos\vartheta_{12}) \tag{2.83}$$

where $P_l(\cos\vartheta_{12})$ is the Legendre polynomial and $\cos\vartheta_{12}$ is expressed by radial variables,

$$\cos\vartheta_{12} = \frac{r_1^2 + r_2^2 - r_{12}^2}{2 r_1 r_2} \tag{2.84}$$

The Legendre polynomial is expanded as a finite series polynomial since $l$ is an integer,

$$P_l(x) = \sum_{n=0}^{l} b_{n,l} x^n \tag{2.85}$$

where $b_{n,l}$ is a coefficient defined in some mathematical books written as the expansion form of the Legendre polynomial. By using the binomial theorem, $P_l(\cos\vartheta_{12})$ is expanded as follows,[19]

$$P_l(\cos\vartheta_{12}) = \sum_{n=0}^{l} \frac{b_{n,l}}{2^n} \sum_{k=0}^{n} {}_nC_k \sum_{m=0}^{k} {}_kC_m (-1)^m r_1^{2k-2m-n} r_2^{n-2k} r_{12}^{2m} \tag{2.86}$$

Substitution Eq. (2.86) into the integral $I_3(l)$ leads to a linear combination of the following type integral,

$$I_4 = \int_0^\infty r_1 dr_1 \int_0^\infty r_2 dr_2 \int_{|r_1-r_2|}^{r_1+r_2} r_{12} dr_{12} \cdot f(r_1, r_2, r_{12}) r_1^a r_2^b r_{12}^c \tag{2.87}$$

The integral $I_4$ can also be expressed as 6-coordinate integration of spherically symmetric type by

$$I_4 = \frac{1}{8\pi^2} \int f(r_1, r_2, r_{12}) r_1^a r_2^b r_{12}^c \cdot d\tau_1 d\tau_2 \tag{2.88}$$

Especially, we want to treat relativistic systems for atoms and molecules, whose wave function has a mild singularity at the poison of the nucleus and the collision point of electrons.[20] Moreover, to recover Ritz-type variational property, we might use the inverse Hamiltonian. To perform the inverse Hamiltonian approach, we have to calculate the expectation value of $H^2$, which includes $r^{-2}$ type singular potential. Even if we do not use the inverse Hamiltonian approach, we must impose some balance conditions to avoid the variational collapse. Even in this approach, the singular potentials ($r^{-2}$ and/or $\ln r$ type) are also appeared. The logarithm type potential ($\ln r$) can also be rewritten as $r^{-2}$ type singular potential. As a result, we have to calculate the following type integral when we use the Slater type orbital,

$$f(r_1, r_2, r_{12}) = r_1^{\gamma_1} \exp(-\alpha_1 r_1) \cdot r_2^{\gamma_2} \exp(-\alpha_2 r_2) \cdot r_{12}^{\gamma_{12}} \exp(-\alpha_{12} r_{12}) \tag{2.89}$$

$$I_5 = \int r_1^{l_1-(1+\delta_1)} \exp(-\alpha_1 r_1) \cdot r_2^{l_2-(1+\delta_2)} \exp(-\alpha_2 r_2) \cdot r_{12}^{l_{12}-(1+\delta_{12})} \exp(-\alpha_{12} r_{12}) \cdot d\tau_1 d\tau_2 \tag{2.90}$$

where $\alpha_1$, $\alpha_2$ and $\alpha_{12}$ are orbital exponents, $\gamma_1$, $\gamma_2$, $\gamma_{12}$, $\delta_1$, $\delta_2$ and $\delta_{12}$ are non-integer values ($\delta_1$, $\delta_2$ and $\delta_{12}$ indicate mild singularity) and $l_1$, $l_2$ and $l_{12}$ are positive integer values in general.

To evaluate the integral $I_5$, a simple way is to use an expansion method for the $r_{12}$ part. The following generalization was introduced by Sack,[12]

$$f(r_{12}) = \sum_{l=0}^{\infty} f_l(r_>, r_<) P_l(\cos\vartheta_{12}) \tag{2.91}$$

where $f(r_{12})$ is a function of $r_{12}$ and $P_l(\cos\vartheta_{12})$ is the Lengendre polynomial. $r_>$ and $r_<$ are defined as $r_> = \max(r_1, r_2)$ and $r_< = \min(r_1, r_2)$, respectively. This approach

was originally introduced by Pestka.[11] He presented some integrations including several $r_{12}$ types without $\exp(-\alpha_{12}r_{12})$ term: real powers of $r_{12}$, integer powers of $r_{12}$ and logarithm term ($\ln r_{12}$). Basically, the Sack expansion continues to infinite series but, in some cases, a summation might be truncated in finite series, for example, the case of the integer powers of $r_{12}$ more than and equal to -1. However, since we want to treat the integrals for relativistic systems, the integrals rather include the non-integer real powers of $r_{12}$ and singular types.[20] For these integrals, especially for singular types, the Sack expansion indicates very slow convergence behavior. In Table I, it is indicated how convergence is slow for the integral of singular types. To accelerate the convergence, a clever technique is known as the Levin's u transformation.[21] Table I also indicates how this transformation is powerful. The Levin's u transformation method indicates good convergence behavior even by the truncation on the small number of summations. However, since the optimum number of finite summations exists, it is difficult to achieve any precision. If you continue to calculate large number of summations, result rather converges to wrong value (show Table I). For the systems including heavy elements or in a strong magnetic field, since numerical instability is easily caused, the calculations of very high precision are needed.

So, we suggest the new integration method based on the Fourie transformation to overcome above problems. Moreover, in our method, the integrals may contain $\exp(-\alpha_{12}r_{12})$ term. In the method based on the Sack expansion, if $\exp(-\alpha_{12}r_{12})$ term is included in the integrals, the derived equations become very complicated. The idea of our method is simple. The summary of our method is follows: first, we transform the real spaces to the Fourie spaces separately performed in $r_1$, $r_2$ and $r_{12}$ and second, the integration over the real spaces is done, and finally, the integration over the Fourie spaces is performed. This procedure is often applied to calculate molecular integrals of Gaussian orbital. We indicate this method also shows good performance for Slater type singular integrals.

First, we summarize the Fourie transformations for some functions in Table II. Here, if the Fourie transformation is not defined (for example, the integrated value converging to infinity), our procedure may become no meaning. However, by using the method of the recursive evaluation,[22] the integrals even not defined Fourie transformation can be calculated. To evaluate the integral $I_5$, $I_5$ is redefined as $\Gamma_{l_1l_2l_{12}}$ : $\Gamma_{l_1l_2l_{12}} = I_5$ and the recurrence formula is written as,[22]

$$\Gamma_{l_1 l_2 l_{12}} = \left(\frac{\partial}{\partial \alpha_1}\right)^{l_1}\left(\frac{\partial}{\partial \alpha_2}\right)^{l_2}\left(\frac{\partial}{\partial \alpha_{12}}\right)^{l_{12}}\Gamma_{000}$$
$$\Gamma_{000} = \int \frac{\exp(-\alpha_1 r_1)}{r_1^{1+\delta_1}} \cdot \frac{\exp(-\alpha_2 r_2)}{r_2^{1+\delta_2}} \cdot \frac{\exp(-\alpha_{12} r_{12})}{r_{12}^{1+\delta_{12}}} \cdot d\tau_1 d\tau_2 \tag{2.92}$$

As a result, we only have to evaluate $\Gamma_{000}$.

Next, we describe the procedure of the integration of $\Gamma_{000}$ from simple cases. The simplest one is the case $\alpha_{12}=0$, $\delta_1=0, \delta_2=0$ and $\delta_{12}=0$,

$$I^{(1)} = \int \frac{\exp(-\alpha_1 r_1)}{r_1} \cdot \frac{\exp(-\alpha_2 r_2)}{r_2} \cdot \frac{1}{r_{12}} \cdot d\tau_1 d\tau_2 \tag{2.93}$$

The Fourie transformations are performed in $r_1$, $r_2$ and $r_{12}$ parts separately by using the equations presented in Table II,

$$I^{(1)} = \frac{1}{\left(8\pi^3\right)^3} \int d\mathbf{r}_1 d\mathbf{r}_2 d\mathbf{q}_1 d\mathbf{q}_2 d\mathbf{p} \cdot e^{i\mathbf{q}_1 \cdot \mathbf{r}_1} e^{i\mathbf{q}_2 \cdot \mathbf{r}_1} e^{i\mathbf{p}\cdot(\mathbf{r}_1 - \mathbf{r}_2)} \cdot \frac{4\pi}{q_1^2 + \alpha_1^2} \cdot \frac{4\pi}{q_2^2 + \alpha_2^2} \cdot \frac{4\pi}{p^2} \tag{2.94}$$

The integration is performed over $\mathbf{r}_1$ and $\mathbf{r}_2$,

$$I^{(1)} = \frac{1}{8\pi^6} \int d\mathbf{q}_1 d\mathbf{q}_2 d\mathbf{p} \cdot \frac{1}{q_1^2 + \alpha_1^2} \cdot \frac{1}{q_2^2 + \alpha_2^2} \cdot \frac{1}{p^2} \cdot 8\pi^3 \delta(\mathbf{q}_1 + \mathbf{p}) \cdot 8\pi^3 \delta(\mathbf{q}_2 - \mathbf{p}) \tag{2.95}$$

where $\delta(\mathbf{x})$ is the Dirac delta function and we used the following integration of the delta function,

$$\int e^{i\mathbf{k}\cdot\mathbf{x}} d\mathbf{x} = 8\pi^3 \delta(\mathbf{k}) \tag{2.96}$$

The integration over $\mathbf{q}_1$ and $\mathbf{q}_2$ is evident,

$$I^{(1)} = 8 \int d\mathbf{p} \cdot \frac{1}{p^2 + \alpha_1^2} \cdot \frac{1}{p^2 + \alpha_2^2} \cdot \frac{1}{p^2} \tag{2.97}$$

Thus, the integral is reduced to one-particle integration. We use the polar coordinates as $\mathbf{p}$ and integrate the angular part,

$$I^{(1)} = 32\pi \int_0^\infty dp \cdot \frac{1}{p^2 + \alpha_1^2} \cdot \frac{1}{p^2 + \alpha_2^2} \tag{2.98}$$

This is a one-dimensional integral and elementally integrated,

$$I^{(1)} = \frac{16\pi^2}{\alpha_1 \alpha_2 (\alpha_1 + \alpha_2)} \tag{2.99}$$

Next, we apply our method to the following singular type integral,

$$I^{(2)} = \int \frac{\exp(-\alpha_1 r_1)}{r_1} \cdot \frac{\exp(-\alpha_2 r_2)}{r_2} \cdot \frac{1}{r_{12}^{\ 2}} \cdot d\tau_1 d\tau_2 \tag{2.100}$$

When using the method based on the Sack expansion, the expansion continues to infinity and indicates very slow convergence. However, when using the based on the Fourie transformation, the integral can be written in a closed form. The procedure of the integration is the same as $I^{(1)}$,

$$\begin{aligned} I^{(2)} &= \frac{1}{\left(8\pi^3\right)^3} \int d\mathbf{r}_1 d\mathbf{r}_2 d\mathbf{q}_1 d\mathbf{q}_2 d\mathbf{p} \cdot e^{i\mathbf{q}_1 \cdot \mathbf{r}_1} e^{i\mathbf{q}_2 \cdot \mathbf{r}_1} e^{i\mathbf{p} \cdot (\mathbf{r}_1 - \mathbf{r}_2)} \cdot \frac{4\pi}{\alpha_1^{\ 2} + q_1^{\ 2}} \cdot \frac{4\pi}{\alpha_2^{\ 2} + q_2^{\ 2}} \cdot \frac{2\pi^2}{p} \\ &= 4\pi \int d\mathbf{p} \cdot \frac{1}{\alpha_1^{\ 2} + p^2} \cdot \frac{1}{\alpha_2^{\ 2} + p^2} \cdot \frac{1}{p} = 16\pi^2 \int_0^\infty dp \cdot \frac{p}{\left(\alpha_1^{\ 2} + p^2\right)\left(\alpha_2^{\ 2} + p^2\right)} \\ &= \begin{cases} 16\pi^2 \ln\left(\dfrac{\alpha_1}{\alpha_2}\right) \dfrac{1}{\alpha_1^{\ 2} - \alpha_2^{\ 2}} & (\alpha_1 \neq \alpha_2) \\ \dfrac{8\pi^2}{\alpha_1^{\ 2}} & (\alpha_1 = \alpha_2) \end{cases} \end{aligned} \tag{2.101}$$

More generally, we introduce the integral including a mild singularity and/or singularity potential, that is, non-integer powers of $r_1$, $r_2$ and $r_{12}$. This integral is appeared when we introduce mild singularities into the wave function to express the boundary conditions at the collision points of two particles,

$$I^{(3)} = \int \frac{\exp(-\alpha_1 r_1)}{r_1^{1+\delta_1}} \cdot \frac{\exp(-\alpha_2 r_2)}{r_2^{1+\delta_2}} \cdot \frac{1}{r_{12}^{1+\delta_{12}}} \cdot d\tau_1 d\tau_2 \tag{2.102}$$

Even in this case, the procedure of the integration is same as $I^{(1)}$ and $I^{(2)}$, but the final one-dimensional integration is difficult to write down an analytical closed form. Therefore, in the final step of the integration, one-dimensional numerical integration is needed. However, the several mathematical tools for one-dimensional numerical integration are available and easy to use. So, we can get the results of any precision without any difficulty,

$$\begin{aligned} I^{(3)} = 32\pi^{\frac{3}{2}} & \frac{\Gamma(1-\delta_1)\Gamma(1-\delta_2)\Gamma(1-\delta_{12}/2)}{2^{\delta_{12}}\Gamma((1+\delta_{12})/2)} \\ & \int_0^\infty dp \cdot \frac{\sin\left((1-\delta_1)\arctan\left(p/\alpha_1\right)\right)\sin\left((1-\delta_2)\arctan\left(p/\alpha_2\right)\right)}{\left(\alpha_1^{\ 2} + p^2\right)^{\frac{1-\delta_1}{2}} \left(\alpha_2^{\ 2} + p^2\right)^{\frac{1-\delta_2}{2}} p^{2-\delta_{12}}} \quad (\delta_1, \delta_2 \neq 1) \end{aligned}$$

(2.103)

$$I^{(3)} = 32\pi^{\frac{3}{2}} \frac{\Gamma(1-\delta_{12}/2)}{2^{\delta_{12}}\Gamma((1+\delta_{12})/2)} \int_0^\infty dp \cdot \frac{\arctan(p/\alpha_1)\arctan(p/\alpha_2)}{p^{2-\delta_{12}}} \quad (\delta_1 = \delta_2 = 1)$$

(2.104)

Finally, we treat the integral including $\exp(-\alpha_{12}r_{12})$ as the most general case,

$$I^{(4)} = \int \frac{\exp(-\alpha_1 r_1)}{r_1^{1+\delta_1}} \cdot \frac{\exp(-\alpha_2 r_2)}{r_2^{1+\delta_2}} \cdot \frac{\exp(-\alpha_{12} r_{12})}{r_{12}^{1+\delta_{12}}} \cdot d\tau_1 d\tau_2 \qquad (2.105)$$

The procedure of the integration is also same as $I^{(1)}$, $I^{(2)}$ and $I^{(3)}$,

$$I^{(4)} = 32\pi \cdot \Gamma(1-\delta_1)\Gamma(1-\delta_2)\Gamma(1-\delta_{12}) \cdot \int_0^\infty dp \cdot \frac{\sin((1-\delta_1)\arctan(p/\alpha_1))\sin((1-\delta_2)\arctan(p/\alpha_2))\sin((1-\delta_{12})\arctan(p/\alpha_{12}))}{(\alpha_1^2+p^2)^{\frac{1-\delta_1}{2}}(\alpha_2^2+p^2)^{\frac{1-\delta_2}{2}}(\alpha_{12}^2+p^2)^{\frac{1-\delta_{12}}{2}} p}$$

$$(\delta_1, \delta_2, \delta_{12} \neq 1)$$

(2.106)

$$I^{(4)} = 32\pi \cdot \Gamma(1-\delta_{12}) \int_0^\infty dp \cdot \frac{\arctan(p/\alpha_1)\arctan(p/\alpha_2)\sin((1-\delta_{12})\arctan(p/\alpha_{12}))}{(\alpha_{12}^2+p^2)^{\frac{1-\delta_{12}}{2}} p}$$

$$(\delta_1 = \delta_2 = 1, \delta_{12} \neq 1)$$

(2.107)

$$I^{(4)} = 32\pi \cdot \Gamma(1-\delta_1)\Gamma(1-\delta_2) \int_0^\infty dp \cdot \frac{\sin((1-\delta_1)\arctan(p/\alpha_1))\sin((1-\delta_2)\arctan(p/\alpha_2))\arctan(p/\alpha_{12})}{(\alpha_1^2+p^2)^{\frac{1-\delta_1}{2}}(\alpha_2^2+p^2)^{\frac{1-\delta_2}{2}} p}$$

$$(\delta_1, \delta_2 \neq 1, \delta_{12} = 1)$$

(2.108)

Table I summarize the numerical tests for the integrals containing some singular and/or mild singular potentials, compared three methods: based on Sack expansion, Levin's u transformation and our method based on the Fourie transformation. In our method, without any difficulty, arbitrary high precision results were obtained. Our method is suitable for numerically unstable systems required the calculations of very high accuracy.

**Table I.** The values of some integrals including singular and/or mild singular potentials are compared among three methods: based on (a) Sack expansion, (b) Livin's u transformation and (c) Fourie transformation. (a), (b): truncated values. The calculated integrals are

(1) $\int \exp(-4.0r_1)/r_1^{0.4} \cdot \exp(-4.0r_2)/r_2^{0.4} \cdot 1/r_{12}^{\ 2} \cdot d\tau_1 d\tau_2$

(2) $\int \exp(-4.0r_1)/r_1^{2.2} \cdot \exp(-4.0r_2)/r_2^{0.4} \cdot r_{12}^{\ 2.2} \cdot d\tau_1 d\tau_2$

(3) $\int \exp(-4.0r_1)/r_1^{2.2} \cdot \exp(-4.0r_2)/r_2^{0.4} \cdot \exp(1.0r_{12})/r_{12}^{\ 2.2} \cdot d\tau_1 d\tau_2$

(a), (b): $l_{max}$ is the maximum number of truncated series and (c): "digits" means the digits calculating the integrals numerically. For (a) and (b), the digits are 35.

| $l_{max}$ or digits | The values of integrals |
|---|---|
| | Integral: (1) |
| $l_{max}$ | Method: (a) / Method: (b) |
| 15 | **0.8**98 568 067 005 019 740 835 326 0 / **0.913 972 803 776** 504 482 961 637 1 |
| 25 | **0.9**04 489 523 947 944 876 268 713 4 / **0.913 972 803 776 404 450 881** 847 7 |
| 35 | **0.907** 123 042 135 819 948 624 077 5 / **0.913 972 803 776 404** 466 732 324 5 |
| 100 | **0.911** 531 057 999 935 220 263 087 6 / 1.14 182 111 755 594 841 692 406 1 |
| 1000 | **0.913** 726 430 237 247 700 212 819 2 / 1.37 213 701 017 433 056 705 955 7 |
| 10000 | **0.913** 948 144 247 432 833 414 951 8 / 1.05 818 605 386 020 691 120 436 6 |
| digits | Method: (c) |
| 15 | **0.913 972 803 776 404** 7 |
| 25 | **0.913 972 803 776 404 450 881 724** 1 |
| 35 | **0.913 972 803 776 404 450 881 724 448 757 147 37** |
| | Integral: (2) |
| $l_{max}$ | Method: (a) / Method: (b) |
| 15 | **36**.7 802 106 933 377 616 144 229 8 / **37.7 950 015 297 81**6 573 616 799 3 |
| 25 | **37**.1 061 336 379 181 798 150 357 7 / **37.7 950 015 297 818 153 006** 232 2 |
| 35 | **37**.2 637 925 828 120 850 653 472 8 / **37.7 950 015 297 818 14**6 249 898 5 |
| 100 | **37**.5 621 025 066 943 999 105 382 7 / 27.0 963 819 413 190 799 516 733 3 |
| 1000 | **37.7** 578 109 341 805 843 491 216 7 / 26.5 463 899 186 041 635 484 954 4 |
| 10000 | **37.7 8**91 027 622 489 510 205 044 8 / 33.7 239 711 718 475 314 487 396 0 |
| digits | Method: (c) |
| 15 | **37.7 950 015 297 818 1** |
| 25 | **37.7 950 015 297 818 153 006 123** 5 |
| 35 | **37.7 950 015 297 818 153 006 124 096 368 611 98** |
| | Integral: (3) |
| digits | Method: (c) |
| 15 | **-32.4 574 194 267 573** |
| 25 | **-32.4 574 194 267 572 455 930 304 4** |
| 35 | **-32.4 574 194 267 572 455 930 304 429 479 573 25** |

**Table II.** The Fourie transformation forms of some functions are tabulated.

| Function: $f(\mathbf{r})$ | Fourie transformation: $F(\mathbf{k})$ |
|---|---|
| $\frac{1}{r}$ | $\frac{4\pi}{k^2}$ |
| $\frac{e^{-\alpha r}}{r}$ | $\frac{4\pi}{\alpha^2+k^2}$ |
| $\frac{1}{r^2}$ | $\frac{2\pi^2}{k}$ |
| $\frac{e^{-\alpha r}}{r^2}$ | $\frac{4\pi}{k}\cdot\arctan\left(\frac{k}{\alpha}\right)$ |
| $\frac{1}{r^{1+\delta}}$ $(\delta<2)$ | $\frac{4\pi^{3/2}}{2^{\delta}}\cdot\frac{\Gamma\left(1-\frac{\delta}{2}\right)}{\Gamma\left(\frac{1+\delta}{2}\right)}\cdot\frac{1}{k^{2-\delta}}$ |
| $\frac{e^{-\alpha r}}{r^{1+\delta}}$ $(\delta<2,\ \delta\neq 1)$ | $4\pi\cdot\Gamma(1-\delta)\cdot\frac{\sin\left((1-\delta)\arctan\left(\frac{k}{\alpha}\right)\right)}{k\left(\alpha^2+k^2\right)^{\frac{1-\delta}{2}}}$ |

## 4. Results

### 4.1 Dirac oscillator

We first performed the ICI calculations of the Dirac oscillator using the scaling $g$ and initial functions given by Eq. (2.34) and (2.35). The Dirac oscillator is simple but unique system, in the sense having the force field expressed as vector potential like systems in a magnetic field and not having scalar potential: $V=0$. Any singularity point is not appeared in the Hamiltonian. We summarize in Table III the calculated energies at the different iteration cycles by using both the inverse and regular DE at the diagonalization step. One can see that as the iteration proceeds, the energy approaches the exact value in the both cases using the inverse and regular DE. Figure 2 shows the convergence behavior of the energy.

When we used the inverse DE at the diagonalization step, the Ritz-type variational property held and the energy approached the exact value from above. However, when we used the regular DE, the energies of the odd number iteration were higher than the

previous ones of the even number iteration. It means the Ritz-type variational property is not always satisfied when using the regular DE. However, as shown in Sec. 2.3, our ICI method has a possibility that the balancing condition that the relativistic Hamiltonian demands is automatically satisfied. Although we do not impose any constraint to the wave function as satisfied balancing condition like the kinetic balance, the energy and wave function approach the exact ones. It means that the ICI wave function is automatically satisfied the balancing – i.e., ICI balance. The free ICI dimensions of the large and small components increases one by one by turns, which indicates that the wave functions of the large and small components are improved by turns at the iteration step.

**Table III.** Relativistic free ICI energy (a.u.) of the Dirac oscillator using the inverse DE and regular DE at the diagonalization step.

| n[a] | M[b] | Energy (Inverse)[c] | Energy (Regular)[d] |
|---|---|---|---|
| 0 | 2 (1,1) | **1.28** 120 131 | **1.05** 622 029 |
| 1 | 3 (1,2) | **1.16** 873 260 | **1.16** 871 363 |
| 2 | 4 (2,2) | **1.03** 096 361 | **1.00** 404 106 |
| 3 | 5 (2,3) | **1.01** 863 331 | **1.01** 862 955 |
| 4 | 6 (3,3) | **1.00** 298 146 | **1.00 0**24 500 |
| 5 | 7 (3,4) | **1.00** 172 325 | **1.00** 172 271 |
| 6 | 8 (4,4) | **1.00 0**22 290 | **0.999** 990 329 |
| 7 | 9 (4,5) | **1.00 0**11 503 | **1.00 0**11 497 |
| 8 | 10 (5,5) | **0.999** 992 070 | **0.999** 974 394 |
| 9 | 11 (5,6) | **0.999** 983 830 | **0.999** 983 825 |
| 10 | 12 (6,6) | **0.999** 974 689 | **0.999 973** 435 |
| 11 | 13 (6,7) | **0.999** 974 103 | **0.999** 974 102 |
| 12 | 14 (7,7) | **0.999 973** 464 | **0.999 973 3**79 |
| 13 | 15 (7,8) | **0.999 973** 424 | **0.999 973** 424 |
| 14 | 16 (8,8) | **0.999 973 3**81 | **0.999 973 376** |
| Exact | | 0.999 973 376 | 0.999 973 376 |

a Iteration number.

b Number of the independent functions for expanding $\psi$ : M ($M_L$, $M_S$).

c Using the inverse DE with energy shift $W = 0$.

d Using the regular DE.

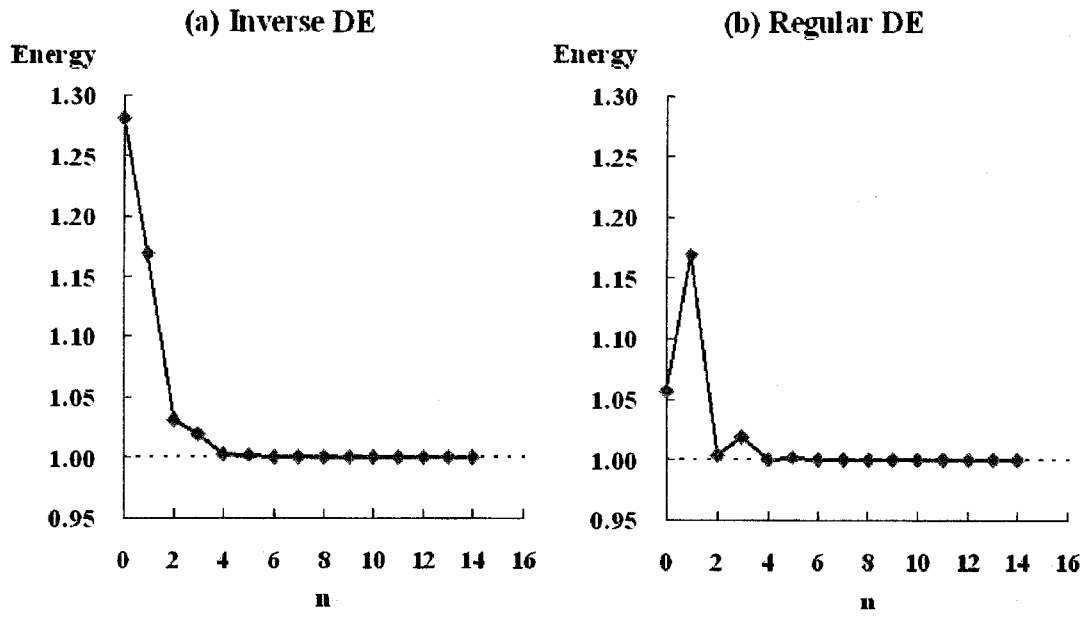


**Fig.2** Convergence behavior of the free ICI energy (a.u.) of the Dirac oscillator during the iteration process. At the diagonalization step, (a) using inverse DE and (b) using regular DE. The dotted line shows the exact energy.

### 4.2 Hydrogenlike atoms

Next application of our theory is to the hydrogen isoelectronic atoms. We performed the calculations for H (Z=1) and $Fe^{25+}$ (Z=26), the relativistic effect is larger for the latter one. The Hamiltonian of these systems contains the Coulomb potential expressed through scalar potential and this potential is singular at the nucleus position. Vector potential is not included in the Hamiltonian: $A = 0$. The case including both scalar and vector potentials will be studied in the next chapter, in which the hydrogen and helium atoms in a magnetic field will be discussed. To overcome the singularity problem, we must use the ICI method based on the scaled DE (SDE) and introduce the $g$ function to eliminate the singularity. Moreover, in the relativistic case, a mild singularity of the boundary condition at the collision point of two particles becomes so important for the rapid convergence of the wave function to the exact one.

We first performed the calculations using the $g$ and initial function given by Eq. (2.44) and Eq. (2.45). This set is the simplest case, which was also used in the nonrelativistic calculations of the hydrogen atom.[4,5] From this set of the $g$ and initial function, the ICI method does not generate the wave functions to express mild singularity. So, too much iteration is needed to represent mild singularity. Table IV

**Table IV.** Relativistic free ICI energy (a.u.) of the hydrogenlike atoms (H and $Fe^{25+}$) using the inverse DE and regular DE at the diagonalization step. The $g$ and initial functions $\psi_0$ are Eq. (2.44) and Eq. (2.45): $g = r$ and $\psi_0^L = \psi_0^S = \exp(-\alpha r)$.

| n[a] | M[b] | Energy (Inverse)[c] | | Energy (Regular)[d] | |
|---|---|---|---|---|---|
| | | H | $Fe^{25+}$ | H | $Fe^{25+}$ |
| 0 | 2 | -0.375 003 751 | -256. 766 190 | -0.375 033 696 | -268. 305 490 |
| 1 | 4 | **-0.491** 029 055 | **-334.** 026 658 | **-0.491** 031 920 | **-334.** 942 314 |
| 2 | 6 | **-0.499** 322 801 | **-340.** 615 512 | **-0.499** 323 117 | **-340.** 773 616 |
| 3 | 8 | **-0.499 960** 719 | **-340.** 974 209 | **-0.499 960** 747 | **-341. 043** 175 |
| 4 | 10 | **-0.500 003** 894 | **-341. 042** 733 | **-0.500 003** 896 | **-341. 097** 636 |
| 5 | 12 | **-0.500 006** 498 | **-341. 047** 632 | **-0.500 006** 499 | **-341. 094** 546 |
| 6 | 14 | **-0.500 006 649** | **-341. 054** 972 | **-0.500 006 649** | **-341. 096** 270 |
| 7 | 16 | **-0.500 006 657** | **-341. 059** 530 | **-0.500 006 657** | **-341. 096** 410 |
| Exact | | -0.500 006 657 | -341. 097 839 | -0.500 006 657 | -341. 097 839 |

a Iteration number.

b Number of the independent functions for expanding. Half and half for the large and small components.

c Using the inverse DE with energy shift $W = 0$.

d Using the regular DE.

shows the calculated energies using both the inverse and regular DE at different iteration cycles. For H (Z=1), when using the inverse DE, the Ritz-type variational property held and the energy approached the exact values from above. Even when we used the regular DE, we had never experienced the variational collapse and the energy approached the exact ones from above as well as using the inverse DE. For $Fe^{25+}$, however, the speed of convergence to the exact values is too slow because the singular behavior at the nucleus position is more important than H (the relativistic effect becomes more dominant than H) and not expressed well by using this set of the $g$ and initial function.

We next performed the calculations using the $g$ and initial functions given by Eq. (2.46) and Eq. (2.47). The $g$ function is same but the initial function is different from the calculations of the previous paragraph: Eq. (2.47) contains a mild singularity term $\gamma_k$ given by Eq. (2.39). The calculated energies are shown in Table V. For H, the results implied the good performance as well as the results in Table IV in the both cases using the inverse and regular DE. Moreover, even for $Fe^{25+}$, we can see the good performance to converge to the exact values in a few iterations. This means that mild singularity is a very important boundary condition to achieve the rapid convergence to the exact solution especially for the atoms including heavier elements.

**Table V.** Relativistic free ICI energy (a.u.) of the hydrogenlike atoms (H and $Fe^{25+}$) using the inverse DE and regular DE at the diagonalization step. The $g$ and initial functions $\psi_0$ are Eq. (2.46) and Eq. (2.47): $g = r$ and $\psi_0^{\,L} = \psi_0^{\,S} = r^{\gamma_k - 1}\exp(-\alpha r)$.

| n[a] | M[b] | Energy (Inverse)[c] | | Energy (Regular)[d] | |
|---|---|---|---|---|---|
| | | H | $Fe^{25+}$ | H | $Fe^{25+}$ |
| 0 | 2 | -0.374 983 782 | -247. 784 272 | -0.375 013 729 | -259. 769 430 |
| 1 | 4 | **-0.49**1 029 607 | **-33**4. 343 616 | **-0.49**1 032 471 | **-33**5. 218 737 |
| 2 | 6 | **-0.499** 322 521 | **-340.** 577 772 | **-0.499** 322 837 | **-340.** 652 714 |
| 3 | 8 | **-0.499** 960 764 | **-341. 0**62 769 | **-0.499** 960 792 | **-341. 0**68 195 |
| 4 | 10 | **-0.500 00**3 884 | **-341. 09**5 716 | **-0.500 00**3 886 | **-341. 09**6 059 |
| 5 | 12 | **-0.500 006** 501 | **-341. 097** 719 | **-0.500 006** 501 | **-341. 097** 739 |
| 6 | 14 | **-0.500 006 648** | **-341. 097 832** | **-0.500 006 648** | **-341. 097 833** |
| 7 | 16 | **-0.500 006 657** | **-341. 097 839** | **-0.500 006 657** | **-341. 097 839** |
| Exact | | -0.500 006 657 | -341. 097 839 | -0.500 006 657 | -341. 097 839 |

a Iteration number.

b Number of the independent functions for expanding. Half and half for the large and small components.

c Using the inverse DE with energy shift $W = 0$.

d Using the regular DE.

In the previous paragraph, we had a mild singularity contained in the initial function. This is a one choice to satisfy the boundary condition at the nucleus position. But, in the hydrogenlike atoms, since we know the exact solutions, the term $\gamma_k$ given by Eq. (2.39) can be adopted the exact one and this may be an artificial choice. To examine our ICI wave function can be converged to the exact solutions by using the arbitrary set of the $g$ and initial functions without variational collapse, we performed the calculations using $g$ and initial functions given by Eq. (2.48) and Eq. (2.49), in which a mild singularity is expressed in the $g$ function. The results are given in Table VI and Figure 3 shows the convergence behavior of the energy using the regular DE for $Fe^{25+}$. In spite of the irresponsible choice of the singular value $g = r^{99/100}$, the energy approaches to the exact value in the both cases using the inverse and regular DE for both H and $Fe^{25+}$. It means that one can be permitted to choose the $g$ and initial functions arbitrary but one should have the wave function satisfy the boundary condition at the nucleus by including mild singularity in the wave function.

In Table VII, we calculated the difference between our ICI wave functions and the exact ones defined by the following equation to describe the convergence behavior of the wave function,

**Table VI.** Relativistic free ICI energy (a.u.) of the hydrogenlike atoms (H and $Fe^{25+}$) using the inverse DE and regular DE at the diagonalization step. The $g$ and initial functions $\psi_0$ are Eq. (2.48) and Eq. (2.49): $g = r^{99/100}$ and $\psi_0^{\,L} = \psi_0^{\,S} = \exp(-\alpha r)$.

| n[a] | M[b] | Energy (Inverse)[c] | | Energy (Regular)[d] | |
|---|---|---|---|---|---|
| | | H | $Fe^{25+}$ | H | $Fe^{25+}$ |
| 0 | 2 | **-0.**375 003 751 | -256. 766 190 | **-0.**375 033 696 | -268. 305 490 |
| 1 | 6 | **-0.**492 424 140 | **-335.** 917 982 | **-0.**493 381 703 | **-336.** 985 793 |
| 2 | 12 | **-0.499** 744 052 | **-340.** 915 434 | **-0.499** 822 155 | **-340.** 983 739 |
| 3 | 20 | **-0.500 002** 351 | **-341. 09**4 866 | **-0.500 00**4 337 | **-341. 096** 421 |
| 4 | 30 | **-0.500 006** 621 | **-341. 097** 814 | **-0.500 006** 642 | **-341. 097 829** |
| 5 | 42 | **-0.500 006 657** | **-341. 097 839** | **-0.500 006 657** | **-341. 097 839** |
| Exact | | -0.500 006 657 | -341. 097 839 | -0.500 006 657 | -341. 097 839 |

a Iteration number.

b Number of the independent functions for expanding. Half and half for the large and small components.

c Using the inverse DE with energy shift $W = 0$.

d Using the regular DE.

$$\Delta_{L\,or\,S} = \left[ \int \left| \psi_{ICI}^{\;L\,or\,S} - \psi_{exact}^{\;L\,or\,S} \right|^2 d\tau \right]^{1/2} \tag{2.109}$$

$\Delta$ of the large and small components using the regular DE for $Fe^{25+}$ was calculated. As shown in Table VII, the ICI wave function itself also converges to the exact one as well as the energy. Moreover, the large and small components are simultaneously improved during the iteration proceeds. This means ICI balance works well for both the large and small components and the variational collapse is not appeared as far as we do ICI. Therefore, it is unnecessary to resort the inverse DE.

**Table VII.** The difference $\Delta$ between the exact and ICI wave function for both large and small components of $Fe^{25+}$ using the regular DE. The $g$ and initial functions $\psi_0$ are Eq. (2.48) and Eq. (2.49): $g = r^{99/100}$ and $\psi_0^{\,L} = \psi_0^{\,S} = \exp(-\alpha r)$.

| n[a] | M[b] | $\Delta^L$ ($Fe^{25+}$) | $\Delta^S$ ($Fe^{25+}$) |
|---|---|---|---|
| 0 | 2 | $3.3 \times 10^{-1}$ | $3.3 \times 10^{-1}$ |
| 1 | 6 | $9.8 \times 10^{-2}$ | $7.1 \times 10^{-2}$ |
| 2 | 12 | $1.6 \times 10^{-2}$ | $1.1 \times 10^{-2}$ |
| 3 | 20 | $1.6 \times 10^{-3}$ | $1.2 \times 10^{-3}$ |
| 4 | 30 | $1.2 \times 10^{-4}$ | $9.0 \times 10^{-5}$ |
| 5 | 42 | $7.2 \times 10^{-6}$ | $5.3 \times 10^{-6}$ |
| Exact | | 0 | 0 |

a Iteration number.

b Number of the independent functions for expanding. Half and half for the large and small components.

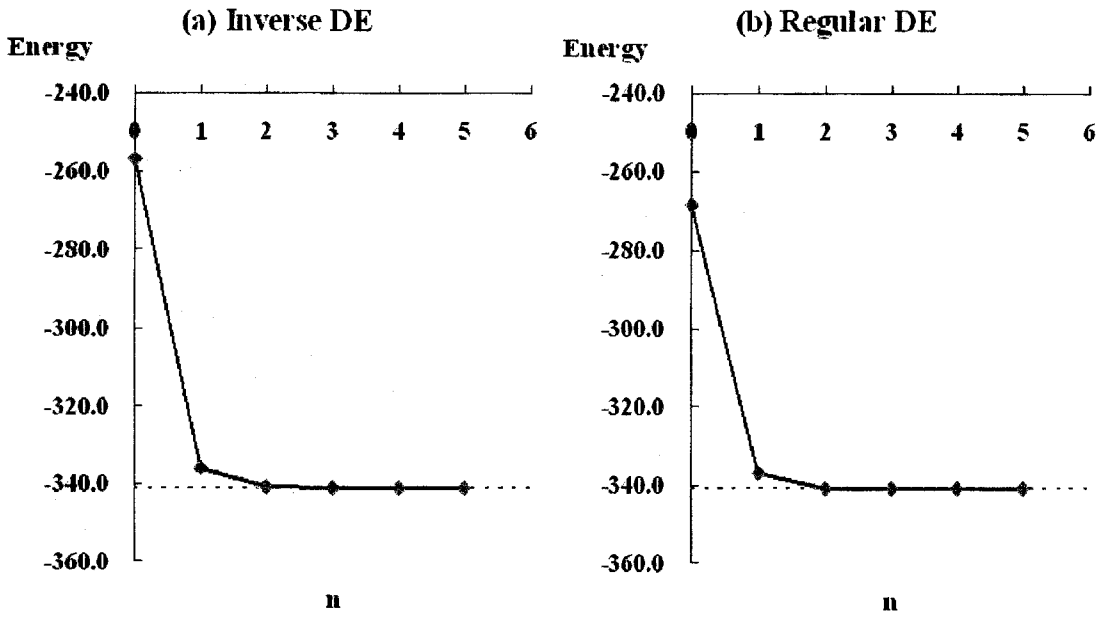


**Fig.3** Convergence behavior of the free ICI energy (a.u.) of $Fe^{25+}$ during the iteration process. The set of $g$ and initial function $\psi_0$ is Eq. (2.48) and Eq. (2.49): $g = r^{99/100}$ and $\psi_0^L = \psi_0^S = \exp(-\alpha r)$. At diagonalization step, (a) using inverse DE and (b) using regular DE. The dotted line shows the exact energy.

### 4.3 Heliumlike atoms

The next application is to the helimulike two-electron atoms. We calculated He (Z=2) and $Th^{88+}$ (Z=90) by using the $g$ and initial functions given by Eq. (2.57) and Eq. (2.58). First, we performed the calculations using the inverse DCE. Table VIII shows the results. One can see that as the iteration proceeds, the energy approaches the reference values from above (actually, the inverse energy converged from below). It means that the method using the inverse DCE at the diagonalization step can be utilized for solving the many-electron DCE, not only for solving the one-electron DE.[13] In Table VIII, for He, the energy of Ref 23 is more accurate than that of Ref 7: the former included $r_{12}$ explicitly, but the latter did not.[7,23] In these reference calculations,[7,23] the wave functions were made as satisfied the kinetic balance condition. We note here that the kinetic balance is an approximate one of the strict balance conditions and it is the simplest $0^{th}$ order of the atomic balance conditions. Moreover, it is difficult to satisfy the kinetic balance strictly for the many-electron DCE. For $Th^{88+}$, the value cited Ref 7 is due to the calculations not including $r_{12}$ explicitly.[7] Since we used the inverse Hamiltonian, the present energy given in Table VIII should be an upper bound of the true energy. For $Th^{88+}$, the reference value is lower than that of our ICI method. To

**Table VIII.** Relativistic free ICI energy (a.u.) of the heliumlike atoms (He and $Th^{88+}$) using the inverse DCE at the diagonalization step.

| n[a] | M[b] | Energy (H)[c] | Energy ($Th^{88+}$)[c] |
|---|---|---|---|
| 0 | 3 (1,1,1) | **-2.**75 008 563 | **-9166.** 575 433 |
| 1 | 12 (4,4,4) | **-2.88** 771 973 | **-9166.** 809 415 |
| 2 | 38 (12,13,13) | **-2.90 3**07 277 | **-9166. 8**58 084 |
| 3 | 105 (29,35,41) | **-2.90 375** 350 | **-9166. 88**1 423 |
| 4 | 224 (66,69,89) | **-2.90 384** 265 | **-9166. 89**4 218 |
| 5 | 482 (145,139,198) | **-2.90 385** 116 | **-9166. 90**3 050 |
| 6 | 852 (257,223,342) | **-2.90 385** 405 | **-9166. 90**7 227 |
| 7 | 1357(458,330,569) | **-2.90 385** 511 | |
| Ref. 7 | | -2.90 263 6 | -9166. 927 2 |
| Ref. 23 | | -2.90 385 7 | |

a Iteration number.

b Number of the independent functions for expanding $\psi$ : M ($M_{ll}$, $M_{ls}$, $M_{ss}$).

c Using the inverse DE with energy shift $W = c$ .

expect the true energy for $Th^{88+}$, we estimated the extrapolation value at the iteration $\infty$ from our results using the inverse DCE. First, we define the difference of the energies $E_n$ as

$$\Delta_{n+1} = E_{n+1} - E_n \tag{2.110}$$

Next, we plot $\Delta_n$ at logarithm order and we assume $\log_{10}(-\Delta_n)$ obeys the involution function, which is determined by the least square method from our results. Finally, the extrapolation value at the large iteration number is estimated by the recursion formula Eq. (2.110). In our case, we obtained $\log_{10}(-\Delta_n) = -0.7014 \cdot n^{0.7074}$ by the least square method from the results shown in Table VIII. The extrapolation value at the iteration $\infty$ was -9166. 910 880. Therefore, the true energy for $Th^{88+}$ might be higher than the reference value and the variational collapse might occur in the reference calculation.[7]

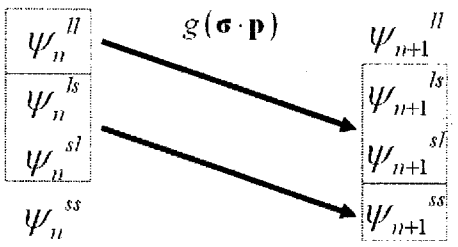


**Fig.4** The new definition of the ICI wave function at the iteration $n$ for using the regular DCE. The enclosed part is the new definition. $\psi_{n+1}$ only includes the functions operated by the directions of the arrows.

**Table IX.** Relativistic free ICI energy (a.u.) of the heliumlike atoms (He and $Th^{88+}$) using the regular DCE at the diagonalization step.

| n[a] | M[b] | Energy (H) | Energy ($Th^{88+}$) |
|---|---|---|---|
| 0 | 8 (1,4,3) | **-2.**75 011 497 | **-9166.** 696 078 |
| 1 | 32 (4,16,12) | **-2.88** 786 145 | **-9166.** 924 096 |
| 2 | 76 (10,37,29) | **-2.90 3**09 958 | **-9166.** 930 884 |
| 3 | 163 (21,75,67) | **-2.90 37**6 145 | **-9166.** 928 998 |
| 4 | 324 (43,156,125) | **-2.90 384** 658 | **-9166.** 919 131 |
| 5 | 603 (84,303,216) | **-2.90 385** 326 | **-9166.** 929 132 |
| Ref. 7 | | -2.90 263 6 | -9166. 927 2 |
| Ref. 23 | | -2.90 385 7 | |

a Iteration number.

b Number of the independent functions for expanding $\psi$ : M ($M_{ll}$, $M_{ls}$, $M_{ss}$).

We also performed the calculation using the regular DCE at the diagonalization step. However, the variational collapse occurred in an earlier stage of the ICI calculation. To overcome it, we redefine the ICI wave function at the iteration $n$ as shown in Fig. 4. We define the enclosed part of Fig. 4 as the new wave function of the iteration $n$. Table IX shows the results. For He, the energy monotonically converges to the reference value from above as well as using the inverse DCE. However, for $Th^{88+}$, the convergence behavior is not good because the energy does not monotonically converge to the fixed value. Therefore, we recommend using the inverse procedure at least at the earlier stage of the ICI calculations.

## 5. Conclusion

We have proposed a method of solving the DE and DCE for atoms and molecules in an analytical expansion form. The relativistic ICI automatically generates the wave function having the exact structure. The exact ICI balancing is done in the iteration process. For the one-electron atoms, we have never experienced any variational problem as far as we do ICI. For the two-electron atoms, we could avoid the variational collapse by introducing the inverse Hamiltonian. Thus, we propose the relativistic free ICI method and the inverse variational method having the Ritz-like property as a general method of calculating the exact solutions of the DCE for many-electron atoms and molecules. This Ritz-like property is very useful in actual calculations where we do not know the true energy.

The ICI method of calculating the analytical exact wave functions has been

confirmed to have a high potentiality for solving the SE of atoms and molecules[4,5] and extended here to solve the relativistic DCE. We have still many things to do in future to develop this new methodology as a really useful method in quantum chemistry.

**ACKNOWLEDGMENTS**

This study has been supported financially by a Grant for Creative Scientific Research from the Ministry of Education, Science, Culture, and Sports of Japan.

## REFERENCES


1. P. A. M. Dirac, *Proc. R. Soc. A* **123**, 714, 1929.
2. H. Nakatsuji, *J. Chem. Phys.* **113**, 2949, 2000., H. Nakatsuji, E. R. Davidson, *J. Chem. Phys.* **115**, 2000, 2001. H. Nakatsuji, *J. Chem. Phys.* **115**, 2465, 2001. H. Nakatsuji, *J. Chem. Phys.* **116**, 1811, 2002. H. Nakatsuji, M. Ehara, *J. Chem. Phys.* **117**, 9, 2002. H. Nakatsuji, M. Ehara, *J. Chem. Phys.* **122**, 194108, 2005.
3. H. Nakatsuji, *Phys. Rev. A* **65**, 052122, 2002.
4. H. Nakatsuji, *Phys. Rev. Lett.* **93**, 030403, 2004.
5. H. Nakatsuji, *Phys. Rev. A* **65**, 062110, 2005.
6. G. Pestka, J. Karwowski, *in Explicitly Correlated Wave Functions in Chemistry and Physics – Theory and Applications, edited by J. Rychlewski (Kluwer, Dordrecht, 2003)*, pp. 331-346.
7. A. Kolakowska, J. D. Talman, K. Aashamar, *Phys. Rev. A* **53**, 168, 1996.
8. M. Moshinski, A. Szczepaniak, *J. Phys. A* **22**, L817, 1989.
9. R. Szmytkowski, M. Gruchowski, *J. Phys. A* **34**, 4991, 2001.
10. J. J. Sakrai, *Advanced Quantum Mechanics (Addison-Wesley, Reading, MA, 1967).*
11. G. Pestka, *J. Phys. B* **31**, 6243, 1998.
12. R. A. Sack, *J. Math. Phys.* **5**, 245, 1964.
13. R. N. Hill, C. Krauthauser, *Phys. Rev. Lett.* **72**, 2151, 1994.
14. G. Pestka, *Physica Scripta* **69**, 203, 2004.
15. E. A. Hylleraas, *Z. Phys.* **54**, 347, 1929.
16. A. R. Edmonds, *Angular Momentum in Quantum Mechanics* (Princeton University Press, Princeton, 1957).
17. G. W. F. Drake, *Phys. Rev. A* **18**, 820, 1978.
18. J. L. Calais, P. O. Löwdin, *J. Mol. Spectrosc.* **8**, 203, 1962.
19. A. M. Frolov, V. H. Smith Jr., *Phys. Rev. A* **53**, 3853, 1996.
20. W. Kutzelnigg, *Lecture Notes in Chemistry* **50**, 353, 1989.
21. D. Levin, *Int. J. Comput. Math. B* **3**, 371, 1973.
22. R. A. Sack, C. C. J. Roothaan, W. Kolos, *J. Math. Phys.* **8**, 1093, 1967.
23. A. Kolakowska, *J. Phys. B* **30**, 2773, 1997.

# Chapter 3

# Hydrogen and Helium Atoms in a Strong Magnetic Field

**Abstract:**

The hydrogen and helium atoms in a strong magnetic field have been studied with both the nonrelativistic and relativistic calculations by using the ICI method. These systems are interesting from the astrophysics, chaotic filed, condensed matter physics and so on, for example, strong magnetic fields exist on the surface of the white dwarf and neutron stars and the spectroscopic studies are very important for studying what atoms exist there. For the hydrogen atom in a strong magnetic filed, very high precision could be achieved with both the non-relativistic and relativistic calculations. Some excited states were also obtained, which were important to discuss the spectra from the white dwarf and neutron stars in the presence of very strong magnetic field. For the helium atom, the excellent results were also obtained. The present study is the first accurate relativistic calculation of the helium atom in a strong magnetic field with explicitly correlated type functions. The ICI method also showed the satisfactory results even for the Zeeman Hamiltonian.

## 1. Introduction

In 1896, since Zeeman first found the splitting of the spectra in a magnetic field, the atoms in a magnetic field have been much studied both theoretically and experimentally. They are interesting from various scientific fields. For example, in the astrophysics, because it has been discovered that a very strong magnetic field exists on white dwarf and neutron stars, the spectra of the hydrogen and helium atoms has been studied.[1,2] In these astrophysical objects, extremely strong magnetic fields ($B \approx 10^7 - 10^8\,G$ on white dwarf stars and $B \approx 10^{10} - 10^{13}\,G$ on neutron stars) are appeared on their surface. They are also interesting from the chaotic field, since the hydrogen atom in a magnetic field is the one of the systems the classical motion displays chaotic behavior in regimes and accurate quantum calculations are possible.[3-5] In others, they are of interests in solid-state condensed matter physics and so on.[6]

Several methodologies to solve these systems have been reported in the literatures.[7-15] Recently, Nakatsuji studied the structure of the exact wave function and established the general method for solving the Schrödinger equation (SE) and proposed the ICI method to construct the exact wave function.[16-20] We have applied the ICI method to the hydrogen, helium, lithium, beryllium and boron atoms and hydrogen molecules and the results were very satisfactory.[18-20] We also extended the ICI theory to the relativistic case for solving the relativistic Dirac equation (DE) and Dirac-Coulomb equation (DCE).[21,22] The relativistic calculations of the Dirac oscillator, hydrogen and helium atoms have been performed.[21,22] However, these systems were solved in no magnetic field and did not contain the vector potential in their Hamiltonian (except for the Dirac oscillator). The systems compete scalar potential (the Coulomb potential) with vector potential are not solved yet. In this chapter, we apply the ICI method to the systems in a magnetic field at both the nonrelativistic and relativistic levels and compare our results with the reference results. We explain the mathematics and computational aspects in Sec. 2. The results are discussed in Sec. 3. The conclusion of this study is given in the last section.

## 2. Formulation

We want to calculate the systems in a magnetic field with the Coulomb potential of the nuclear-electron attraction and the electron-electron repulsion. The Coulomb potential is written as scalar potential $V$ but the magnetic interaction is accomplished

through vector potential $\mathbf{A}$. For one-electron system, the nonrelativistic Hamiltonian of the SE is written as

$$H_S = \frac{1}{2}p^2 + \frac{1}{2c^2}A^2 + \frac{1}{c}\mathbf{A}\cdot\mathbf{p} + \frac{1}{2c}\boldsymbol{\sigma}\cdot rot\mathbf{A} + V \tag{3.1}$$

where $\mathbf{p}$ is the momentum operator and $c$ is the velocity of light. The relativistic Hamiltonian of one-electron system is written as

$$H_D = c\boldsymbol{\alpha}\cdot\boldsymbol{\pi} + \beta c^2 + VI_4 \tag{3.2}$$

$$H_D = \begin{pmatrix} (V+c^2)I_2 & c\left(\boldsymbol{\sigma}\cdot\left(\mathbf{p}+\frac{\mathbf{A}}{c}\right)\right) \\ c\left(\boldsymbol{\sigma}\cdot\left(\mathbf{p}+\frac{\mathbf{A}}{c}\right)\right) & (V-c^2)I_2 \end{pmatrix} \tag{3.3}$$

The vector potential is included in the substitution of $\mathbf{p}$ for $\boldsymbol{\pi} = \mathbf{p} + \mathbf{A}/c$. $\boldsymbol{\alpha}$ and $\beta$ are defined as

$$\boldsymbol{\alpha} = \begin{pmatrix} 0 & \boldsymbol{\sigma} \\ \boldsymbol{\sigma} & 0 \end{pmatrix}, \beta = \begin{pmatrix} I_2 & 0 \\ 0 & -I_2 \end{pmatrix} \tag{3.4}$$

where $\boldsymbol{\sigma}$ is the Pauli matrix. The nonrelativistic Hamiltonian Eq. (3.1) is rather derived from the relativistic Hamiltonian Eq. (3.2) by taking the nonrelativistic limit $c \to \infty$ with the Coulomb gauge $div\mathbf{A} = 0$. For the hydrogenlike atoms in a uniform magnetic field $\mathbf{B}$, the Coulomb potential and vector potential are written as

$$V = -\frac{Z}{r} \tag{3.5}$$

$$\mathbf{A} = \frac{\mathbf{B}}{2}\times\mathbf{r} \tag{3.6}$$

with nuclear charge $Z$. The atomic unit of magnetic field is $2.35*10^9$ G. We adopt the Coulomb gauge for vector potential: $div\mathbf{A} = 0$. If the direction of the uniform magnetic field is $z$ axis, $\mathbf{B}$ is expressed as $\mathbf{B} = (0,0,B)$.

The Hamiltonian of two-electron system in a uniform magnetic field is simply extended from one-electron system. The nonrelativistic Hamiltonian of the SE is written as

$$H_S = \sum_{i=1}^{2}\left(\frac{1}{2}p_i^2 + \frac{1}{2c^2}A_i^2 + \frac{1}{c}\mathbf{A}_i\cdot\mathbf{p}_i + \frac{1}{2c}\boldsymbol{\sigma}_i\cdot rot\mathbf{A}_i\right) + V \tag{3.7}$$

The relativistic Dirac-Coulomb Hamiltonian is written as

$$H_D = \begin{pmatrix} (V+2c^2)I_4 & c\left(\boldsymbol{\sigma}_2 \cdot \left(\mathbf{p}_2 + \frac{\mathbf{A}_2}{c}\right)\right) & c\left(\boldsymbol{\sigma}_1 \cdot \left(\mathbf{p}_1 + \frac{\mathbf{A}_1}{c}\right)\right) & 0 \\ c\left(\boldsymbol{\sigma}_2 \cdot \left(\mathbf{p}_2 + \frac{\mathbf{A}_2}{c}\right)\right) & VI_4 & 0 & c\left(\boldsymbol{\sigma}_1 \cdot \left(\mathbf{p}_1 + \frac{\mathbf{A}_1}{c}\right)\right) \\ c\left(\boldsymbol{\sigma}_1 \cdot \left(\mathbf{p}_1 + \frac{\mathbf{A}_1}{c}\right)\right) & 0 & VI_4 & c\left(\boldsymbol{\sigma}_2 \cdot \left(\mathbf{p}_2 + \frac{\mathbf{A}_2}{c}\right)\right) \\ 0 & c\left(\boldsymbol{\sigma}_1 \cdot \left(\mathbf{p}_1 + \frac{\mathbf{A}_1}{c}\right)\right) & c\left(\boldsymbol{\sigma}_2 \cdot \left(\mathbf{p}_2 + \frac{\mathbf{A}_2}{c}\right)\right) & (V-2c^2)I_4 \end{pmatrix}$$

(3.8)

where $\boldsymbol{\sigma}_1$ and $\boldsymbol{\sigma}_2$ are defined as $\boldsymbol{\sigma}_1 = \boldsymbol{\sigma} \otimes I_2$ and $\boldsymbol{\sigma}_2 = I_2 \otimes \boldsymbol{\sigma}$, respectively. The wave function is composed of 16 components. Scalar and vector potentials of the heliumlike atoms in a uniform magnetic field are written as

$$V = -\frac{Z}{r_1} - \frac{Z}{r_2} + \frac{1}{r_{12}} \tag{3.9}$$

$$\mathbf{A}_i = \frac{\mathbf{B}}{2} \times \mathbf{r}_i \tag{3.10}$$

To solve the nonrelativistic SE or relativistic DCE in a magnetic field, we use the ICI method for both the nonrelativistic and relativistic cases,[16-22] in which the ICI wave function is defined by a recurrence formula as

$$\psi_{n+1} = \left[1 + C_n g\left(H - E_n\right)\right]\psi_n \tag{3.11}$$

where $C_n$ is a variational parameter at the iteration $n$. The scale factor $g$ is introduced to avoid the singularity problem of the Coulomb potential. It is proved in the literatures that the ICI wave function of Eq. (3.11) gives the exact wave function at convergence.[16-19] We introduce the free ICI method to accelerate the convergence speed, in which the wave function at the iteration $n+1$ is expressed as

$$\psi_{n+1} = \sum_{i}^{all} c_i \phi_i \tag{3.12}$$

where $\{\phi_i\}$ is the independent function included in $\psi_{n+1}$ and $c_i$ is its independent variational parameter of $\phi_i$. In the relativistic calculations, the so-called variational collapse may be an obstacle to perform the variational calculations. To overcome this problem, one method is using the inverse Hamiltonian $H^{-1}$ at the diagonalization step.

The other method is to satisfy some balancing conditions to the wave function. The ICI method automatically generates the wave function satisfied the balancing condition – i.e., ICI balance, in this case, we need not use the inverse Hamiltonian and may use the regular Hamiltonian $H$.[21,22] More details of the ICI method were discussed in the previous chapter and the literatures.[16-22]

First, we apply the ICI method to solve the SE and DCE of the hydrogen atom in a uniform magnetic field. In the ICI method, at first, we need determine the two freedoms: the $g$ and initial functions $\psi_0$. The choice of these functions is so important because it determines the speed of convergence to the exact solution. For the nonrelativistic SE of the hydrogen atom, the exact solutions are understood in the two limits ($B=0$ or $Z=0$), and they gives us some hints to construct the exact wave function of the no limit case ($B\neq 0$ and $Z\neq 0$). In the limit $B=0$, as well known, the exact solution is expressed as the Slater orbital in the polar coordinates,

$$\psi_{exact}^{B=0}=\sum_i r^i \exp(-\alpha r)\cdot Y_l^m(\vartheta,\varphi) \tag{3.13}$$

where $Y_l^m$ is the spherical harmonic with the quantum numbers: $l$ and $m$. In the limit $Z=0$, the exact solution is expressed as the Landau orbital in the cylindrical coordinates,

$$\psi_{exact}^{Z=0}=\sum_i \rho^i \exp(-\beta\rho^2)\cdot\exp(im\varphi+ip_z z) \tag{3.14}$$

where $\rho$ is defined as $\rho=\sqrt{x^2+y^2}$ and $m$ and $p_z$ are quantum numbers.[23] Considering these two exact limits, we adopted the following initial function for the nonrelativistic calculations,

$$\psi_0{}^S=e^{-\alpha r-\beta\rho^2}\cdot Y_l^m(\vartheta,\varphi) \tag{3.15}$$

We calculated the s state (even parity state) and the lowest p state of the Zeeman splitting (odd parity state). In the relativistic case, we should introduce so-called mild singularity to express the boundary condition at the nucleus position in addition to the nonrelativistic case,

$$\psi_0{}^D=\begin{pmatrix} C_0{}^L r^{\gamma-1}e^{-\alpha r-\beta r^2\sin^2\vartheta}\cdot\Theta_{j,j_z,\pi}{}^L(\vartheta,\varphi) \\ C_0{}^S r^{\gamma-1}e^{-\alpha r-\beta r^2\sin^2\vartheta}\cdot\Theta_{j,j_z,\pi}{}^S(\vartheta,\varphi)\end{pmatrix} \tag{3.16}$$

where $\Theta_{j,j_z,l}$ is composed of two components and the eigenfunction of the total

angular momentum, its $z$ component and parity: $j$, $j_z$ and $\pi$. $C_0$ is also composed of two components. We use the following simple $g$ function to avoid the singularity of the Coulomb potential,

$$g = r \tag{3.17}$$

When we use these $g$ and initial functions, the ICI method automatically generates the following functional space in the polar coordinates,

$$\phi = r^{\gamma-1+n} e^{-\alpha r - \beta r^2 \sin^2 \vartheta} \cdot (\cos\vartheta)^a (\sin\vartheta)^b \cdot e^{im\varphi} \tag{3.18}$$

This type functions are similar to the basis set introduced by Chen and Goldman.[8,9] Although these functions cover the wide range of magnetic field strength, the functions expressed by the cylindrical or parabolic coordinates may become better choice in the extremely strong magnetic field like on the neutron starts.

Next, we apply our method to the helium atom in a uniform magnetic field. In the extremely strong magnetic field, the functions or basis set should be expressed in the cylindrical or parabolic coordinates to expect more rapid convergence to the exact solution, similar to the hydrogen atom. In the middle range of magnetic filed, the spherical and cylindrical symmetries compete each other. For the ICI method, we want to choose the $g$ and initial functions as well as the hydrogen atom like Eq. (3.15) to Eq. (3.17). However, if the initial function contains the term $\exp(-\beta\rho^2)$, the generated functions are difficult to evaluate the integrals to estimate matrix elements. Therefore, we use the initial function of spherical type. The ICI method automatically generates the functions having cylindrical symmetry. Nevertheless, since the rapid convergence is expected by the term $\exp(-\beta\rho^2)$, we try to solve their integral problem and the results will be discussed elsewhere. In the nonrelativistic case, we calculated the two states correspond to the $^1S_0$ and $^3P_0$ symmetries in the $B = 0$. The $^1S_0$ state has totally zero angular momentum, in which both the spin and orbital angular momentums are zero, so this state has an anti-magnetic property. In contrast, the $^3P_0$ state is triplet, so this state has a ferro-magnetic property and the energy becomes more stable at higher magnetic fields. For the ICI method, the $g$ function we chose was a summation type as

$$g = 1 + r_1 + r_2 + r_{12} \tag{3.19}$$

We adopted the spherical type initial function,

$$\psi_0^{\,S} = \left(1 + (-1)^{p_{12}} P_{12}\right)\left(e^{-\alpha_1 r_1 - \alpha_2 r_2} \cdot \Theta^M_{L,l_1,l_2}(\vartheta_1, \varphi_1, \vartheta_2, \varphi_2)\right) \tag{3.20}$$

where $P_{12}$ is the permutation operator exchange electrons and for the singlet state, $p_{12}=1$ and for the triplet state, $p_{12}=-1$. $\Theta^{M}_{L,l_1,l_2}$ is the eigenfunction of the spatial angular momentum made from a linear combination of the product of the one-electron spherical harmonics by the angular momentum composite theorem given in the Edmond's book.[24] In the relativistic calculation, we calculated the $S_0$ state by using the inverse method at the diagonalization step. The initial function is given by

$$\psi_0^{\,D}=\begin{pmatrix} C_0^{\,ll}A\left\{r_1^{\gamma-1}r_2^{\gamma-1}\exp\left(-\alpha_1 r_1-\alpha_2 r_2\right)\cdot\Theta^{J_z,\Pi}_{J,J_1,J_2,\pi_1,\pi_2}{}^{ll}(\vartheta_1,\varphi_1,\vartheta_2,\varphi_2)\right\} \\ C_0^{\,ls}\begin{cases} r_1^{\gamma-1}r_2^{\gamma-1}\exp\left(-\alpha_1 r_1-\alpha_2 r_2\right)\cdot\Theta^{J_z,\Pi}_{J,J_1,J_2,\pi_1,\pi_2}{}^{ls}(\vartheta_1,\varphi_1,\vartheta_2,\varphi_2) \\ -r_1^{\gamma-1}r_2^{\gamma-1}\exp\left(-\alpha_1 r_1-\alpha_2 r_2\right)\cdot\Theta^{J_z,\Pi}_{J,J_1,J_2,\pi_1,\pi_2}{}^{sl}(\vartheta_1,\varphi_1,\vartheta_2,\varphi_2) \end{cases} \\ C_0^{\,ll}A\left\{r_1^{\gamma-1}r_2^{\gamma-1}\exp\left(-\alpha_1 r_1-\alpha_2 r_2\right)\cdot\Theta^{J_z,\Pi}_{J,J_1,J_2,\pi_1,\pi_2}{}^{ss}(\vartheta_1,\varphi_1,\vartheta_2,\varphi_2)\right\} \end{pmatrix} \tag{3.21}$$

where $A$ is the anti-symmetrizer defined as $A=1-P_{12}$. $\Theta^{J_z,\Pi}_{J,J_1,J_2,\pi_1,\pi_2}$ is the composite eigenfunction of the total angular momentum and parity made from the one-electron eigenfunctions. When we use the $g$ and initial functions given in Eq. (3.19) to Eq. (3.21), the generated functional space is written as Slater type orbital with the spherical harmonics,

$$\phi=r_1^{\gamma_1-1+n_1}r_2^{\gamma_2-1+n_2}r_{12}^{\,n_{12}}e^{-\alpha_1 r_1-\alpha_2 r_2}\cdot Y_{l_1}^{m_1}(\vartheta_1,\varphi_1)Y_{l_2}^{m_2}(\vartheta_2,\varphi_2) \tag{3.22}$$

Although this form is not suitable for extremely strong magnetic field, the necessary formulation and integrals are almost same as the systems of $B=0$ and they were already given in the previous chapter. For extremely strong magnetic field, the mathematics based on the cylindrical coordinates will be studied elsewhere.

Finally, for convenience, we give some formulation and integrals to evaluate matrix elements for the present systems. The formulation is given in the polar coordinates. First, we derive the operation of $\boldsymbol{\sigma}\cdot\mathbf{A}$, which is appeared in the relativistic calculation including vector potential to express magnetic field. In a uniform magnetic field of the $z$ direction, vector potential is written as follows in the polar coordinates,

$$\begin{aligned}\mathbf{A}&=\frac{1}{2}\mathbf{B}\times\mathbf{r}=\frac{1}{2}\left(B_y z-B_z y,B_z x-B_x z,B_x y-B_y x\right)\\&=\frac{1}{2}\left(-By,Bx,0\right)=\frac{B}{2}\left(-r\sin\vartheta\sin\varphi,r\sin\vartheta\cos\varphi,0\right)\end{aligned} \tag{3.23}$$

Therefore, the operation of $\boldsymbol{\sigma}\cdot\mathbf{A}$ is expressed in the polar coordinates as

$$\begin{aligned}\boldsymbol{\sigma}\cdot\mathbf{A} &= \sigma_x A_x + \sigma_y A_y + \sigma_z A_z \\ &= \frac{Br}{2}\left(-\sin\vartheta\sin\varphi\cdot\sigma_x, \sin\vartheta\cos\varphi\cdot\sigma_y, 0\right) \\ &= \frac{-iBr}{2}\begin{pmatrix} 0 & \sin\vartheta\cdot e^{-i\varphi} \\ -\sin\vartheta\cdot e^{i\varphi} & 0 \end{pmatrix}\end{aligned} \tag{3.24}$$

If we consider the magnetic field introduced by the nuclear magnetic moment $\boldsymbol{\mu}$, vector potential is written in the point nucleus model as

$$\mathbf{A} = \frac{1}{2}\mathbf{B}\times\mathbf{r} + \boldsymbol{\mu}\times\frac{\mathbf{r}}{r^3} \tag{3.25}$$

In this case, the formulation of the second term of Eq. (3.25) is similar to the first term,

$$\boldsymbol{\sigma}\cdot\mathbf{A} = -i\left(\frac{Br}{2} + \frac{\mu}{r^2}\right)\begin{pmatrix} 0 & \sin\vartheta\cdot e^{-i\varphi} \\ -\sin\vartheta\cdot e^{i\varphi} & 0 \end{pmatrix} \tag{3.26}$$

However, the singular potential $r^{-2}$ is appeared in vector potential. In the relativistic calculations, the inverse method was proposed to avoid the variational collapse,[21,22,25] in which we need the expectation values of the square Hamiltonian $H^2$. Since Eq. (3.26) contains the singular potential $r^{-2}$, the square Hamiltonian $H^2$ includes divergence terms. To overcome this problem, we have to use the $g$ function even at the diagonalization step or use a finite nucleus model. The details will be studied elsewhere. The formulation of $\boldsymbol{\sigma}\cdot\mathbf{p}$ in the polar coordinates is expressed as

$$\boldsymbol{\sigma}\cdot\mathbf{p} = -i\boldsymbol{\sigma}\cdot\hat{\mathbf{r}}\left\{\frac{\partial}{\partial r} - \frac{1}{r}\left(\boldsymbol{\sigma}\cdot\mathbf{L}\right)\right\} \tag{3.27}$$

The $\boldsymbol{\sigma}\cdot\hat{\mathbf{r}}$ and $\boldsymbol{\sigma}\cdot\mathbf{L}$ operate the angular coordinates and written as

$$\boldsymbol{\sigma}\cdot\hat{\mathbf{r}} = \begin{pmatrix} \cos\vartheta & \sin\vartheta\cdot e^{-i\varphi} \\ \sin\vartheta\cdot e^{i\varphi} & -\cos\vartheta \end{pmatrix} \tag{3.28}$$

$$\boldsymbol{\sigma}\cdot\mathbf{L} = \begin{pmatrix} L^z & L^- \\ L^+ & -L^z \end{pmatrix} \tag{3.29}$$

The operators of the spatial angular momentum are expressed in the polar coordinates as

$$\begin{aligned} L^z &= -i\frac{\partial}{\partial\varphi} \\ L^+ &= L^x + iL^y = e^{i\varphi}\frac{\partial}{\partial\vartheta} + ie^{i\varphi}\frac{\cos\vartheta}{\sin\vartheta}\frac{\partial}{\partial\varphi} \\ L^- &= L^x - iL^y = -e^{-i\varphi}\frac{\partial}{\partial\vartheta} + ie^{-i\varphi}\frac{\cos\vartheta}{\sin\vartheta}\frac{\partial}{\partial\varphi} \end{aligned} \tag{3.30}$$

For the helium atom, when we use the $g$ and initial functions given in Eq. (3.19) to Eq. (3.21), the integrals appeared in the evaluation of matrix elements are same as the calculations of $B=0$. These integrals were already discussed in the previous chapter. For the hydrogen atom, when we use the $g$ and initial functions given in Eq. (3.15) to Eq. (3.17), the necessary integral is written as

$$\begin{aligned} I &= \int e^{-\alpha r-\beta(r\sin\vartheta)^2}\cdot r^{\gamma}(\cos\vartheta)^{a}(\sin\vartheta)^{b}e^{im\varphi}\cdot d\mathbf{r} \\ &= 2\pi\int_0^{\infty}dr\cdot r^{\gamma+2}e^{-\alpha r}\int_0^{\pi}d\vartheta\cdot e^{-\beta(r\sin\vartheta)^2}(\cos\vartheta)^{a}(\sin\vartheta)^{b+1} \\ &= 2\pi\frac{\Gamma\left(\frac{b+2}{2}\right)\Gamma\left(\frac{a+1}{2}\right)}{\Gamma\left(\frac{a+b+3}{2}\right)}\int_0^{\infty}dr\cdot r^{\gamma+2}e^{-\alpha r}\,{}_1F_1\left(\frac{b+2}{2};\frac{a+b+3}{2};-\beta r^2\right) \end{aligned} \tag{3.31}$$

where ${}_1F_1$ is the confluent geometric function. In the final step, we need perform an one-dimensional numerical integration. In Eq. (3.31), if $m\neq 0$ or $a=odd$, $I=0$. This integration was first derived by Chen and Goldman.[8,9]

### 3. Results

We first discuss about the nonrelativistic calculation of the hydrogen atom in a uniform intense magnetic field. In the ICI method, we used the scaling $g$ and initial functions given in Eq. (3.17) and Eq. (3.15), respectively. The nonlinear parameters of the initial functions are $\alpha=1,\beta=B/4$ for $B=1$, $\alpha=5,\beta=B/4$ for $B=500$ and $\alpha=10,\beta=B/4$ for $B=5000$. Table I shows the calculated energies of the $1s_{1/2}$ state in the magnetic field $B=1$ at different iteration cycles of the ICI recurrence formula. In the present free ICI method, the obtained value considerable exceeded the reference value given at the bottom of the table.[7] We obtained the energy of the accuracy about 33-35 digits at the iteration 20 with the dimension 860. The set of the $g$ and initial functions given in Eq. (3.17) and Eq. (3.15) indicates good performance even in the systems compete the Coulomb potential with the magnetic field. Table II shows the energies of the $1s_{1/2}$ states at the iteration 20 with the dimension 860 and the $2p_{3/2}$ states at the iteration 15 with the dimension 496 in the magnetic field $B=1,500,5000$. In the magnetic field $B=1$, the free ICI energy of the $2p_{3/2}$ state also shows good performance as well as the $1s_{1/2}$ state. However, in the very strong magnetic field $B=500,5000$, the reference values are slightly better than our ICI results. In the reference study, the basis functions are written in the parabolic coordinates. This is a

clever choice for very strong magnetic field because the wave function is extremely distorted from spherical symmetry. To achieve the rapid convergence, the functional space generated by the ICI method is so important and the coordinates we select are also important to determine the suitable independent free ICI functions for the systems. In the present calculations, the $g$ and initial functions and the coordinates are suitable for middle range of magnetic field strength but may not be the best choice for extremely strong magnetic field. At least, the coordinates should be cylindrical or parabolic coordinates.

**Table I.** Hydrogen atom of the $1s_{1/2}$ state in a magnetic field B=1 by the nonrelativistic calculation.

| n[a] | M[b] | Energy (a.u.) |
|---|---|---|
| 0 | 1 | **-0.802** 823 296 270 760 288 697 137 002 693 579 228 |
| 1 | 5 | **-0.830** 651 472 238 754 549 986 109 910 670 042 259 |
| 2 | 14 | **-0.831 156** 821 764 373 528 659 267 608 173 969 909 |
| 3 | 27 | **-0.831 168** 644 226 326 985 625 750 272 165 327 973 |
| 4 | 44 | **-0.831 168 89**1 478 990 877 775 432 971 706 712 803 |
| 5 | 65 | **-0.831 168 896** 622 351 813 515 796 169 966 885 950 |
| 6 | 90 | **-0.831 168 896 73**0 799 301 599 214 073 626 700 088 |
| 7 | 119 | **-0.831 168 896 733** 107 530 408 437 806 273 932 988 |
| 8 | 152 | **-0.831 168 896 733 15**6 949 708 188 274 214 704 640 |
| 9 | 189 | **-0.831 168 896 733 158 0**12 194 316 101 778 651 053 |
| 10 | 230 | **-0.831 168 896 733 158 035** 104 415 809 763 186 529 |
| 11 | 275 | **-0.831 168 896 733 158 035 5**99 352 789 454 242 416 |
| 12 | 324 | **-0.831 168 896 733 158 035 610** 061 024 550 874 661 |
| 13 | 377 | **-0.831 168 896 733 158 035 610 29**3 085 313 968 647 |
| 14 | 434 | **-0.831 168 896 733 158 035 610 298** 122 577 941 181 |
| 15 | 495 | **-0.831 168 896 733 158 035 610 298 23**2 067 649 271 |
| 16 | 560 | **-0.831 168 896 733 158 035 610 298 234** 450 479 382 |
| 17 | 629 | **-0.831 168 896 733 158 035 610 298 234 50**2 401 738 |
| 18 | 702 | **-0.831 168 896 733 158 035 610 298 234 503** 534 418 |
| 19 | 779 | **-0.831 168 896 733 158 035 610 298 234 503 559** 153 |
| 20 | 860 | **-0.831 168 896 733 158 035 610 298 234 503 559 694** |
| Ref. 7 | | -0.831 168 896 733 158 035 610 2 |

a Iteration number.

b Number of the independent functions.

**Table II.** Hydrogen atom of the $1s_{1/2}$ and $2p_{3/2}$ states in a magnetic field B=1, B=500 and B= 5000 by the nonrelativistic calculation. Iteration number: n and number of independent functions: M are n=20, M=860 for $1s_{1/2}$ and n=15, M=496 for $2p_{3/2}$.

| B | State | Energy (a.u.) | Ref. 7 |
|---|---|---|---|
| 1 | $1s_{1/2}$ | **-0.831 168 896 733 158 035 610 298 234 503 559 694** | -0.831 168 896 733 158 035 610 2 |
| | $2p_{3/2}$ | **-0.456 597 058 423 752 111 164 921 868** 213 | -0.456 597 058 423 752 111 164 |
| 500 | $1s_{1/2}$ | **-6.25 708 767 468 056 188** 188 | -6.25 708 767 468 056 189 04 |
| | $2p_{3/2}$ | **-4.53 124 638 073 446** 570 868 | |
| 5000 | $1s_{1/2}$ | **-11.8 734 182 826 810** 767 626 | -11.8 734 182 826 812 097 44 |
| | $2p_{3/2}$ | **-9.04 139 866 234** 804 765 484 | |

Next, we summarize the results of the relativistic calculations of the hydrogen atom in the same magnetic fields as the nonrelativistic calculations. We performed the calculations using the inverse and regular Hamiltonian at the diagonalization step. The $g$ and initial functions we selected were given in Eq. (3.17) and Eq. (3.16). We used the same nonlinear parameters of the initial functions as the nonrelativistic case: $\alpha = 1, \beta = B/4$ for $B = 1$, $\alpha = 5, \beta = B/4$ for $B = 500$ and $\alpha = 10, \beta = B/4$ for $B = 5000$. Table III shows the calculated energies of the $1s_{1/2}$ state in the magnetic field $B = 1$. When we use the inverse Hamiltonian at the diagonalization step, the energy is improved as approaching the exact solution from above, which indicates the Ritz type variational property holds. When we used the regular Hamiltonian at the diagonalization step, the obtained energies at the even number iteration converged to the exact solution but the energies at the odd number iteration indicated the variational collapse. It suggests that the ICI balance to perform the variational calculations is satisfied at the even number iteration and the balancing condition of the large and small components is improved by turns of the iterations. At the even number iteration, the functions to satisfy the balancing condition are generated. In contrast, at the odd number iteration, the functions to extend the functional space are generated but the functions to satisfy the balancing condition are not generated yet at least for electronic states. As shown in Table III, the energies we obtained improved the reference values about 6 decimal figures.[8] Table IV shows the energies of the $1s_{1/2}$ states at the iteration 16 with the dimension 867 (192,225,225,225) and the $2p_{3/2}$ states at the iteration 16 with the dimension M=902 (200,234,234,234) in the magnetic field $B = 1, 500, 5000$ by using both the inverse and regular Hamiltonian at the diagonalization step. In the all magnetic field $B = 1, 500, 5000$, our results are more accurate than the reference values.[8] Similar to the nonrelativistic case, to expect more rapid convergence in very strong magnetic

**Table III.** Hydrogen atom of the $1s_{1/2}$ state in a magnetic field B=1 by the relativistic calculation using both inverse and regular DE at the diagonalization step.

| N[a] | M[b] | Energy (a.u.) (Inverse) | Energy (a.u.) (Regular) |
|---|---|---|---|
| 0 | 3 (0,1,1,1) | **-0.802** 823 887 449 331 513 | **-0.802** 826 512 118 055 045 |
| 1 | 12 (2,6,2,2) | **-0.827** 945 467 012 769 097 | -2.37 861 661 357 269 493 |
| 2 | 27 (3,8,8,8) | **-0.830** 662 045 709 567 475 | **-0.830** 663 055 005 888 350 |
| 3 | 48 (10,18,10,10) | **-0.831** 120 466 080 318 975 | -4.20 019 929 515 919 493 |
| 4 | 75 (12,21,21,21) | **-0.831 162** 248 268 893 111 | **-0.831 162** 255 449 890 315 |
| 5 | 108 (24,36,24,24) | **-0.831 172** 214 323 411 421 | -6.00 745 202 757 182 890 |
| 6 | 147 (27,40,40,40) | **-0.831 172** 989 037 674 849 | **-0.831 172** 989 132 705 172 |
| 7 | 192 (44,60,44,44) | **-0.831 173 205** 517 109 161 | -7.79 264 876 379 615 195 |
| 8 | 243 (48,65,65,65) | **-0.831 173 220** 849 895 160 | **-0.831 173 220** 851 463 187 |
| 9 | 300 (70,90,90,90) | **-0.831 173 225** 511 341 426 | -9.56 201 169 362 397 590 |
| 10 | 363 (75,96,96,96) | **-0.831 173 225** 822 871 031 | **-0.831 173 225** 822 907 250 |
| 11 | 432 (102,126,102,102) | **-0.831 173 225 923** 172 682 | -11.3 196 540 321 204 703 |
| 12 | 507 (108,133,133,133) | **-0.831 173 225 929** 607 197 | **-0.831 173 225 929** 608 049 |
| 13 | 588 (140,168,140,140) | **-0.831 173 225 931** 765 080 | -13.0 682 214 956 495 016 |
| 14 | 675 (147,176,176,176) | **-0.831 173 225 931 899** 483 | **-0.831 173 225 931 899** 504 |
| 15 | 768 (184,216,184,184) | **-0.831 173 225 931 945** 943 | -14.8 095 050 911 257 600 |
| 16 | 867 (192,225,225,225) | **-0.831 173 225 931 948** 773 | **-0.831 173 225 931 948** 774 |
| Ref. 8 | | -0.831 173 226 | -0.831 173 226 |

a Iteration number.

b Number of the independent functions for expanding $\psi$ : M ($M_{L1}$, $M_{L2}$, $M_{S1}$, $M_{S2}$).

field, we should use the cylindrical or parabolic coordinates. The relativistic correction from the nonrelativistic energy is small for the hydrogen atom ($Z=1$) but the difference between the nonrelativistic and relativistic energies becomes slightly large by increasing magnetic field strength. This differences $\Delta E = E_{rel} - E_{nonrel}$ are $-4.3\times10^{-6}$, $5.5\times10^{-5}$ and $3.3\times10^{-4}$ for $B=1$, $B=500$ and $B=5000$, respectively.

**Table IV.** Hydrogen atom of the $1s_{1/2}$ and $2p_{3/2}$ states in a magnetic field B=1, B=500 and B= 5000 by the relativistic calculation using both inverse and regular DE at the diagonalization step. Iteration number: n and number of independent functions: M are n=16, M=867 (192,225,225,225) for $1s_{1/2}$ and n=16, M=902 (200,234,234,234) for $2p_{3/2}$.

| B | State | Energy (a.u.) (Inverse) | Energy (a.u.) (Regular) | Ref. 8 |
|---|---|---|---|---|
| 1 | $1s_{1/2}$ | **-0.831 173 225 931 948** 773 | **-0.831 173 225 931 948** 774 | -0.831 173 226 |
| | $2p_{3/2}$ | **-0.456 597 236 750 452** 001 | **-0.456 597 236 750 452** 004 | -0.456 597 24 |
| 500 | $1s_{1/2}$ | **-6.25 703 258 758** 308 998 | **-6.25 703 258 758** 402 | -6.25 703 26 |
| | $2p_{3/2}$ | **-4.53 121 620** 594 537 | **-4.53 121 620** 672 520 | |
| 5000 | $1s_{1/2}$ | **-11.8 730 884 0**06 583 | **-11.8 730 884 0**25 355 | -11.8 730 8 |
| | $2p_{3/2}$ | **-9.04 121 822** 465 259 | **-9.04 121 823** 350 083 | |

**Table V.** Helium atom of the $^1S_0$ and $^3P_0$ states in a magnetic field B=0.5, B=1 and B=5 by the nonrelativistic calculation.

| n[a] | $^1S_0$ | | $^3P_0$ | |
|---|---|---|---|---|
| | M[b] | Energy (a.u.) | M[b] | Energy (a.u.) |
| **B=0.5** | | | | |
| 0 | 1 | **-2.**71 875 000 000 | 1 | -1.26 374 742 798 |
| 1 | 11 | **-2.85** 517 267 872 | 20 | **-2.47** 646 119 926 |
| 2 | 91 | **-2.85 62**1 994 405 | 169 | **-2.48 0**20 243 581 |
| 3 | 438 | **-2.85 623** 669 370 | 913 | **-2.48 053** 807 174 |
| Ref. 13 | | | | |
| Ref. 14 | | -2.85 585 9 | | |
| Ref. 15 | | | | |
| **B=1** | | | | |
| 0 | 1 | **-2.**62 500 000 000 | 1 | -1.60 437 242 798 |
| 1 | 11 | **-2.72** 918 264 280 | 20 | **-2.7**0 899 955 438 |
| 2 | 91 | **-2.73 03**5 725 975 | 169 | **-2.73** 068 040 588 |
| 3 | 438 | **-2.73 037 8**49 564 | 913 | **-2.73** 355 366 641 |
| Ref. 13 | | -2.73 037 3 | | |
| Ref. 14 | | -2.72 950 8 | | |
| Ref. 15 | | -2.73 038 | | -2.73 748 |
| **B=5** | | | | |
| 0 | 1 | 3.28 125 000 000 | 1 | 3.69 438 014 403 |
| 1 | 11 | **-0.5**33 042 840 793 | 20 | **-3.**54 852 315 575 |
| 2 | 91 | **-0.57**3 897 655 725 | 169 | **-3.8**5 616 533 898 |
| 3 | 438 | **-0.575 6**30 909 124 | 913 | **-3.91 6**80 071 945 |
| Ref. 13 | | -0.575 5 | | |
| Ref. 14 | | -0.574 877 | | |
| Ref. 15 | | | | |

a Iteration number.

b Number of the independent functions.

We next performed the nonrelativistic ICI calculations of the helium atom in a magnetic field. We summarize in Table V the calculated energies of the $^1S_0$ and $^3P_0$ states in the magnetic field $B = 0.5, 1, 5$. In ICI, we used the $g$ and initial functions given in Eq. (3.19) and Eq. (3.20). The nonlinear parameters in the initial functions are $\alpha = 2$, $\alpha = 2$ and $\alpha = 4$ for $B = 0.5$, $B = 1$ and $B = 5$, respectively. For more stronger magnetic field than $B = 5$, the spherical functional space we used may poorly represents the wave function of cylindrical shape, so we did not calculate them in this thesis. However, in our calculations, since the wave function contains the explicitly

correlated terms $r_{12}$, accurate electron correlations may be represented in the wave function. As shown in Table V, the energy appears to converge to the exact solution and the agreement with the reference calculations.[13-15] For the $^1S_0$ state, our results at the iteration 3 are the best values compared to the literature values in the all magnetic field strength. For the $^3P_0$ state, the ICI method also indicates good performance. Since the $^3P_0$ state has the parallel spin, the energy becomes stable by increasing magnetic filed strength. In contrast, since the $^1S_0$ state has the unparallel spin, this state indicates an anti-ferromagnetic property. In the magnetic field $B = 0$ and $B = 0.5$, the ground state is the $^1S_0$ state. However, in the magnetic field $B = 1$ and $B = 5$, the ground state changes from $^1S_0$ state to the triplet state. Calculating the ground and many excited states is important to study spectra in the astrophysics.

**Table VI.** Helium atom of the $^1S_0$ state in a magnetic field B=0.5, B=1 and B=5 by the relativistic calculation using inverse DE at the diagonalization step.

| n[a] | M[b] | Energy (a.u.) (Inverse) |
|---|---|---|
| **B=0.5** | | |
| 0 | 7 (1,2,4) | -2.71 884 542 381 |
| 1 | 88 (35,41,12) | -2.85 528 180 967 |
| 2 | 534 (229,133,172) | -2.85 628 511 025 |
| Nonrelativistic | | -2.85 623 669 370 |
| **B=1** | | |
| 0 | 7 (1,2,4) | -2.62 512 463 617 |
| 1 | 88 (35,41,12) | -2.72 935 006 715 |
| 2 | 534 (229,133,172) | -2.73 017 320 172 |
| Nonrelativistic | | -2.73 037 849 564 |
| **B=5** | | |
| 0 | 7 (1,2,4) | 0.374 059 092 990 |
| 1 | 88 (35,41,12) | -0.513 296 152 963 |
| 2 | 534 (229,133,172) | -0.550 498 994 370 |
| Nonrelativistic | | -0.575 630 909 124 |

a Iteration number.

b Number of the independent functions for expanding $\psi$ : M ($M_{ll}$, $M_{ls}$, $M_{ss}$).

Finally, we performed the relativistic calculations of the helium atom of the $^1S_0$ state in the magnetic field $B = 0.5, 1, 5$. To avoid the variational collapse, we used the inverse Hamiltonian at the diagonalization step. We chose the $g$ and initial functions given in Eq. (3.19) and Eq. (3.21) and we used the same nonlinear parameters in the initial function as the nonrelativistic calculations: $\alpha = 2$, $\alpha = 2$ and $\alpha = 4$ for $B = 0.5$, $B = 1$ and $B = 5$, respectively. We summarize the calculated energies in Table VI. Our wave functions include the correlation terms $r_{12}$ explicitly, therefore, this thesis is the first accurate calculations of the helium atom in a magnetic field at the relativistic level. Although the Hamiltonian contained vector potential with scalar potential, the variational collapse did not occur as far as ICI and using the inverse Hamiltonian. As shown in Table VI, the energy appears to converge to the exact solution from above without any variational problem in the all magnetic field. The relativistic corrections from the nonrelativisitc results are also small same as the hydrogen atom. The differences between the relativistic and nonrelativistic energies $\Delta E = E_{rel} - E_{nonrel}$ are $-4.8\times10^{-5}$, $2.1\times10^{-4}$ and $2.5\times10^{-2}$ for $B = 0.5$, $B = 1$ and $B = 5$, respectively. The relativistic corrections become large by increasing the magnetic field strength and the sign of $\Delta E$ changes from $B = 0.5$ to $B = 1$, this is the same trends as the hydrogen atom.

## 4. Conclusion

We have studied the hydrogen and helium atoms in a uniform magnetic field by using the ICI method in the nonrelativistic and relativistic calculations. The ICI method also indicates very good performance even for the systems in a magnetic field. In not only the nonrelativistic calculations but also the relativistic calculations, the variational calculations are performed and the energy of the ICI converges to the exact solution from above without any variational collapse.

For the hydrogen atom in the nonrelativistic calculations, we obtained the energy of the accuracy about 33-35 digits and improve the best literature value in the magnetic field strength $B = 1$. However, in the extremely strong magnetic field, the speed of the convergence to the exact solution was slow because the coordinates we used were suitable for middle range of magnetic field strength but not suitable for extremely strong field, in whose systems cylindrical or parabolic coordinates may be best choice. We will perform the calculations in these coordinates elsewhere. Also in the relativistic

calculations, our ICI energies improved the reference values. The variational collapse did not occur even when we used the regular Hamiltonian at the diagonalization step.

For the helium atom in the nonrelativistic calculations, we could obtain the very accurate results and improve the literature values in almost cases. Similar to the hydrogen atom, the choice of the coordinates is important and we should choose the cylindrical or parabolic coordinates for extremely strong magnetic field. In the relativistic level, this thesis is the first accurate calculation includes the explicitly correlated terms $r_{12}$ in the wave functions. We used the inverse Hamiltonian at the diagonalization step and any variational collapse did not occur.

By using the ICI method, it becomes possible to calculate the systems in a strong magnetic field accurately at both the nonrelativistic and relativistic levels. More accurate calculations for extremely strong magnetic field and more interesting physical properties will be discussed elsewhere.

**ACKNOWLEDGMENTS**

This study has been supported financially by a Grant for Creative Scientific Research from the Ministry of Education, Science, Culture, and Sports of Japan.

## REFERENCES


1. J. C. L. Guillow, J. Z. Justin, *Ann. Phys.* S. **147**, 57, 1983.
2. S. Jordan, P. Schmelcher, W. Becken, *Astron. Astrophys.* **376**, 614, 2001.
3. T. S. Monteiro, G Wunner, *Phys. Rev. Lett.* **65**, 1100, 1990.
4. D. Delande, J. C. Gay, *Phys. Rev. Lett.* **57**, 2006, 1986.
5. D. Wintgen, A. Hönig, *Phys. Rev. Lett.* **63**, 1467, 1989.
6. H. C. Praddaude, *Phys. Rev. A* **6**, 1321, 1972.
7. C. Stubbins, K. Das, Y. Shiferaw, *J. Phys. B* **37**, 2201, 2004.
8. Z. Chen, S. P. Goldman, *Phys. Rev. A* **45**, 1722, 1992.
9. Z. Chen, S. P. Goldman, *Phys. Rev. A* **48**, 1107, 1993.
10. A. Poszwa, A. Rutkowski, *Phys. Rev. A* **63**, 043418, 2001.
11. A. Poszwa, A. Rutkowski, *Phys. Rev. A* **69**, 023403, 2004.
12. C. R. Liu, A. F. Starace, *Phys. Rev. A* **35**, 647, 1987.
13. M. Hesse, D. Baye, *J. Phys. B* **37**, 3937, 2004.
14. W. Becken, P. Schmelcher, F. K. Diakonos, *J. Phys. B* **32**, 1557, 1999.
15. A. Scrinzi, *Phys. Rev. A* **58**, 3879, 1998.
16. H. Nakatsuji, *J. Chem. Phys.* **113**, 2949, 2000., H. Nakatsuji, E. R. Davidson, *J. Chem. Phys.* **115**, 2000, 2001. H. Nakatsuji, *J. Chem. Phys.* **115**, 2465, 2001. H. Nakatsuji, *J. Chem. Phys.* **116**, 1811, 2002. H. Nakatsuji, M. Ehara, *J. Chem. Phys.* **117**, 9, 2002. H. Nakatsuji, M. Ehara, *J. Chem. Phys.* **122**, 194108, 2005.
17. H. Nakatsuji, *Phys. Rev. A* **65**, 052122, 2002.
18. H. Nakatsuji, *Phys. Rev. Lett.* **93**, 030403, 2004.
19. H. Nakatsuji, *Phys. Rev. A* **72**, 062110, 2005.
20. Y. Kurokawa, H. Nakashima, H. Nakatsuji, *Phys. Rev. A* **72**, 062502, 2005.
21. H. Nakatsuji, H. Nakashima, *Phys. Rev. Lett.* **95**, 050407, 2005.
22. H. Nakashima, H. Nakatsuji, *unpublished.*
23. L. D. Landau, E. M. Lifschitz, *Quantum Mechanics: Non-Relativistic Theory* (Pergamon, Oxford, 1977).
24. A. R. Edmonds, *Angular Momentum in Quantum Mechanics* (Princeton University Press, Princeton, 1957).
25. R. N. Hill, C. Krauthauser, *Phys. Rev. Lett.* **72**, 2151, 1994.

# Part II

# Theoretical Study for the Reversible $O_2$ Binding Mechanism of Fe-Porphyrin Complex and its Isomers

# Chapter 4

# On the Reversible $O_2$ Binding of Fe-Porphyrin Complex

**Abstract:**

Electronic mechanism of the reversible $O_2$ binding by heme was studied by using Density Functional Theory calculations. The ground state of oxyheme was calculated to be open singlet state (Fe(S=1/2)+$O_2$(S=1/2)). The potential energy surface for the singlet state is associative, while that for triplet state is dissociative. Since the ground state of the $O_2$ + deoxyheme system is triplet in the dissociation limit (Fe(S=2)+$O_2$(S=1)), the $O_2$ binding process requires relativistic spin-orbit interaction to accomplish the intersystem crossing from triplet to singlet states. Owing to the singlet-triplet crossing, the activation energies for both $O_2$ binding and dissociation become moderate and hence reversible. We also found that the deviation of the Fe atom from the porphyrin plane is also important reaction coordinate for $O_2$ binding. The potential surface is associative/dissociative when the Fe atom locates in-plane/out-of-plane.

## 1. Introduction

Hemoglobin and myoglobin play indispensable roles in the living body: transport and storage of dioxygen. These processes have been studied in detail both theoretically and experimentally.[1-10] Hemoglobin and myoglobin have the same active site, heme (Fe-porphyrin complex), and the tertiary structure of a subunit of hemoglobin is very similar to that of myoglobin. However, the $O_2$ binding process is quite different between the two molecules. In hemoglobin, the $O_2$ dissociation curve shows so called S-form due to the allosteric effect, while in myoglobin the $O_2$ dissociation curve is hyperbolic. In hemoglobin, the present allosteric model proposes that the change of the quarternary structure between T- and R-forms controls the $O_2$ affinity. The T- and R-forms have low and high oxygen affinity, respectively.[11,12]

The $O_2$ affinity of myoglobin and hemoglobin has been studied experimentally from mainly two perspectives: with regard to substitution of the amino acid residue[3-5] and substitution of heme itself by a similar modified heme (Fe-porphycene, Fe-azaporphyrin etc.).[13-17] The former studies concern the allosteric mechanism of hemoglobin. Hemoglobin has 4 subunits connected each other by salt bridges, hydrogen bonds and van der Waals interactions. Although there is no firm conclusion on the allosteric effect, it is known that these interactions control the structure of the active site, heme, in hemoglobin.[11,12] Therefore, it is worth investigating how the structure change affects the $O_2$ binding. In the latter studies, Hayashi.et al. reported that the replacement of heme itself (Fe-porphyrin) by the modified heme (Fe-porphycene) in myoglobin had extremely high $O_2$ affinity (compared to the native myoglobin, more than 1,000 times).[16,17] This result shows that the electronic structure of the active site itself is very important in the $O_2$ affinity. Therefore, quantum mechanical calculation on the active site could draw important conclusion.

The electronic structures of oxyheme and deoxyheme have been theoretically studied at several theoretical levels, MNDO/d,[18] QM/MM,[19-21] DFT using LSD schemes,[22-24] CASSCF,[25-27] CASPT2[28] and SAC/SAC-CI[29] calculations.[30] These studies mainly addressed the electronic structures of oxyheme and deoxyheme but not the change in the electronic structure during the $O_2$ binding process. In this study, we focus the $O_2$ binding process. The electronic structures of oxyheme and deoxyheme and their stabilities are rather subtle problems, because of the existence of many possible spin states and the electron correlations. Therefore, we will discuss these problems, comparing our

calculations with several theoretical studies.

There are two important aspects in the dioxygen binding process in the active site of myoglobin and hemoglobin: the change in the spin state and the change in the structure of heme.[31] Intersystem crossing is necessary in the $O_2$ binding process. The ground states of deoxyheme and $O_2$ molecule are in quintet (S=2) and triplet state (S=1), respectively, and the total system is triplet. In oxyheme, the spin multiplicity becomes low-spin singlet state (S=0) after the $O_2$ binding.[32,33] A large structural change is also seen in the $O_2$ binding process. Oxyheme has the Fe atom in the same plane as the porphyrin ring, while there are large deviations from the plane in the deoxyheme (myoglobin: 0.3-0.4 Å, hemoglobin: 0.5-0.6 Å).[34-38]

In this study, we investigated these two aspects that could be important in the reversible $O_2$ binding process in myoglobin and hemoglobin. We studied the electronic structure of oxy-/deoxyheme and the potential energy surface for the $O_2$ binding process using the Density Functional Theory to understand how these factors control the oxygen affinity.

## 2. Computational details

We studied model systems: $O_2$-Fe(II)-Porphin(Por)-Imidazole(Im) for oxyheme and Fe(II)-Por-Im for deoxyheme (Fig. 1). DFT (UB3LYP) calculations were performed with the following basis set and geometries using the Gaussian98 program package.[39] The basis set used was 6-31g* for Fe, O and pyrrole N atoms and 6-31g for the other atoms.[40]

To identify the spin-multiplicity of the ground state, we determined the energy-minimum structure of deoxyheme in singlet, triplet and quintet states and oxyheme in singlet and triplet states.

Next, we calculated the potential energy surfaces of the $O_2$ binding process in the singlet and triplet states as functions of two reaction coordinates: d (the deviation of the Fe atom from the porphyrin plane) and the distance R between Fe and $O_2$ (Fig. 1). We selected 46 points which were placed at intervals of 0.1 Å for coordinate d and at intervals of 0.2 Å (or 0.1 Å near minimal point) about coordinate R. In this calculation, other atomic coordinates except for d and R were changed linearly between the optimized geometry for the singlet state of oxyheme ($O_2$-binding state) and that for the triplet state of oxyheme (dissociation limit). We first optimized the atomic coordinates

for $O_2$-binding state ($X_{bind}$) and dissociation limit ($X_{dis}$). With a parameter $\lambda$ ($0 \leq \lambda \leq 1$), the atomic coordinates between the two structures were linearly defined as Eq.(4.1). At each point, the Fe-$O_2$ distance, R, was changed, keeping all other geometric parameters fixed.

$$\mathbf{X} = \lambda \mathbf{X}_{bind} + (1-\lambda)\mathbf{X}_{dis} \tag{4.1}$$

We later checked the relaxation effects on the potential energy surface and found that the structural relaxation gave only minor changes in the potential surface as described in section 3.2.

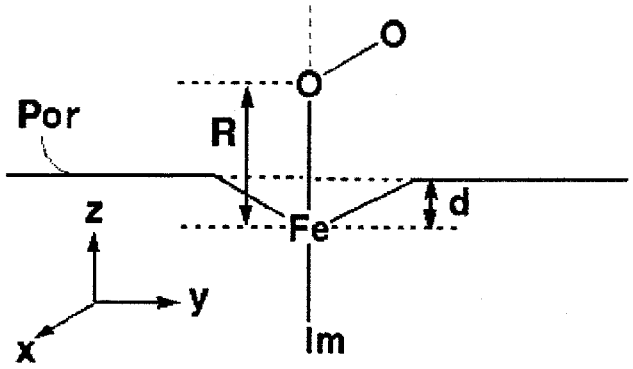


**Fig.1** Illustration of the calculation model. Two reaction coordinates are defined: d (Å) (the deviation of Fe from the porphyrin plane) and R (Å) (the distance between Fe and dioxygen). In this figure, "Im" means imidazole and "por" means porphyrin ring.

## 3. Results and Discussion

### 3.1 Ground states of deoxyheme and oxyheme

First, we investigated the geometries and electronic structures of the ground-state of deoxyheme and oxyheme. Table I shows the optimized geometry and relative energy in each spin multiplicity. The ground state of deoxyheme was calculated to be a quintet state, and the triplet and singlet states locate 0.67 kcal/mol and 6.48 kcal/mol higher than the quintet state, respectively. Although the energy difference among these states are very small, the present conclusion agrees with the previous experimental study: in a heme model, Fe(II)-OEP(OctaEthylPorphyrin)-(2-MeIm),[41] and the active sites of myoglobin and hemoglobin protein[31-33], the ground-state spin-multiplicity is quintet.

The optimized geometry of the quintet state is quite different from those of the triplet and singlet states. In the quintet state, the Fe atom lies out of the porphyrin plane by d = 0.429 Å, which is much larger than the cases of the triplet state (0.190 Å) and the singlet state (0.201 Å). The calculated geometry for the quintet state agrees with the results

obtained by X-ray crystallographic data for both myoglobin and biomimetic complexes,[34-38] in which this deviation of Fe distributes around 0.3-0.4 Å (0.34 Å for a biomimetic deoxymyoglobin model[37]). The electronic reason of the position of the Fe atom is relevant to the occupation of the $d_{x^2-y^2}$ orbital in the quintet state (the $d_{x^2-y^2}$ orbital is unoccupied in the triplet and singlet states). Since the $d_{x^2-y^2}$ orbital has anti-bonding interaction with the lone-pair of the pyrrole N in the porphyrin plane, the out-of-plane position becomes stable. As shown in Table I, the dihedral angle, Pyr N – Fe – Im N- Im C, of quintet deoxyheme (0.204 deg.) is different from those of triplet (44.8 deg.) and singlet deoxyheme (44.9 deg.). In the quintet state, the $d_{x^2-y^2}$ orbital interacts with the $\pi$ orbital of imidazole, and this interaction results in the change of the dihedral angle. The geometrical parameters agree reasonably well with those of a biomimetic deoxymyoglobin model as shown in Table I.[37]

The ground state of oxyheme is the singlet state, and the triplet state locates 8.36 kcal/mol higher than the singlet state. As shown in Table I, the optimized geometry of the singlet state is in reasonable agreement with the experimental X-ray crystallographic data for both myoglobin and biomimetic complexes.[34-38] The Fe atom locates inside the porphyrin-plane. The distance between Fe and $O_2$ was 1.85 Å. The O-O bond length was 1.29 Å, which is very close to free $O_2$. In the triplet state, the Fe atom lies out of porphyrin-plane by 0.394 Å. The Fe-O and O-O distance is 2.91 Å and 1.22 Å, respectively. The Fe-O distance of the triplet oxyheme is by 1.0 Å larger than that of the singlet oxyheme. The imidazole plane is parallel to the Fe-pyrrole N plane in contrast to the 45°-rotated structure in the singlet state. These results indicate that the electronic structure of the triplet ground state is described as Fe(S=2) + $O_2$(S=1): the electronic structure of the Fe-Por-Im moiety is very close to that of the quintet state of deoxyheme, Fe(S=2). Therefore, the triplet state of oxyheme does not bind $O_2$ strongly, as we see in section 3.2. Most theoretical and experimental studies suggested that the heme binds $O_2$ in singlet ground state.[18-24,26,27,29] We will discuss the electronic structure of the $O_2$ binding state in section 3.3 in more detail.

### 3.2 The potential energy surface for the $O_2$ binding process

We investigated the potential energy surface for the $O_2$ binding process in triplet and singlet states as functions of d and R (see Figure 1) to understand the mechanism of the $O_2$ binding.

**Table I.** The optimized geometries and total energy of deoxyheme and oxyheme in each spin state: for deoxyheme, the quintet state, triplet state and singlet state; for oxyheme, the triplet state and singlet state. For deoxyheme, the total energy of the quintet state is set at 0.00 kcal/mol and for oxyheme, the total energy of the singlet state is set at 0.00 kcal/mol.

| | Deoxyheme | | | Oxyheme | |
|---|---|---|---|---|---|
| | quintet[a] | triplet | singlet | triplet | singlet[b] |
| **Relative energy (kcal/mol)** | **0.00** | **0.671** | **6.48** | **8.36** | **0.00** |
| **Optimized geometry** | | | | | |
| **distance (Å)** | | | | | |
| Fe - Im N | 2.13(2.134) | 2.21 | 1.91 | 2.14 | 2.07(2.07) |
| Fe - Pyr N | 2.09(2.075) | 2.01 | 2.00 | 2.09 | 2.01(1.97-1.99) |
| Fe – O | - | - | - | 2.91 | 1.85(1.75) |
| O – O | - | - | - | 1.22 | 1.29(1.15-1.32) |
| Fe - Por plane | **0.429(0.34)** | **0.190** | **0.201** | **0.394** | **0.0253(0.03)** |
| **angle (degree)** | | | | | |
| Pyr N - Fe - Pyr N | 88.8 | 89.1 | 89.6 | 89.0 | 89.6 |
| | 88.7 | 90.4 | 89.8 | 88.9 | 90.7 |
| Pyr N - Fe - Im N | 98.6 | 94.2 | 94.7 | 99.1 | 89.5 |
| Fe - O - O | - | - | - | 119.7 | 118.1(129-133) |
| **dihedral angle (degree)** | | | | | |
| Pyr N – Fe - Im N - Im C | 0.204 | 44.8 | 44.9 | 2.67 | 44.2 |

[a] The values in the parenthesis are the X-ray structural data for the biomimetic myoglobin model.[37]

[b] The values in the parenthesis are the X-ray structural data for the biomimetic oxymyoglobin model[38].

As seen in Figure 2 (a), the potential energy surface of the triplet state is entirely dissociative. In the dissociation limit, the total electronic structure is Fe(S=2) + $O_2$(S=1): the ground states of deoxyheme (quintet state) and $O_2$ (triplet state). The Fe atom locates the out-of-plane position in the dissociation limit, as in the ground state of deoxyheme. One exception is the case that the parameter d (distance from the porphyrin plane) is fixed to around zero. The potential curve becomes slightly associative, even though the binding energy is very small.

On the other hand, the potential energy surface of the singlet state is entirely associative. In the energy minimal structure, the Fe atom locates in the porphyrin plane. We also found that the character of the potential curve depends on the parameter d. With the Fe atom fixed around the porphyrin plane (d $\approx$ 0.0) the potential curve is highly associative, while the curve becomes dissociative when the Fe atom is fixed at out of

the plane.

As explained in section 2, the structural parameters except for R and d were linearly changed between the binding structure and the dissociation limit in calculating the potential energy surfaces. We describe here the effect of the structural relaxation to the potential surfaces. To confirm the results shown in Figure 2, we carried out geometry optimization with fixed R and d at structures (i) near to $O_2$ binding state (small R and small d), (ii) near the dissociation limit (large R and large d), and (iii) intermediate between them (middle R and middle d). First, there was no crucial difference between the partially optimized and linearly changed structures in all cases (i-iii). Second, the error in the potential surfaces due to the lack of the structure relaxation is expected to be at most 1 kcal/mol. Since we performed the optimization of all structural parameters for both the binding state and dissociation limit, the linearly-changed structures around (i) and (ii) would be reliable. For the structure around (iii), the energy change due to the relaxation was calculated to be 1.08 kcal/mol in the singlet state, which was the worst example in the examinations.

Thus, two important conclusions are derived: *(1) Heme binds $O_2$ only in its singlet state, because the potential surface is entirely associative. (2) The potential curve becomes associative when the Fe atom locates close to the porphyrin plane, while the potential curve changes into dissociative when the Fe atom lies out of the plane.* The former indicates the importance of the relativistic effect, spin-orbit interaction, in the $O_2$ binding. The latter indicates that the $O_2$ affinity can be controlled by tuning the geometry parameter d, the deviation of the Fe atom from the porphyrin ring. Table II summarizes the oxygen affinity in terms of the spin multiplicity and the deviation of the Fe atom.

**Table II.** $O_2$ affinity of heme in single and triplet states and in different deviation of the Fe atom.

| Spin multiplicity | Deviation of Fe | Potential curve | Oxygen affinity |
|---|---|---|---|
| Singlet | in plane | Associative | High |
| Singlet | out of plane | Slightly associative | Very low |
| Triplet | in plane | Slightly associative | Very low |
| Triplet | out of plane | Dissociatibve | None |

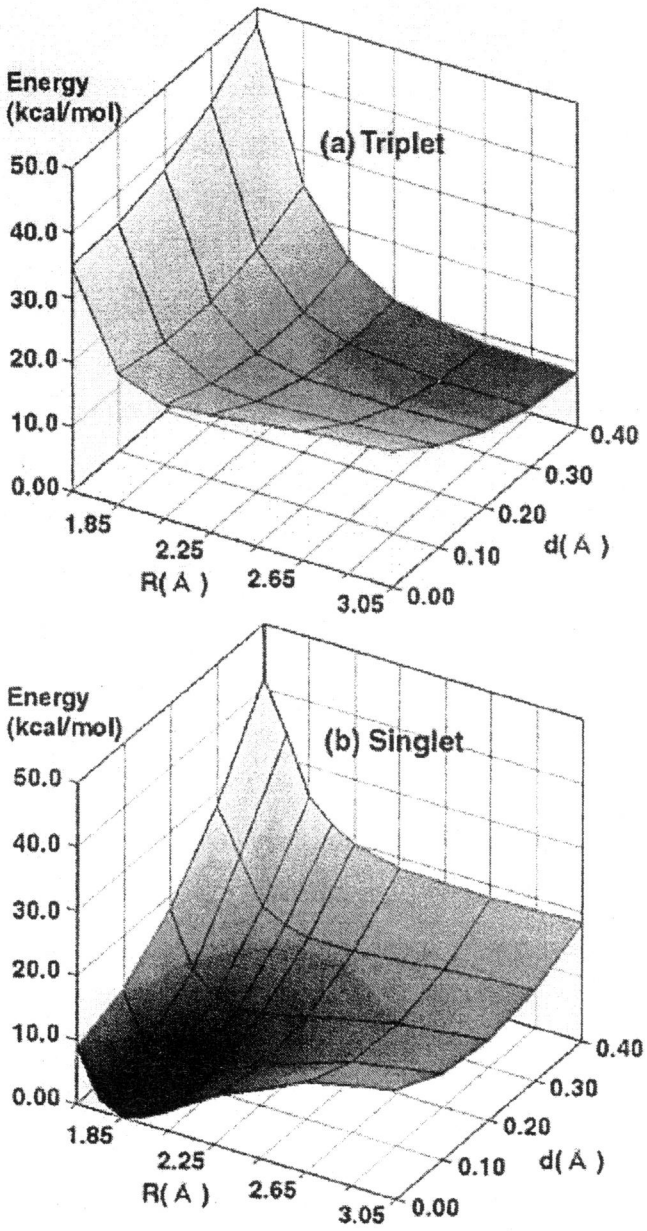


**Fig.2** The potential energy surface in each spin state as a function of two reaction coordinates: d (Å) (the deviation of Fe from the porphyrin plane) and R (Å) (the distance between Fe and dioxygen). A darker color shows greater stability.

### 3.3 The electronic structure and the $O_2$ affinity

The $O_2$ affinity is mainly controlled by (1) the spin multiplicity of the oxyheme and (2) the deviation of the Fe atom from the porphyrin plane. We analyze these results from the electronic structural view point.

(1) Spin state: As shown in Table II, oxyheme has high $O_2$ affinity only in the singlet state. In the triplet state of oxyheme, an unpaired electron occupies the Fe($d_x2_{-y}2$) orbital,

while the electron is in the Fe($d_{yz}$) orbital as paired electron in the singlet state. This would be one reason of the difference in the $O_2$ affinity between the triplet and singlet states. Since the Fe($d_x2_{-y}2$) orbital and the N(lone-pair) of pyrrole have anti-bonding interaction, the Fe atom prefers to be out of the porphyrin plane. The electronic structure of the Fe-Por-Im moiety is very similar to that of deoxyheme in the quintet state.

(2) Deviation of the Fe atom from the porphyrin plane: Since the Fe($d_z2$) orbital forms σ-bond with the $O_2(\pi^*)$ orbital, this orbital could be related to the dependency between the $O_2$ affinity and the position of the Fe atom. When the Fe atom locates in-plane, the Fe($d_z2$) orbital cannot interact with the π orbitals of the porphyrin ring due to symmetry. However, when the Fe atom locates out of plane, the Fe($d_z2$) orbital can interact with the π orbital of the porphyrin ring due to the broken symmetry. This makes the Fe($d_z2$) orbital stable because π-electron of the porphyrin flows into the Fe($d_z2$) orbital. Therefore, the interaction between the Fe($d_z2$) and the $O_2(\pi^*)$ orbitals becomes weaker.

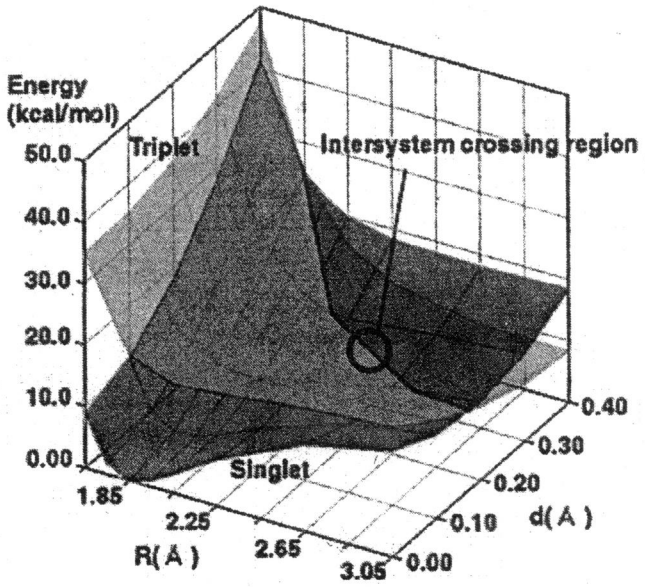


**Fig.3** The potential energy surface with the singlet state on the triplet state. A dark color shows the singlet state surface and a bright color shows the triplet state surface. The intersystem crossing area appears at d = 0.2-0.4 Å and R = 2.2-2.5 Å.

### 3.4 Intersystem crossing in the $O_2$ binding process

In Figure 3, the singlet and triplet potential surfaces were compared. The ground state of oxyheme is singlet in the binding region, while triplet state is the ground state in the dissociation limit. In addition, the potential surface of the triplet state is entirely dissociative. Therefore, intersystem crossing is indispensable in the $O_2$ binding process. The interaction which allows the crossing is the spin-orbit interaction. In this sense, *relativistic effect is essentially important for the $O_2$ binding in the living bodies.*

Next, we analyze the potential energy surface with the singlet state upon the triplet state, as shown in Fig. 3. There is a region where the intersystem crossing occurs. Since the energy levels of single and triplet states become degenerate in this region, the spin conversion is expected to happen easily, even though the spin-orbit interaction is very small. The area of the crossing appears in the range d=0.2-0.4 Å, and there is no crossing in d=0.0-0.1 Å. Since the $O_2$ actual binding process occurs approximately along the energy-minimum pathway, the actual intersystem crossing area would be around d=0.2-0.3 Å and R=2.2-2.5 Å.

### 3.5 On the Reversible $O_2$ binding

To understand the $O_2$ binding process, we extract energy-minimal $O_2$ binging pathway from Figure 3. As seen in Figure 4 (a), starting with the dissociation limit, the system in triplet state reaches to the intersystem crossing point by climbing over an energy barrier of 3.0 kcal/mol. At the crossing point, the triplet state converts into the singlet state due to the spin-orbit interaction. The system then proceeds to the $O_2$ binding state on the singlet potential energy surface. Consequently, the system gains 8.4 kcal/mol of the binding energy. In the $O_2$ dissociation, the system in singlet state needs 11.4 kcal/mol to reach the intersystem crossing region. After the spin state changes into the triplet state, oxyheme releases $O_2$ and reaches to the dissociation limit. If the $O_2$ binding occurs only along the singlet surface, the activation energy would be approximately 20 kcal/mol, which makes the $O_2$ release process very difficult. In this sense, the relativistic effect plays an important role in the reversible $O_2$ binding.

Using the calculated potential surface, we estimated the equilibrium constant for the $O_2$ binding and compared with that of human myoglobin. Our result shown in Figure 4(a) might be close to the situation in human myoglobin, since myoglobin does not show the allosteric effect.

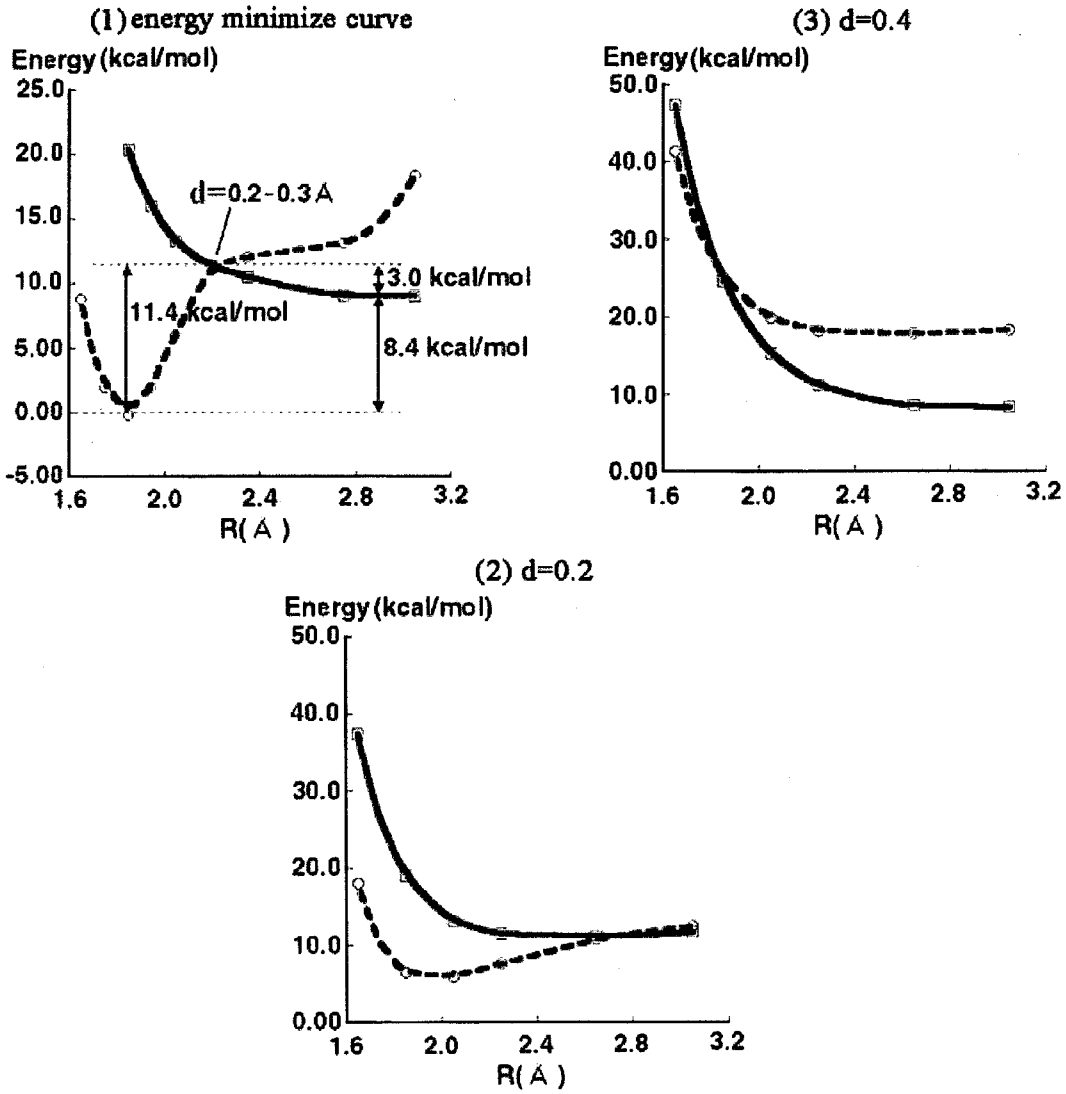


**Fig.4** The one dimensional potential energy curve for the $O_2$ binding for the singlet (the dotted line) and triplet (the solid line). (1) Approximate energy-minimum potential curve extracted from Figure 3. The intersystem-crossing occurs around d = 0.2 ~ 0.4 Å. (2, 3) The cross-section view of the Figure 3 at d=0.2 (2) and d=0.4 (3).

$$K = e^{-\frac{\Delta G}{RT}} \approx e^{-\frac{\Delta E}{RT}} \tag{4.2}$$

In Eq. (4.2), we assume that the entropy effects are constant and estimate the equilibrium constant from the binding energy (ΔE) instead of free energy (ΔG). The theoretically estimated equilibrium constant obtained from Eq. (4.2) was $1.8 \times 10^6$ [$M^{-1}$] at 20°C. The experimental value obtained for human myoglobin protein is $1.1 \times 10^6$ [$M^{-1}$] at pH 7.0 and 20°C.[42] Although we did not consider the effects of the surrounding

**Table III**. Spin population of oxyheme in the $O_2$ binding state, the crossing region, and the $O_2$ dissociation limit

| | $O_2$ binding state (singlet) | Crossing region (d=0.2,R=2.25) (singlet) | $O_2$ dissociation limit (triplet) |
|---|---|---|---|
| Gross orbital spin population: | | | |
| $d_{x^2-y^2}$ | 0.0733 | 0.1792 | 0.7992 |
| $d_{z^2}$ | 0.1306 | 0.4958 | 0.8025 |
| $d_{yz}$ | 0.4386 | 0.3470 | 0.9454 |
| $d_{xz}$ | 0.4368 | 0.6234 | 0.9281 |
| $d_{xy}$ | 0.0288 | 0.0519 | 0.1123 |
| Atomic spin population: | | | |
| Fe | 1.1520 | 1.7703 | 3.8825 |
| $O_2$ | -1.0864 | -1.6933 | -1.9944 |

protein, the estimated equilibrium constant is close to the experimental value. This may indicate that the interaction between heme and $O_2$ dominates the binding process more than that with the surrounding protein residues.

Next we examined a situation where an external confinement restricts the geometry: An external force acts on the imidazole, and the Fe atom moves out of the porphyrin ring. This was mimicked with the fixed parameter d. Figure 4(b) and (c) are cross-section view of the Figure 3 at d = 0.2 and 0.4 Å, respectively. In the case of d = 0.2 Å, the valley of the singlet-state potential curve becomes shallow, while there is little change in the triplet-state potential curve. The activation energy for the $O_2$ dissociation significantly decreased to about 5 kcal/mol. Approximately 6 kcal/mol of energy should be used for pulling the Fe-Imidazole moiety toward outside. In the case of d = 0.4 Å, the potential curve for the singlet states turns to dissociative, while the triple state shows only minor change in the potential curve. There is almost no energy barrier to dissociate $O_2$ molecule.

In summary, owing to the relativistic effect, the spin-orbit interaction in this case, heme obtains high reversibility in the $O_2$ binding. When heme is free from the structural confinement by the protein environment, it is natural for the system to go along the energy-minimal pathway and to bind $O_2$ with the activation barrier of only 3.0 kcal/mol, as shown in Figure 4 (a). Change of the structural parameter d from in-plane to out-of-plane significantly switches the singlet-state potential curve from associative to disscociativey. When one assumes that heme has an external confinement forcing the

Fe-Imidazole unit to be out of the porphyrin ring, oxyheme easily releases $O_2$ molecule without large activation energy.

### 3.6 The electronic-structure of oxyheme and its changes during the $O_2$ binding

In this section, we describe the electronic structure of oxyheme in the $O_2$ binding process. Figure 5 illustrates the changes of the electronic structure. Table III shows the spin population on each orbital and on each atom. In the $O_2$ dissociation limit, the spin multiplicity is triplet: heme and $O_2$ are in quintet (S=2) and triplet (S=1) states, respectively (Mulliken spin population: Fe:3.8825, $O_2$:-1.9944).

The $O_2$ molecule approaches to the intersystem crossing point, and the spin multiplicity converts into the singlet state. In this transition, an electron in the $d_{x^2-y^2}$ orbital flips its spin state and moves to the $d_{yz}$ orbital. This is seen in Table III. The spin population of the $d_{x^2-y^2}$ orbital 0.80 decreases to 0.18 and, that of the $d_{yz}$ orbital 0.95 decreases to 0.35. The $O_2$ molecule is still has two unpaired electron in this structure (spin population on Fe and $O_2$ is 1.77 and -1.69, respectively).

Finally, the $O_2$ molecule reaches to the binding state. Heme forms σ-bond between the Fe($d_{z^2}$) orbital and $O_2(\pi^{*,\parallel})$ orbital, where $\pi^{*,\parallel}$ denotes $\pi^*$ orbital parallel to the mirror plane (yz-plane) of the molecule. In the binding state, there is no apparent π-bond (π-back donation) between the Fe atom and $O_2$ molecule. As shown in Figure 5, the ground state of oxyheme is an open-shell singlet state: a biradical state having unpaired elections in each Fe($d_{xz}$) and $O_2(\pi^{*,\perp})$ orbitals (Mulliken spin population: Fe:1.15, $O_2$:-1.09). The $\pi^{*,\perp}$ orbital denotes $\pi^*$ orbital perpendicular to the mirror plane (yz plane) of the molecule. These two orbitals show little interaction each other, not like the ground state of $O_3$ molecule (a biradical electronic structure with singlet coupling). Therefore, the electronic structure in the ground state of oxyheme is different from Goddard model[43] and characterized as σ-bonding between Fe($d_{z^2}$) orbital and $O_2(\pi^{*,\parallel})$ and non-interacting unpaired electrons in Fe($d_{xz}$) and $O_2(\pi^{*,\perp})$ orbitals. The present result is compared with the previous studies. The DFT studies using LSD schemes also suggested an open-shell singlet ground state,[22-24] which is the same as our results. In contrast, the CASSCF study and the SAC/SAC-CI study suggested that the Hartree-Fock configuration is the main configuration in the ground state, although the weight of the Hartree-Fock configuration was rather small. These results indicates that these strong configuration interaction describes the biradical electronic structure.[26,27,29]

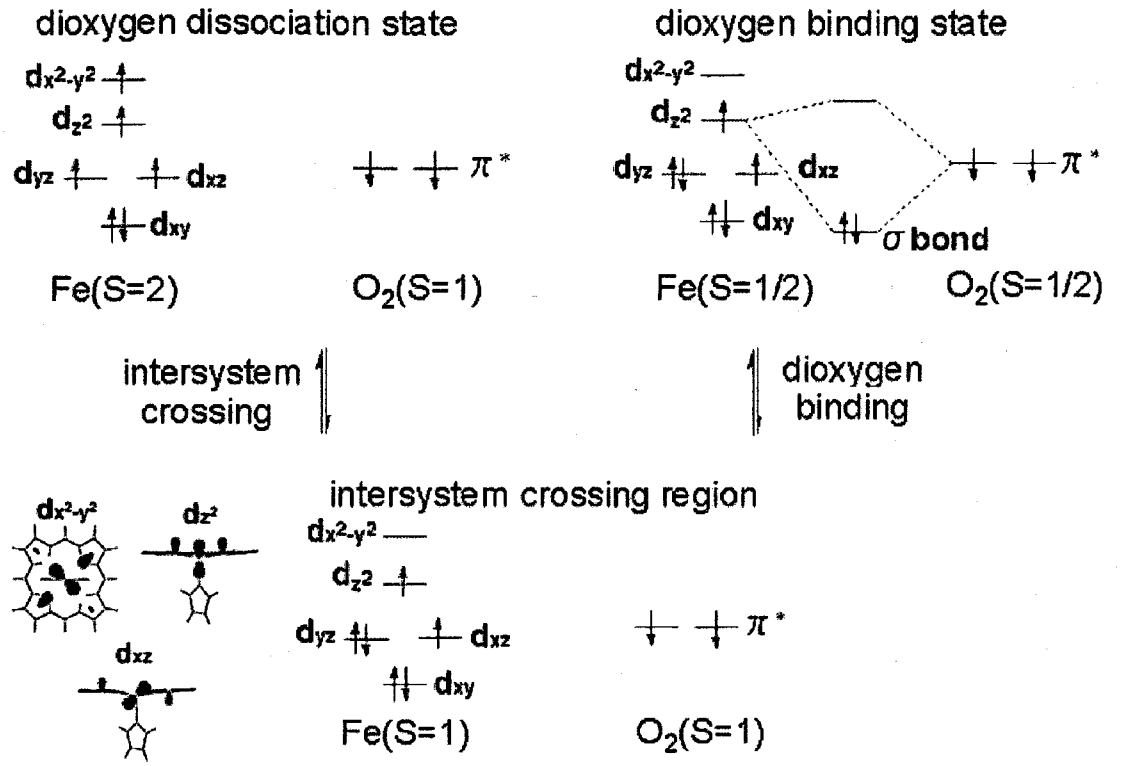


**Fig.5** The $d_{x^2-y^2}$, $d_{z^2}$ and $d_{xz}$ orbitals, and the change in electronic structure upon dioxygen binding.

$Fe(d_{xz})$ and $Fe(d_{yz})$ orbitals are almost equivalent by the symmetry reason. However, $Fe(d_{yz})$ orbital is slightly lower than $Fe(d_{xz})$ orbital by the effect of imidazole and Fe-$O_2$ plane. Therefore, the state in which the $Fe(d_{yz})$ orbital is occupied by two electrons is more stable than that the $Fe(d_{xz})$ orbital occupied by two electrons.

We examined the $S^2$ values of the calculated wave functions. In deoxyheme, the $S^2$ values of the quintet, triplet and singlet states were 6.0, 2.1, and 0.0, respectively. These values are pure spin multiplicities in each spin state. In oxyheme, these values of the $O_2$ dissociation limit (triplet : Fe(S=2) + $O_2$ (S=1)) and the $O_2$ binding state (singlet : Fe(S=1/2) + $O_2$ (S=1/2)) were 4.0 and 0.9, respectively. In the $O_2$ dissociation limit (triplet), the triplet and higher-spin state (septet) are degenerate. The $S^2$ value : 4.0 is the just median of the values of these two states (triplet : 2.0, septet : 6.0). In the $O_2$ binding state, as above-mentioned, the non-interacting unpaired electrons are left in $Fe(d_{xz})$ and $O_2(\pi^{*\perp})$ orbitals. Therefore, the singlet and higher-spin state (triplet) are almost degenerate. The $S^2$ value : 0.9 is also the middle of these two states (singlet : 0.0, triplet : 2.0) the same as in the $O_2$ dissociation limit. This is the drawback of the single-determinant description for the biradical states. Even though the optimized

structures agree well with the X-ray ones, more advanced method should be necessary to confirm the potential surfaces.

## 4. Conclusion

We investigated the mechanism of the reversible $O_2$ binding in heme by using Density Functional Theoretical calculations. First, we optimized the geometries of deoxyheme and oxyheme in their spin-multiplicities to determine the ground state.

In deoxyheme, the ground state is the quintet state where the Fe atom deviates greatly from the porphyrin plane. In oxyheme, the ground state is the singlet state where the Fe atom locates in the porphyrin plane. These results are in good agreement with experimental findings. These facts indicate that the electronic structure of the active site (heme) controls the geometry (planarity), rather than the surrounding protein effects.

Next, we studied the potential energy surfaces as functions of the deviation of the Fe atom from the porphyrin ring and the Fe-$O_2$ distance. The results indicate that the potential energy surface is entirely associative in singlet state, while it is dissociative in triplet state. The potential curve becomes associative when the Fe atom locates close to the porphyrin plane, while the potential curve changes into dissociative when the Fe atom lies out of the plane. This is because the large deviation of the Fe atom prevents $\sigma$ bond formation between the Fe atom and $O_2$ molecule. Comparing the potential energy surfaces of the singlet and triplet states, we found the intersystem crossing area (d: 0.2-0.3 Å, R: 2.2-2.5 Å), where the singlet and triplet states accidentally degenerate. Thus, the $O_2$ binding process proceeds from the triplet to the singlet states due to the spin-orbit interaction. We applied the present potential surface to estimate the equilibrium constant. The calculated $1.8\times 10^6\,[M^{-1}]$ is close to the experimental value $1.1\times 10^6\,[M^{-1}]$, indicating that the $O_2$ affinity is controlled by the electronic structure of oxyheme rather than the surrounding protein effects.

The transition probability by spin-orbit interaction is generally expected to be not so large. However, for the living bodies to survive, the intersystem crossing should be easily accomplished. Therefore, the $O_2$ binding reaction pathway should be firm and stable. It would be interesting to say that the relativistic effect works every time when we breathe.

We also studied the potential curve of the $O_2$ binding with the parameter d fixed to 0.2 and 0.4 Å. Although the triplet state was insensitive to the parameter d, the singlet

state shows significant changes in the potential curve. With the larger d, the potential curve becomes shallower. At d = 0.4 Å, the potential curve becomes dissociative. These results indicate that the change of d, the deviation of the Fe atom from the porphyrin ring, would be important reaction coordinate which controls the $O_2$ affinity.

Change of the electronic structure during the binding process was also studied. In the $O_2$ dissociation limit, the whole system in the triplet state includes heme in the quintet state and dioxygen in the triplet state. When $O_2$ approaches to heme and arrives at the intersystem crossing point, the spin state of the system changes from the triplet state to the singlet state by the spin-orbit coupling, so the spin state of heme moiety becomes the triplet state. The Fe($d_{xz}$) and Fe($d_z2$) orbitals are SOMO in the triplet state. When the $O_2$ further approaches to heme and arrives at the $O_2$ binding state, $\sigma$ bond is formed between the Fe($d_z2$) orbital of the Fe atom and the $O_2$ ($\pi^*$) orbital of dioxygen, while there is no strong $\pi$ bond. The electronic structure of $O_2$ binding state is an open-shell singlet state, namely a biradical state with singlet coupling, in which both the $d_{xz}$ orbital of Fe and the one $\pi^*$ orbital of dioxygen have non-zero spin density distribution. There is a strong $\sigma$ bond, but no $\pi$ bond formed between the $d_{xz}$ orbital of Fe and the $\pi^*$ orbital of dioxygen. Therefore, the electronic structure of the $O_2$ binding state is a biradical state with non-interacting singlet coupling, which is different from that of ozone.

**ACKNOWLEDGMENTS**

This study has been supported by the Grant for Creative Scientific Research from the Ministry of Education, Science, Sports and Culture. A part of the computations was performed in the Research Center for Computational Science, Okazaki, Japan.

## REFERENCES


1. J. D. Bernal, I. Fankuchen, J. F. Perutz, *Nature* **141**, 523, 1938.
2. J. Monod, J. Wyman, J. P. Changeux, *J. Mol. Biol.* **12**, 88, 1965.
3. J. J. Englander, J. N. Rumbley, S. W. Englander, *J. Mol. Biol.* **284**, 1707, 1998.
4. S. Bettati, A. Mozzarelli, M. F. Perutz, *J. Mol. Biol.* **281**, 581, 1998.
5. H. W. Kim, T. J. Shen, N. T. Ho, M. Zou, M. F. Tam, C. Ho, *Biochemistry* **35**, 6620, 1996.
6. Y. Tokita, H. Nakatsuji, *J. Phys. Chem. B* **101**, 3281, 1997.
7. P. Jewsbury, S. Yamamoto, T. Minato, M. Saito, T. Kitagawa, *J. Phys. Chem.* **99**, 12677, 1995.
8. S. Obara, H. Kashiwagi, *J. Chem. Phys.* 77, 3155, 1982.
9. A. Ghosh, D. F. Bocian, *J. Phys. Chem.* **100**, 6363, 1996.
10. P. Jewsbury, S. Yamamoto, T. Minato, M. Saito, T. Kitagawa, *J. Am. Chem. Soc.* **116**, 11586, 1994.
11. R. Liddington, Z. Derewenda, G. Dodson, D. Harris, *Nature* **331**, 725, 1998.
12. W. A. Eaton, E. R. Henry, J. Hofrichter, A. Mozzarelli, *Nature Struct. Biol.* **6**, 351, 1999.
13. S. Neya, T. Kaku, N. Funasaki, Y. Shiro, T. Iizuka, K. Imai, H. Hori, *J. Biol. Chem.* **270**, 13118, 1995.
14. S. Neya, H. Hori, K. Imai, Y. Kawamura-Konishi, H. Suzuki, Y. Shiro, T. Iizuka, N. Funasaki, *J. Biochem.* **121**, 654, 1997.
15. S. Neya, M. Tsubaki, H. Hori, T. Yonetani, N. Funasaki, *Inorg. Chem.* **40**, 1220, 2001.
16. T. Hayashi, H. Dejima, T. Matsuo, H. Sato, D. Murata, Y. Hisaeda, *J. Am. Chem. Soc.* **124**, 11226, 2002.
17. T. Matsuo, H. Dejima, S. Hirota, D. Murata, H. Sato, T. Ikegami, H. Hori, Y. Hisaeda, T. Hayashi, *J. Am. Chem. Soc.* **126**, 16007, 2004.
18. A. G. Taranto, J. W. M. Carneiro, F. G. Oliveira, *J. Mol. Struct. (Theochem)* **539**, 267, 2001.
19. J. Marechal, G. Barea, F. Maseras, A. Lledos, L. Mouawad, D. Perahia, *J. Comput. Chem.* **21**, 282, 2000.
20. F. Maseras, *New. J. Chem.* 327, 1998.
21. G. Barea, F. Maseras, A. Lledos, *Int. J. Quantum Chem.* **85**, 100, 2001.

22. C. Rovira, K. Kunc, J. Hutter, P. Ballone, M. Parrinello, *Int. J. Quantum Chem.* **69**, 31, 1998.
23. C. Rovira, M. Parrinello, *Int. J. Quantum Chem.* **70**, 387, 1998.
24. C. Rovira, M. Parrinello, *Int. J. Quantum Chem.* **80**, 1172, 2000.
25. Y. Choe, T. Hashimoto, H. Nakano, K. Hirao, *Chem. Phys. Lett.* **295**, 380, 1998.
26. S. Yamamoto, H. Kashiwagi, *Chem. Phys. Lett.* **161**, 85, 1989.
27. S. Yamamoto, H. Kashiwagi, *Chem. Phys. Lett.* **205**, 306, 1993.
28. Y. Choe, T. Nakajima, K. Hirao, R. Lindh, *J. Chem. Phys.* **111**, 3837, 1999.
29. H. Nakatsuji, J. Hasegawa, H. Ueda, M. Hada, *Chem. Phys. Lett.* **250**, 379, 1996.
30. I. Bytheway, M. B. Hall, *Chem. Rev.* **94**, 639, 1994.
31. W. R. Scheidt, C. A. Reed, *Chem. Rev.* **81**, 543, 1981.
32. L. Pauling, C. N. Coryell, *Proc. Natl. Acad. Sci. USA* **22**, 210, 1936.
33. M. Montenteau, C. A. Reed, *Chem. Rev.* **94**, 659, 1994.
34. S. E. V. Phillips, *Nature* **273**, 247, 1978.
35. S. E. V. Phillips, *J. Mol. Biol.* **142**, 531, 1980.
36. G. Fermi, *J. Mol. Biol.* **97**, 237, 1975.
37. M. Momenteau, W. R. Scheidt, C. W. Eigenbrot, C. A. Reed, *J. Am. Chem. Soc.* **110**, 1207, 1988.
38. G. M. Jameson, G. A. Rodley, W. T. Robinson, R. R. Gagne, C. A. Reed, J. P. Collman, *Inorg. Chem.* **17**, 850, 1978.
39. M. J. Frisch, G. W. Trucks, H. B. Schlegel, et al., *Gaussian98, Gaussian Inc., Pittsburgh, PA*, 1998.
40. P. C. Hariharan, J. A. Pople, *Theoret. Chim. Acta* **28**, 213, 1973.
41. T. Kitagawa, J. Teraoka, *Chem. Phys. Lett.* **63**, 443, 1979.
42. B. A. Springer, S. G. Sligar, J. S. Olson, G. N. Phillips Jr., *Chem. Rev.* **94**, 699, 1994.
43. W. A. Goddard III, B. D. Olasfson, *Proc. Natl. Acad. Sci. US* 72, 2335, 1975.

# Chapter 5

# On the $O_2$ Binding of Fe-Porphyrin, Fe-Porphycene and Fe-Corrphycene Complexes

**Abstract:**

Based on our previous study for the $O_2$ binding of the Fe-Por complex, this study investigates the $O_2$ binding mechanism in the Fe-porphyrin isomers, Fe-porphycene (FePc) and Fe-corrphycene (FeCor) complexes. By calculating the potential energy surface of the $O_2$ binding, the present study explains the reason for the dramatic increase of $O_2$ affinities observed in the FePc complex. In the case of FeCor-$O_2$, the $O_2$ binding process includes the intersystem crossing from triplet to singlet state, as in FePor-$O_2$ complex. However, FePc-$O_2$ uses only singlet surface. This is because the ground state of FePc complex in the deoxy state is triplet state, while those of FePor and FeCor are quintet states. Such difference originates from character of the SOMO. We estimated equilibrium constants for the $O_2$ binding, which reasonably reproduced the trends observed in the experiments.

## 1. Introduction

Hemoglobin and myoglobin play important roles in our daily life through the transport and storage of $O_2$. These processes have been studied in detail both theoretically and experimentally.[1-10] Hemoglobin and myoglobin are well-known heme proteins. They are also useful for engineering applications.[11-26] To understand and control their functions, myoglobin has been subjected to extensive modifications. They are classified into two categories: amino-acid mutation[11-15] and replacements of the protoporphyrin by artificial porphyrin isomers.[16-26] The former approach is mainly suitable for regulating delicate physiological reactions. In contrast, the latter approach is expected either to improve its functions or to introduce new functions, since the active center itself is replaced by another one. Several modified myoglobins have been experimentally realized using the latter approach. For example, the protoporphyrin has been replaced by aza-porphyrin, diaza-porphyrin, tetra-aza porphyrin, porphycene, corrphycene, etc.[16-22]

Among the interesting properties that the reconstituted myoglobins exhibit, we particularly focus on the $O_2$ binding property. Hayashi et. al. reported that the replacement of porphyrin by porphycene in myoglobin had extremely high $O_2$ affinity, which is by more than 1000 times higher than that of the native myoglobin.[19,20] This finding indicates a possibility to realize tailor-made functional protein.[20] In contrast, Neya et. al. reported that the replacement by corrphycene lowered the $O_2$ affinity (about 1/100 times).[21,22] These dramatic changes were introduced only by the substitution of the porphyrin ring. Porphycene[19,20] and corrphycene[21,22] are porphyrin isomers that have (2,0,2,0) and (2,1,0,1) carbon atoms between each pyrrole rings, respectively, as shown in Figure 1. These isomers interact to the Fe atom in different ways, and the electronic structures could be unique among the reconstituted heme. In this case, a theoretical study would provide important information about the electronic-structure basis to understand the $O_2$ affinity. It would be difficult only by the experimental studies to conclude which factor controls the $O_2$ binding properties.

In our previous study,[27] we investigated the electronic mechanism of the reversible $O_2$ binding by heme (FePor). For the $O_2$ binding process, we found that the spin state was primarily important. Out-of-plane deviation of the Fe atom from the porphyrin plane was also an important factor. Our conclusion for oxyheme is as follows. (i) The potential energy surface of the lowest singlet state is associative, while that of the

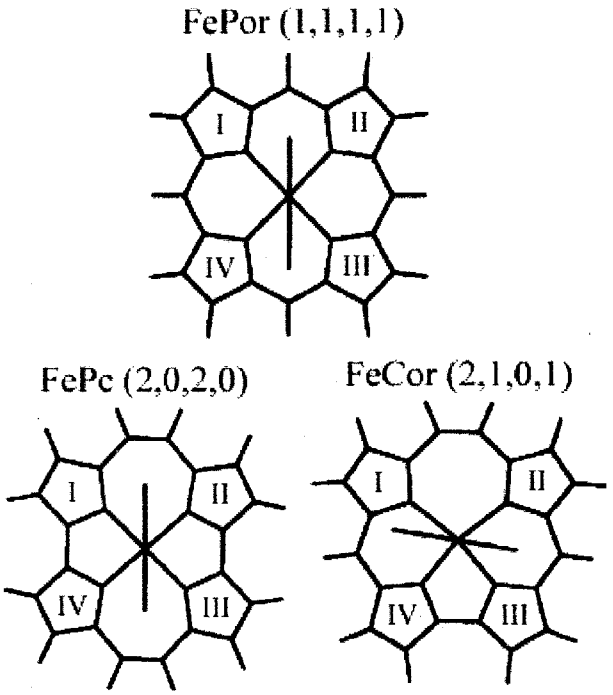


**Fig.1** Structures of Fe-porphyrin (FePor), Fe-porphycene (FePc) and Fe-corrphycene (FeCor) complexes. Porphyrin has (1,1,1,1) carbons, porphycene has (2,0,2,0) carbons and corrphycene has (2,1,0,1) carbons between pyrrole rings. The numbers in the parenthesis, ($n_{I\text{-}II}$, $n_{II\text{-}III}$, $n_{III\text{-}IV}$, $n_{IV\text{-}I}$) are number of the carbon atoms between the pyrrole rings. The "$n_{I\text{-}II}$", "$n_{II\text{-}III}$", "$n_{III\text{-}IV}$", and "$n_{IV\text{-}I}$" denotes the number of the carbon atoms between the rings I and II, II and III, III and IV, and IV and I, respectively.

lowest triplet state is dissociative. (ii) The Fe atom locates in-plane in the singlet state, while that is out-of-plane in the triplet state. (iii) The $O_2$ binding process obviously include intersystem crossing from triplet to singlet states. (iv) This crossing requires relativistic spin-orbit interaction. (v) Owing to such intersystem crossing, the activation energies for both $O_2$ binding and dissociation become moderate and hence reversible. (vi) The electronic structure of the ground state of the oxyheme would be open singlet state.

In this study, we have extended our previous study to the Fe(II)-porphycene-Imidazole (FePc) and Fe-corrphycene-Imidazole (FeCor) isomers and clarified the potential surfaces of the $O_2$ binding processes. Based on these calculations, a reasonable explanation has been given to the previous experimental results. In sections 3.1 and 3.2, the electronic and molecular structures of the deoxy-states and oxy-states are discussed, respectively. In section 3.3 and 3.4, the

potential energy surfaces and the $O_2$ binding processes are discussed. In section 3.5, we estimate the equilibrium constant for the $O_2$ binding, and the result are compared with the experimental data.

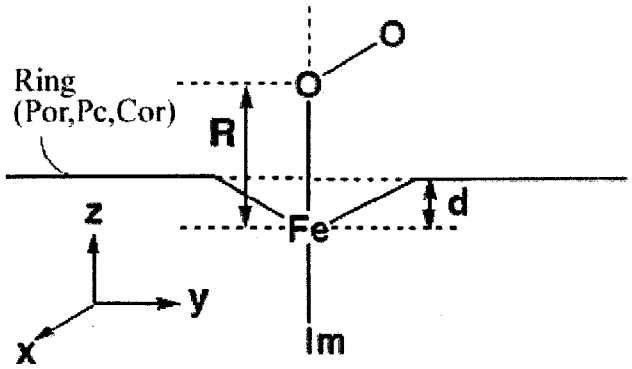


**Fig.2** The computational model and the two reaction coordinates, "d" (the deviation of the Fe atom from the ring plane) and "R" (the distance between Fe and $O_2$). The "Im", "Por", "Pc", and "Cor" denote imidazole, porphyrin, porphycene and corrphycene rings, respectively.

## 2. Computational details

DFT (UB3LYP) calculations were performed with the Gaussian98 program package.[28] The heme model used in this study is $O_2$-Fe(II)-X-Imidazole complex.[27] For FePor, FePc, and FeCor, "X" is porphin, porphycenes, and corrphycene, respectively. The basis sets for the Fe, O and pyrrole N atoms were 6-31g* set.[29] The rest of atoms are treated by 6-31g set for the other atoms.[29]

To determine the electronic structure of the ground states, we performed the geometry optimizations both for oxy- and deoxy-complexes. Then, we calculated the two-dimensional potential energy surfaces of the $O_2$ binding process in the singlet and triplet states. The reaction coordinates are (i)the deviation of the Fe atom from the ring plane and (ii)the distance between Fe and $O_2$. These two reaction coordinates are referred as "d" and "R", respectively. See Fig. 2 for the graphical representations. We calculated 46, 38 and 46 points on the potential surface for FePor, FePc and FeCor, respectively. The intervals are 0.1 and 0.2 Å for the coordinates d and R, respectively. For the R, a finer grid of 0.1 Å interval was taken near minimal point. In this calculation, other atomic coordinates except for d and R were changed linearly between the optimized geometry for the $O_2$ binding states and that for $O_2$ dissociation limit. We first optimized the atomic coordinates for $O_2$ binding state ($X_{bind}$) and $O_2$ dissociation limit

($X_{dis}$). With a parameter $\lambda$ ($0 \leq \lambda \leq 1$), the atomic coordinates between the two structures were linearly defined as Eq. (5.1),

$$\mathbf{X} = \lambda \mathbf{X}_{bind} + (1-\lambda)\mathbf{X}_{dis} \tag{5.1}$$

In each geometry, the Fe-$O_2$ distance, R, was changed without changing all other geometric parameters. Although the other structural parameters were not optimal in terms of the energy, the structural relaxation gave only minor changes to the potential surface as described in section 3.2 of the previous paper.[27]

## 3. Results and Discussion

### 3.1 Ground states of the deoxy complexes: Electronic structure and geometry

The spin-multiplicity and the geometry of the deoxy complexes were determined by the geometry optimization in each spin multiplicity. Table I shows some important structural parameters and relative energies of the complexes.

The ground state of FePor was calculated to be a quintet state.[27] The triplet and singlet states located by 0.67 and 6.48 kcal/mol higher than the quintet state, respectively. The optimized geometry of the quintet state was quite different from those of the triplet and singlet states. In the quintet state, the deviation of the Fe atom from the ring plane was 0.421 Å, which was much larger than the case of the triplet (0.190 Å) and the singlet states (0.201 Å). The calculated geometry for the quintet state is in good agreement with the experimental X-ray crystallographic data[27] for myoglobin and a biomimetic complexes.[30-34]

For FeCor, the ground state was also a quintet state as in FePor. The energy gaps between the quintet state and the other states were, however, larger than the case of FePor. The Fe atom dislocation was 0.513 Å, which was larger than that of the triplet (0.213 Å) and singlet states (0.224 Å).

On the other hand, the ground state of FePc was calculated to be a triplet state. The quintet and singlet states lay by 4.70 and 9.97 kcal/mol higher than the triplet state, respectively. Moreover, the Fe atom deviation was not so significant (0.260 Å), which was clearly different from the case of FePor (0.421 Å). The triplet (0.231 Å) and singlet (0.233 Å) states showed similar deviations to the case of FePor as shown in Table I.

Among these three complexes, the optimized geometries and stabilities of the quintet states shows characteristic feature. To figure out the reason, we analyzed the orbital energy of the complexes in the quintet state as shown in Figure 3. The orbitals shown

**Table I.** The optimized geometries and total energies of the deoxy complexes in quintet, triplet and singlet state. The total energy of ground state is taken as 0.00 kcal/mol.

| | FePor | | | FePc | | | FeCor | | |
|---|---|---|---|---|---|---|---|---|---|
| | quintet | triplet | singlet | quintet | triplet | singlet | quintet | triplet | singlet |
| **Relative energy (kcal/mol)** | **0.00** | **0.671** | **6.48** | **4.70** | **0.00** | **9.97** | **0.00** | **3.59** | **12.6** |
| | | | | **Optimized geometry** | | | | | |
| **Distance (Å)** | | | | | | | | | |
| Fe - Im N | 2.13 | 2.21 | 1.91 | 2.12 | 2.21 | 1.92 | 2.12 | 2.19 | 1.92 |
| Fe - Pyr $N_I$ | 2.09 | 2.01 | 2.01 | 1.95 | 1.95 | 1.95 | 2.09 | 2.06 | 2.05 |
| Fe - Pyr $N_{II}$ | 2.09 | 2.01 | 2.02 | 1.95 | 1.95 | 1.95 | 2.10 | 2.07 | 2.05 |
| Fe - Pyr $N_{III}$ | 2.09 | 2.01 | 2.01 | 1.95 | 1.95 | 1.95 | 2.10 | 1.95 | 1.96 |
| Fe - Pyr $N_{IV}$ | 2.09 | 2.01 | 2.01 | 1.95 | 1.95 | 1.95 | 2.10 | 1.95 | 1.96 |
| Fe - ring plane | **0.429** | **0.190** | **0.201** | **0.260** | **0.231** | **0.233** | **0.513** | **0.213** | **0.224** |
| **Angle (degree)** | | | | | | | | | |
| Pyr $N_I$ - Fe - Pyr $N_{II}$ | 88.8 | 89.1 | 89.7 | 94.2 | 96.2 | 96.1 | 107.6 | 102.7 | 103.4 |
| Pyr $N_{II}$ - Fe - Pyr $N_{III}$ | 88.7 | 90.4 | 89.6 | 84.1 | 82.9 | 83.1 | 85.0 | 88.5 | 88.3 |
| Pyr $N_{III}$ - Fe - Pyr $N_{IV}$ | 88.6 | 89.0 | 89.6 | 94.4 | 96.2 | 96.1 | 74.2 | 78.6 | 78.5 |
| Pyr $N_{IV}$ - Fe - Pyr $N_I$ | 88.7 | 90.4 | 89.7 | 84.1 | 82.9 | 83.1 | 85.6 | 88.7 | 88.3 |
| Pyr $N_I$ - Fe - Im N | 98.6 | 94.2 | 95.2 | 96.3 | 94.5 | 94.6 | 100.9 | 95.7 | 95.1 |
| Pyr $N_{II}$ - Fe - Im N | 99.9 | 94.2 | 94.2 | 96.4 | 94.5 | 94.5 | 98.0 | 94.7 | 94.5 |
| Pyr $N_{III}$ - Fe - Im N | 96.6 | 93.9 | 94.6 | 97.3 | 95.5 | 95.1 | 102.3 | 93.5 | 94.0 |
| Pyr $N_{IV}$ - Fe - Im N | 99.9 | 93.9 | 94.2 | 97.4 | 95.4 | 95.1 | 101.1 | 94.9 | 94.4 |
| **Dihedral angle (degree)** | | | | | | | | | |
| Pyr $N_I$ – Fe - Im N – Im C | 90.4 | 135.4 | 135.0 | 46.5 | 46.8 | 46.9 | 105.8 | 149.7 | 142.6 |
| Pyr $N_{II}$ – Fe - Im N – Im C | 0.204 | 44.7 | 45.0 | -48.5 | -49.8 | -49.6 | -4.01 | 46.4 | 38.6 |
| Pyr $N_{III}$ – Fe - Im N – Im C | -90.1 | -44,5 | -44.9 | -133.3 | -133.1 | -133.1 | -90.6 | -42.4 | -50.0 |
| Pyr $N_{IV}$ – Fe - Im N – Im C | -179.9 | -135.2 | -135.0 | 131.3 | 130.1 | 130.3 | -166.7 | -121.2 | -128.7 |

are characterized as Fe(d-orbital), Ring($\pi$), and Ring($\pi^*$) of porphyrin. The orbital energy in in-plane (d=0.0) and out-of-plane geometries are also compared.

Based on the diagram, the character of the highest singly-occupied MO (HSOMO) explains why the Fe atom in FePor and FeCor prefer out-of-plane position. The HSOMO of FePor and FeCor is the Fe $d_x2_{-y}2$ orbital, while that of FePc is Ring($\pi^*$) orbital. Since the Fe $d_x2_{-y}2$ orbital has anti-bonding character with the lone-pair of the pyrrole N, the $d_x2_{-y}2$ orbital becomes significantly stable when the Fe atom is in the out-of-plane position. The amount of the stabilization is 49.8 and 41.6 mH for FePor and FeCor, respectively. This would be the reason why the Fe atom stays in out-of-plane

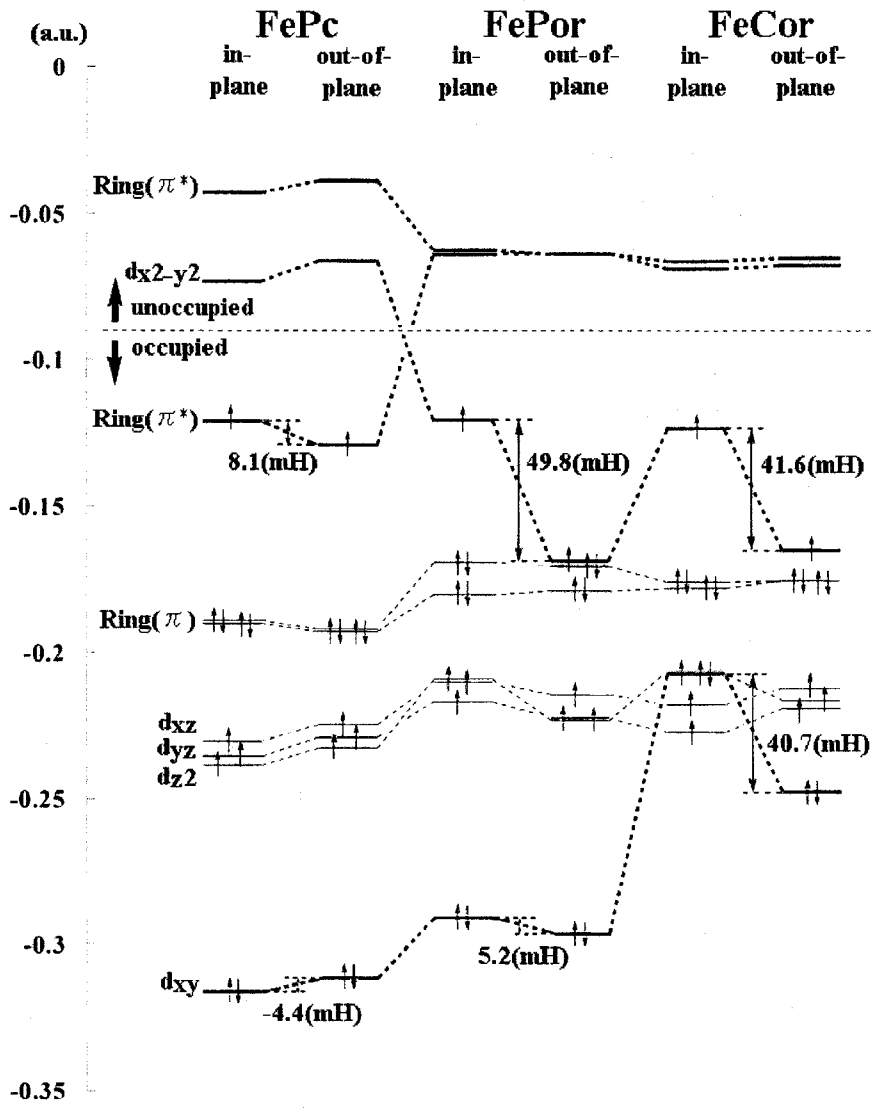


**Fig.3** Molecular orbital energy diagram of the deoxy complexes in the quintet states. The results for the two structures, in-plane (d=0.0) and out-of-plane, are compared.

position in quintet state of FePor and FeCor.

In contrast, the HSOMO of FePc is Ring($\pi^*$) orbital. The Ring($\pi$) and Ring($\pi^*$) orbitals originates from the four-orbitals of the porphyrin.[35,36] The energy levels of Ring($\pi^*$) orbitals are very close each other in FePor, because of the symmetry. However, in FePc, one of Ring($\pi^*$) orbital is significantly more stable than the other. This is related to the orbital energy levels of $C_{20}H_{20}^{2+}$ perimeter model as clearly explained by a previous study.[37,38] As a result, the lowest quintet state of FePc has unpaired electron in one of the Ring($\pi^*$) orbital, not in the Fe $d_{x^2-y^2}$ orbital. This is clearly different from the case of FePor and FeCor. In other word, FePc has a radical in the porphycene ring, and

the Fe atom is in quartet state (Fe(S=3/2) + Pc(S=1/2)). In contrast, FePor and FeCor have Fe(II) ion in the quintet state (Fe(S=2) + Por(S=0)). Therefore, FePc cannot be stable even when Fe atom is in the out-of-position. The amount of the stabilization is 8.1 mH (49.8 and 41.6 mH for FePor and FeCor, respectively).

Another remarkable orbital is $d_{xy}$ orbital, which is the lowest energy d-orbital of Fe atom for FePor and FePc. However, in FeCor, since the ring plane is distorted (symmetry broken), $d_{xy}$ orbital interacts to the lone-pair of the pyrrole N with anti-bonding character. As a result, this orbital is destabilized in in-plane geometry but stabilized in out-of plane geometry (the same reason for the stabilization of $d_{x^2-y^2}$ orbital). In contrast, in FePor and FePc, the anti-bonding interactions vanishes, since the ring planes have high symmetry. The amount of the stabilization is 5.2, -4.4 and 40.7 mH for FePor, FePc and FeCor, respectively. As a result, the quintet state of FeCor becomes more stable than that of FePor in out-of-plane geometry.

### 3.2 Ground states of the oxy-complex: Electronic structure and geometry

Next, we investigated the geometry and electronic structures of the ground state of the oxy-complexes. Table II shows the optimized geometry and the relative energies in each spin multiplicity.

The ground states of the oxy-complex, FePor, FePc, and FeCor, were calculated to be a singlet states. There was no remarkable difference in the optimized geometries among the complexes in the single ground state. The Fe atom located in-plane position, and the deviations were calculated to be almost 0.0 Å. The Fe-$O_2$ and O-O distances were about 1.85 and 1.29 Å, respectively. The electronic structures of the oxy-complexes in the ground state were also very similar. As shown in the previous paper,[27] the Fe $d_{z^2}$ and the $O_2$ $\pi^*$ orbital interacts and compose $\sigma$-bonding orbital. There is no apparent $\pi$-bonding orbital. Therefore, the electronic structure of the oxy-complexes is biradical character: spin population in the Fe $d_{xz}$ and the other $\pi^*$ orbital. Thus, there were no large differences regarding either the optimized geometry or the electronic structure among any of the complexes.

On the other hand, the triplet states located higher than that of the singlet states by 8.36, 13.8, and 6.54 kcal/mol for FePor-$O_2$, FePc-$O_2$ and FeCor-$O_2$, respectively. The Fe-$O_2$ and O-O distances were very close among the complexes. One characteristic feature was that the Fe atom located out of plane by 0.394, 0.256, and 0.468 Å in

**Table II.** The optimized structural parameters and total energies of the oxy-complexes in the triplet and singlet states. The total energy of the singlet state is taken to be 0.00 kcal/mol for all complexes

| | FePor-$O_2$ | | FePc-$O_2$ | | FeCor-$O_2$ | |
|---|---|---|---|---|---|---|
| | triplet | singlet | triplet | singlet | triplet | singlet |
| **Relative energy (kcal/mol)** | **8.36** | **0.00** | **13.8** | **0.00** | **6.54** | **0.00** |
| | | | **Optimized geometry** | | | |
| **Distance (Å)** | | | | | | |
| Fe - Im N | 2.14 | 2.07 | 2.12 | 2.08 | 2.12 | 2.06 |
| Fe - Pyr $N_I$ | 2.09 | 2.01 | 1.95 | 1.95 | 2.09 | 2.04 |
| Fe - Pyr $N_{II}$ | 2.09 | 2.03 | 1.95 | 1.96 | 2.10 | 2.07 |
| Fe - Pyr $N_{III}$ | 2.09 | 2.03 | 1.95 | 1.96 | 2.09 | 1.97 |
| Fe - Pyr $N_{IV}$ | 2.08 | 2.01 | 1.95 | 1.95 | 2.10 | 1.96 |
| Fe - O | 2.91 | 1.85 | 3.01 | 1.86 | 2.91 | 1.84 |
| O - O | 1.22 | 1.29 | 1.21 | 1.29 | 1.21 | 1.29 |
| Fe - ring plane | **0.394** | **0.0253** | **0.256** | **0.00141** | **0.468** | **0.0326** |
| **Angle (degree)** | | | | | | |
| Pyr $N_I$ - Fe - Pyr $N_{II}$ | 88.8 | 90.8 | 94.4 | 96.9 | 108.4 | 104.9 |
| Pyr $N_{II}$ - Fe - Pyr $N_{III}$ | 88.9 | 88.9 | 84.1 | 82.8 | 85.4 | 87.6 |
| Pyr $N_{III}$ - Fe - Pyr $N_{IV}$ | 89.0 | 90.7 | 94.5 | 97.0 | 74.4 | 79.0 |
| Pyr $N_{IV}$ - Fe - Pyr $N_I$ | 89.0 | 89.6 | 84.1 | 83.2 | 85.7 | 88.4 |
| Pyr $N_I$ - Fe - Im N | 98.9 | 89.7 | 95.7 | 89.0 | 99.8 | 88.5 |
| Pyr $N_{II}$ - Fe - Im N | 96.2 | 89.5 | 96.2 | 88.9 | 97.1 | 88.5 |
| Pyr $N_{III}$ - Fe - Im N | 99.1 | 89.4 | 96.7 | 89.1 | 101.2 | 90.6 |
| Pyr $N_{IV}$ - Fe - Im N | 97.7 | 89.5 | 96.8 | 89.1 | 100.0 | 90.8 |
| Fe - O - O | 119.7 | 118.1 | 116.6 | 118.5 | 118.3 | 118.4 |
| **Dihedral angle (degree)** | | | | | | |
| Pyr $N_I$ – Fe - Im N – Im C | 86.6 | 135.7 | 38.0 | 45.3 | 103.7 | 136.6 |
| Pyr $N_{II}$ – Fe - Im N – Im C | -3.15 | 44.9 | -57.1 | -51.7 | -6.40 | 31.6 |
| Pyr $N_{III}$ – Fe - Im N – Im C | -93.0 | -44.0 | -141.9 | -134.5 | -93.1 | -56.0 |
| Pyr $N_{IV}$ – Fe - Im N – Im C | 176.8 | -134.7 | 122.7 | 128.5 | -169.0 | -135.0 |

FePor-$O_2$, FePc-$O_2$ and FeCor-$O_2$ complexes, respectively. Compared with FePor-$O_2$ and FeCor-$O_2$, the out-of-ring deviation was small in FePc-$O_2$. The amount of the deviation is related to the structure of the deoxy-complexes in its ground state. The out-of-ring deviation was 0.429, 0.231, and 0.513 Å in FePor, FePc, and FeCor complexes, respectively. This is because the electronic structures of the triplet states can be described as the combination of the deoxy-complex and $O_2$ in their ground-states.

They are described as Fe(S=2) + $O_2$(S=1) for FePor-$O_2$ and FeCor-$O_2$ and Fe(S=1) + $O_2$(S=1) for FePc-$O_2$. This fact explains the reason why the triplet state of FePc-$O_2$ is unstable compared with those of FePor-$O_2$ and FeCor-$O_2$ and why the out-of-ring deviation of the Fe atom is small for FePc-$O_2$.

### 3.3 The potential energy surfaces for the $O_2$ binding processes

To understand the mechanism of $O_2$ binding, we studied the potential energy surfaces in the $O_2$ binding for the singlet and triplet states. Figure 4 shows the potential energy surfaces for the singlet and triplet states. See Figure 2 for the reaction coordinate, "d" and "R".

#### 3.3.1 The potential energy surface for FePor-$O_2$ and FeCor-$O_2$ complex

For FePor-$O_2$, the details have been described in the previous paper.[27] As shown in Figure 4, the potential energy surface of the singlet state is associative over the entire surface. In contrast, the triplet surface is dissociative over the entire area. Since the FePor moiety becomes the quintet ground state in the $O_2$ dissociation limit, the Fe atom locates in the out-of-plane position. The potential surface clearly shows that the $O_2$ binding requires the intersystem crossing from triplet to singlet state. The crossing region would be around d=0.2-0.3 Å, R=2.2-2.5 Å. The $O_2$ binding process should include the intersystem crossing region to reach the singlet $O_2$ binding state.

The $O_2$ binding potential surface for the FeCor-$O_2$ complex resembles that for FePor-$O_2$. The ground state is singlet in the $O_2$ binding state and changes into triplet state in the dissociation limit. There is intersystem-crossing region around d=0.1-0.2 Å and R=2.1-2.5 Å. Therefore, the $O_2$ binding process would be very similar to that of FePor-$O_2$.

#### 3.3.2 The potential energy surface for FePc-$O_2$ complex

Next, we explain the potential energy surface of the porphycenes complex. As seen in Figure 4, the potential energy surface of the singlet state is associative, and that of the triplet state is dissociative. This is the same feature generally seen in the porphyrin isomer complex. However, the important difference in the Pc case is that the singlet state is more stable than the triplet state in the dissociation limit. This is because the ground state of the deoxy complex is triplet, not quintet as the case of porphyrin and corrphycene as described in section 3.1. The FePc + $O_2$ system is singlet (Fe(S=1) +

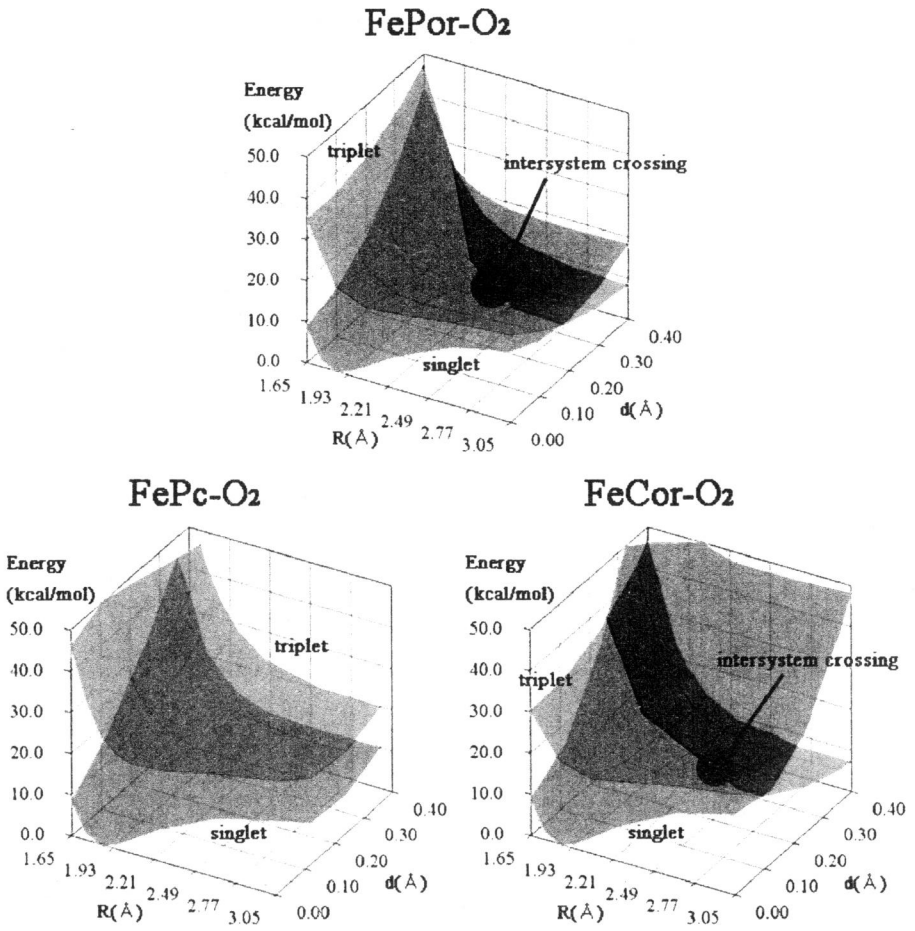


**Fig.4** The potential energy surfaces of FePor-$O_2$, FePc-$O_2$, and FeCor-$O_2$ in the lowest singlet and triplet states. The intersystem crossing could occur around d=0.2-0.3 Å and R=2.2-2.5 Å in FePor-$O_2$ and around d=0.1-0.2 Å and R=2.1-2.5 Å in FeCor-$O_2$. There is no intersystem crossing region in the FePc-$O_2$ potential surface.

$O_2$(S=1)) in the $O_2$ dissociation limit. The FePc-$O_2$ complex is also singlet after the $O_2$ binding as described in section 3.2. Therefore, the $O_2$ binding process does not require intersystem-crossing. In this sense, the mechanism of $O_2$ binding in the FePc-$O_2$ complex is fundamentally different from that in the FePor-$O_2$ and FeCor-$O_2$ complexes.

### 3.4 The $O_2$ binding mechanism

As shown in Figure 5, we extracted the energy-minimum pathway along the $O_2$ binding process from the potential surface. For FePor-$O_2$, the details have been reported in the previous paper.[27] In the $O_2$ binding process, the complex reaches the intersystem crossing point on the triplet potential energy surface after climbing the energy barrier of 3.0 kcal/mol. The spin multiplicity changes into the singlet state, and Fe-$O_2$ bond is

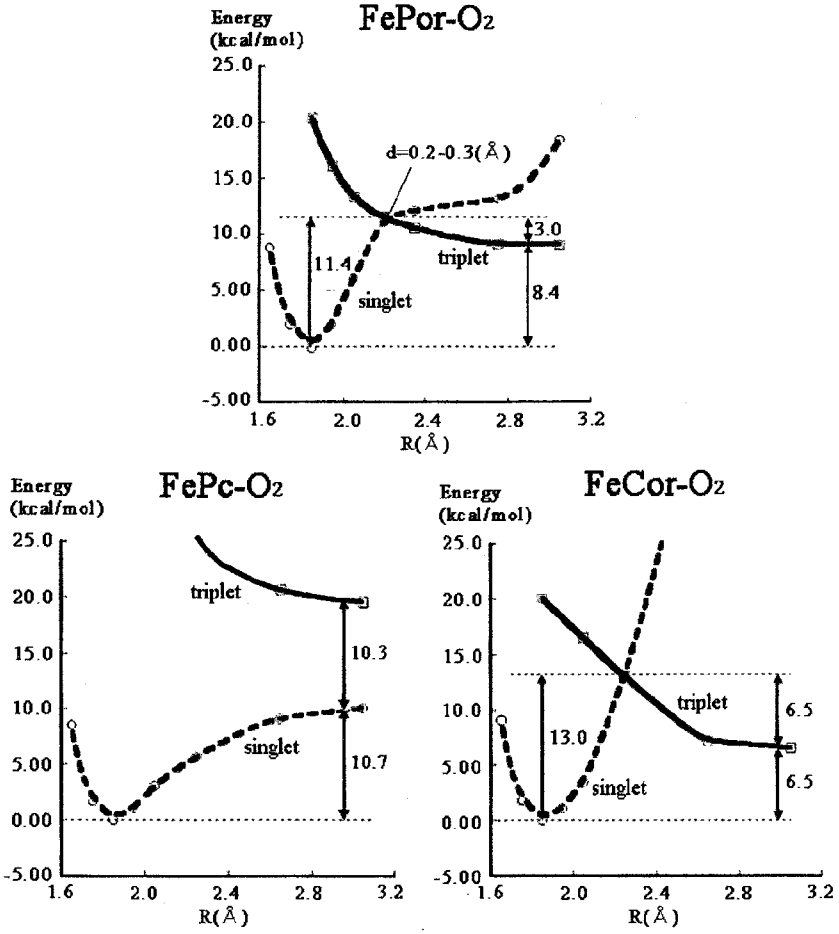


**Fig.5** Potential curves for the $O_2$ binding along the energy minimum pathway. The solid line (——) and dashed line (- - - -) denote the triplet and singlet states, respectively.

formed. The overall reaction energy is 8.4 kcal/mol. In the $O_2$ dissociation process, the system needs 11.4 kcal/mol to reach the intersystem-crossing point.

The potential curve of the FeCor-$O_2$ as shown in Figure 5 is very similar to that of FePor-$O_2$. The activation energy for the $O_2$ binding is 6.5 kcal/mol, and the reaction energy is 6.5 kcal/mol as binding energy. In the $O_2$ dissociation, the energy barrier is calculated to be 13.0 kcal/mol.

In contrast, FePc-$O_2$ complex only uses the singlet surface for the $O_2$ binding/dissociation without spin conversion. The binding energy is 10.7 kcal/mol. The $O_2$ binding process has no energy barrier. We note that our calculations included only the $O_2$-Fe-Porphycene-Imidazole and the $O_2$ binding would be barrier-less within the complex. In the actual system, the pathway to the heme might include some energy barrier due to van der waals interactions between $O_2$ and the protein residues.

The $O_2$ binding energy of the FePc-$O_2$ complex is the largest, and that of FeCor-$O_2$ is

the smallest of the three porphyrin isomers. This tendency qualitatively explains the experimental fact that the FePc reconstituted heme exhibits very high $O_2$ binding affinity[19,20] and the FeCor one shows only small $O_2$ binding affinity.[21,22]

### 3.5 On the equilibrium constant of $O_2$ binding

Using the calculated potential surfaces, we estimated the equilibrium constant for the $O_2$ binding in each complex and compared with the experimental results observed in human myoglobin and its reconstituted ones.

$$K = e^{\frac{\Delta G}{RT}} \approx e^{\frac{\Delta E}{RT}} \tag{5.2}$$

In Eq. (5.2), we assumed that the entropy effects were constant and used the binding energy ($\Delta$E) instead of free energy ($\Delta$G). The theoretically estimated equilibrium constants obtained from eq.(2) and the experimental values[19-22] are compared in Table III. The theoretically estimated value of FePor-$O_2$ is $1.8\times10^6$ [$M^{-1}$] at 20 °C, which is close to the experimental value $1.1\times10^6$ [$M^{-1}$] at 20 °C. For FePc-$O_2$, our estimation is $7.0\times10^7$ [$M^{-1}$] at 25 °C and is around 50 times larger than that for FePor-$O_2$. The experimental value is $1.1\times10^9$ [$M^{-1}$] at 25 °C, which is around 1000 times larger than natural myoglobin including FePor-$O_2$. Our estimation shows the same tendency observed in the experiment, which indicates that the FePc-$O_2$ moiety of the heme explains the large portion of the high $O_2$ affinity in the reconstituted myoglobin.[19-20] For FeCor-$O_2$, the theoretical and experimental values at 20 °C are $7.0\times10^4$ [$M^{-1}$] and $1.5\times10^4$ [$M^{-1}$], respectively. The theoretical estimation decreases and reproduced the small $O_2$ affinity seen in the experiment.[21-22]

The present estimations for the equilibrium constant reasonably agrees to the trend observed in the experiments for three isomers.[21-22] The active site of the complex, especially the potential energy surface, should play important roles in the $O_2$ binding. Therefore, the present results could be a reasonable explanation for the experimental findings.[19-22]

## 4. Conclusion

There are several porphyrin isomers, porphycene and corrphycene. They were used for the alternative to the porphyrin in myoglobin. Such reconstituted myoglobins show singular $O_2$ affinity which is quite different from the native myoglobin. We theoretically

**Table III.** Equilibrium constants estimated by the reaction energy. The experimental values are also shown for the comparison.

| K [$M^{-1}$] | Theoretical estimation | Experimental value |
|---|---|---|
| FePor | $1.8 \times 10^6$ (20 °C ) | $1.1 \times 10^6$ (20 °C ) |
| FePc | $7.0 \times 10^7$ (25 °C ) | $1.1 \times 10^9$ (25 °C ) |
| FeCor | $7.0 \times 10^4$ (20 °C ) | $1.5 \times 10^4$ (20 °C ) |

investigated the mechanism of $O_2$ binding to FePor, FePc and FeCor complexes using the Density Functional Theory calculations.

First, the ground state of the deoxy and oxy complexes were determined. In deoxy complexes, the ground states of both FePor and FeCor are quintet states, and the Fe atom significantly deviates from the ring plane. In contrast, the ground state of FePc is triplet state, and the Fe atom shows moderate deviation from the ring plane. In the quintet states, the $d_x2_{-y}2$ orbital (SOMO) is stabilized when the Fe atom locates the out-of-plane positions. This is because the $d_x2_{-y}2$ orbital has anti-bonding character between the Fe $d_x2_{-y}2$ and the porphyrin $\pi$ orbitals. However, the $d_x2_{-y}2$ orbital is not occupied in the quintet state of FePc. Instead, the porphycene's Ring($\pi^*$) orbital becomes SOMO. Therefore, the quintet state of FePc is not stabilized as those of FePor and FeCor. This is the electronic-structural origin of the high $O_2$ affinity in the porphycenes reconstituted myoglobin. In the oxy complexes, the ground states were calculated to be the singlet states for all complexes, and the Fe atom locates in-plane position. There are no large differences in the optimized geometries and the electronic structures among the isomers. The electronic structures of the triplet states are Fe(S=2) + $O_2$(S=1), and the Fe-Ring-Im moieties are very close to that of the quintet states in deoxy complexes.

Next, we investigated the potential energy surfaces for the $O_2$ binding. In all complexes, the potential energy surfaces of the singlet state are associative, while they are dissociative for the triplet states. For FePor-$O_2$ and FeCor-$O_2$, there is the intersystem crossing regions between the singlet and triplet states. This area is also the transition state in the $O_2$ binding pathway. Therefore, the $O_2$ binding process for both FePor-$O_2$ and FeCor-$O_2$ includes the intersystem crossing. In contrast, for FePc-$O_2$, the triplet state is more unstable than the singlet state, and there is no crossing between the two surfaces. Therefore, the $O_2$ binding of the FePc-$O_2$ complex proceeds only on the singlet surface. There is no energy barrier in the $O_2$ binding. These potential surfaces qualitatively explain the $O_2$ affinity observed in the experiments.

We discussed the $O_2$ affinities by estimating the equilibrium constant. The theoretical estimation reproduced the trend of the experimental equilibrium constant. This result also indicate that the potential energy surface reasonably explains major part of the $O_2$ affinities, FePc-$O_2$ > FePor-$O_2$ > FeCor-$O_2$, observed in the experiments.

**ACKNOWLEDGMENTS**

This study has been supported by the Grant for Creative Scientific Research from the Ministry of Education, Science, Sports and Culture. A part of the computations was performed in the Research Center for Computational Science, Okazaki, Japan.

## REFERENCES


1. J. D. Bernal, I. Fankuchen, M. F. Perutz, *Nature* **141**, 523, 1938.
2. J. Monod, J. Wyman, J. P. Changeux, *J. Mol. Biol.* **12**, 88, 1965.
3. J. J. Englander, J. N. Rumbley, S. W. Englander, *J. Mol. Biol.* **284**, 1707, 1998.
4. S. Bettati, A. Mozzarelli M. F. Perutz, *J. Mol. Biol.* **281**, 581, 1998.
5. H. W. Kim, T. J. Shen, N. T. Ho, M. Zou, M. F. Tam, C. Ho, *Biochemistry* **35**, 6620, 1996.
6. Y. Tokita, H. Nakatsuji, *J. Phys. Chem. B* **101**, 3281, 1997.
7. P. Jewsbury, S. Yamamoto, T. Minato, M. Saito, T. Kitagawa, *J. Phys. Chem.* **99**, 12677, 1995.
8. S. Obara, H. Kashiwagi, *J. Chem. Phys.* 77, 3155, 1982.
9. A. Ghosh, D. F. Bocian, *J. Phys. Chem.* **100**, 6363, 1996.
10. P. Jewsbury, S. Yamamoto, T. Minato, M. Saito, T. Kitagawa, *J. Am. Chem. Soc.* **116**, 11586, 1994.
11. B. A. Springer, S. G. Sligar, J. S. Olson, G. N. Phillips Jr., *Chem. Rev.* **94**, 699, 1994.
12. C. T. Allocatellli, F. Cutruzzola, A. Brancaccio, B. Vallone, M. Brunori, *FEBS Lett.* **352**, 63, 1994.
13. P. Turano, Y. Lu, *In Handbook on Metalloproteins,* S. Sigel, H. Sigel, Eds. Marcel Dekker New York, pp 269-356, 2001.
14. E. L. Raven, A. G. Mauk, *In Advances in Inorganic Chemistry,* A. G. Sykes, G. Mauk, Eds. Academic Press: San Diego, 51, pp 1-51, 2001.
15. S. Ozaki, M. P. Roach, Y. Watanabe, *Acc. Chem. Res.* **34**, 818, 2001.
16. S. Neya, T. Kaku, N. Funasaki, Y. Shiro, T. Iizuka, K. Imai, H. Hori, *J. Biol. Chem.* **270**, 13118, 1995.
17. S. Neya, H. Hori, K. Imai, Y. Kawamura-Konishi, H. Suzuki, Y. Shiro, T. Iizuka, N. Funasaki, *J. Biochem.* **121**, 654, 1997.
18. J. P. Fitzgerald, B. S. Haggerty, A. L. Rheingold, L. May, G. A. Brewer, *Inorg. Chem.* **31**, 2006, 1992.
19. T. Hayashi, H. Dejima, T. Matsuo, H. Sato, D. Murata, Y. Hisaeda, *J. Am. Chem. Soc.* **124**, 11226, 2002.
20. T. Matsuo, H. Dejima, S. Hirota, D. Murata, H. Sato, T. Ikegami, H. Hori, Y. Hisaeda, T. Hayashi, *J. Am. Chem. Soc.* **126**, 16007, 2004.

21. S. Neya, M. Tsubaki, H. Hori, T. Yonetani, N. Funasaki, *Inorg. Chem.* **40**, 1220, 2001.
22. S. Neya, N. Funasaki, H. Hori, K. Imai, S. Nagatomo, T. Iwase, T. Yonetani, *Chem. Lett.* **28**, 989, 1999.
23. T. Hayashi, Y. Hisaeda, *Acc. Chem. Res.* **35**, 35, 2002.
24. V. Heleg-Shabtai, T. Gabriel, I. Willner, *J. Am. Chem. Soc.* **121**, 3220, 1999.
25. F. Christopher Jr., T. Takimura, J. L. Sessler, Abstracts of Papers 213th ACS National Meeting San Francisco CA: American Chemical Society: Washington D. C., INOR-519, 1997.
26. C. Sotiriou-Leventis, C. K. Chang, *Inorg. Chim. Acta* **311**, 113, 2000.
27. H. Nakashima, J. Hasegawa, H. Nakatsuji, *J. Comput. Chem.*, in press.
28. M. J. Frisch, G. W. Trucks, H. B. Schlegel, et al., *Gaussian98, Gaussian Inc., Pittsburgh, PA,* 1998.
29. P. C. Hariharan, J. A. Pople, *Theoret. Chim. Acta* **28**, 213, 1973.
30. S. E. V. Phillips, *Nature* **273**, 247, 1978.
31. S. E. V. Phillips, *J. Mol. Biol.* **142**, 531, 1980.
32. G. Fermi, *J. Mol. Biol.* **97**, 237, 1975.
33. M. Momenteau, W. R. Scheidt, C. W. Eigenbrot, C. A. Reed, *J. Am. Chem. Soc.* **110**, 1207, 1988.
34. G. M. Jameson, G. A. Rodley, W. T. Robinson, R. R. Gagne, C. A. Reed, J. P. Collman, *Inorg. Chem.* **17**, 850, 1978.
35. M. Gouterman, *The Porphyrins, Academix Press, New York* pp1-156, 1978.
36. M. Gouterman, *J. Mol. Spectrosc.* **6**, 138, 1961.
37. J. Waluk, M. Müller, P. Swiderek, M. Köcher, E. Vogel, G. Hohlneicher, J. Michl, *J. Am. Chem. Soc.* **113**, 5511, 1991.
38. J. Waluk, J. Michl, *J. Org. Chem.* **56**, 2729, 1991.